Final Report

for

Feasibility Study of a Noncontacting, Remote Sensing Displacement Transducer

Contract No.: NAS5-10345

Prepared by

Electro-Optical Systems, Inc.
A Xerox Company
300 North Halstead Street
Pasadena, California 91107

for

Goddard Space Flight Center
Greenbelt, Maryland 20771

Final Report

for

Feasibility Study of a Noncontacting, Remote Sensing Displacement Transducer

N68 24511

Contract No.: NAS5-10345

Goddard Space Flight Center

Contracting Officer: S. Provenzano
Technical Monitor: Allen Sherman

Prepared by

Electro-Optical Systems, Inc.
A Xerox Company
300 North Halstead Street
Pasadena, California 91107

Project Manager: T. L. Ward

for

Goddard Space Flight Center
Greenbelt, Maryland 20771

FOREWORD

This feasibility study of a noncontacting, remote sensing, displacement transducer was conducted by the Measurement Systems Division of Electro-Optical Systems, Inc., Pasadena, California, under National Aeronautics and Space Administration Contract Number NAS5-10345. The contract was issued and administered by the Goddard Space Flight Center, Greenbelt, Maryland. A. Sherman was the GSFC Technical Officer, and T. Ward was the EOS Principal Investigator. This study was conducted during the period from 17 April 1967 to 12 January 1968. This study did not develop data applicable to the "New Technology" clause of the contract.

ABSTRACT

This report presents the results of a feasibility-design study of a laser-based displacement transducer. The work included a preliminary verification of the suitability of the laser approach, a systems analysis and design, and layouts of the electrical, optical, and mechanical design. It was concluded that the layout design is capable of remotely measuring displacements with a resolution on the order of 10^{-9} inch. It is recommended that a prototype transducer be constructed and tested.

CONTENTS

CONTENTS (Contd)

CONTENTS (Contd)

ILLUSTRATIONS

ILLUSTRATIONS (contd)

ILLUSTRATIONS (contd)

SECTION 1

INTRODUCTION

This section describes the scope and purpose of the report, gives a general background of the project, and provides a breakdown of the project into its functional systems and subsystems. A brief summary of the work performed during the reporting period is included.

1.1 SCOPE AND PURPOSE OF REPORT

This feasibility study (Ref. 1) consisted of two phases, a research phase and a feasibility-design study phase. The research phase was a review of the state of the art in low-level displacement sensing devices. Based on the results (Ref. 2) of that phase, a laser technique was selected for the feasibility-design study phase. This report presents in detail the results of the latter phase.

Section 2 is a summary of the measurement theory that is generally applicable to any displacement transducer. It also includes a summary of the techniques investigated during the research phase and a discussion of the bases for selecting the laser technique. Section 3 is a qualitative discussion of those aspects of gas laser operation that are of interest to persons considering their use in displacement measurement. Sections 4 through 7 consider the system, electrical, optical, and mechanical design. Section 8 discusses the applicability of the basic sensor in the measurement of velocity, acceleration, pressure, force, and impulse through electronic operation on the sensor output signal. Techniques for alignment, calibration, and operation are covered in Section 9.

1.2 BACKGROUND OF THE PROJECT

There are numerous instrumentation applications that require the measurement of extremely small, yet rapidly changing, displacements. Thrust measurement of small, pulsed, rocket engines is an example of a particularly demanding application. Such engines may be mounted on thrust stands that have a deflection that is directly proportional to thrust under steady-state conditions. For pulsed operation, the natural frequency of the test stand becomes important. If it is desired to know the peak thrust to about 5 percent, then a rule-of-thumb requirement (Ref. 3) is that the natural period of the structure, if it is damped to within 0.4 or 0.7 of critical, should not exceed about one-third the pulse duration. In the more frequent case of lightly-damped thrust stands an even shorter natural period is required, say one-fifth the pulse length. Shorter natural periods inevitably mean stiffer structure, lower deflections, and increased demands upon the sensitivity of the displacement transducer.

In one investigation (Ref. 4), a Resistojet engine was supported by a wire-in-tension thrust stand. Using a then-available displacement transducer with a minimum detectable displacement of 3×10^{-7} inches, a minimum thrust level of 10^{-4} pounds could be resolved when the stand was adjusted to have a natural frequency of 40 Hz (a natural period of 25 ms). The investigators recognized that the displacement transducer imposed limitations. They pointed out that minimum thrust level could have been lowered to 6×10^{-6} lbs, but only at the expense of a 10 Hz natural frequency. Similarly, if it was required that the natural frequency be raised to 640 Hz, the minimum detectable thrust would be increased to 2.6×10^{-2} lbs.

The example of the Resistojet is not unique. In the case of any mechanical system, improving the dynamic response by increasing stiffness results

in decreased deflection. Any system that relies on the measurement of such deflections (e.g., see Section 8) would be aided by the availability of a displacement sensor with improved sensitivity. This investigation was undertaken to determine the extent to which such improvement is possible.

1.3 PROJECT FUNCTIONAL BREAKDOWN

This feasibility-design study of a displacement sensor was based on the use of a helium-neon laser operating in the visible portion of the spectrum. Reduced to its most elemental form the gas laser consists of a discharge tube located between two mirrors. The mirrors form a resonant optical cavity, the length of which determines the frequency of the light produced. Changing the length of the cavity, for example, by moving one mirror, changes the frequency of the light and affords the opportunity for the measurement of displacement

In order to construct a practical displacement transducer other components must be added to the elemental laser just described. The discharge tube and other optical components must have mechanical supports that provide required adjustments and movements. A control system is frequently provided to insure that the laser frequency will stay within prescribed limits despite environmental effects. And, in the case of a laser used to sense displacement, a means of generating the appropriate electrical output is required.

Although these elements are clearly interrelated, some functional breakdown was required for the purpose of the design study. Broadly, these functions were systems design, optical design, electrical design, and mechanical design. Systems design was concerned with the operation of the complete instrument as a displacement transducer, and the other three are largely self-explanatory. The results of the design study in each of the four areas are presented in Sections 4 through 7.

1.4 SUMMARY OF WORK

As previously mentioned, this report deals primarily with the work of the feasibility-design study phase. This phase extended from 13 July 1967 to 12 December 1967.

A study was made of a variety of factors that affect laser design and operation. Particular attention was directed toward those characteristics important in displacement measurement. The most general results of this initial analysis were that special provisions would have to be made to assure single-mode operation and that closed-loop control would be required to maintain frequency within the operating range. A system that combined these functions with the ability to measure small displacements was laid out. The feasibility-design study was completed by a systems analysis, and feasibility studies of the optical, electrical, and mechanical design. Consideration was given to the measurement of velocity, acceleration, pressure, force, and impulse by means of appropriate modifications to the basic sensor.

SECTION 2

DISPLACEMENT MEASUREMENT THEORY

The most demanding requirements of the target design specifications given in Subsection 4.1 are the 10^{-6} and 10^{-9} inch sensitivity, and the 0 to 1000 Hz frequency response. These requirements are interrelated, since, in the design of most measuring systems, it is possible to improve resolution at the expense of bandwidth, and conversely. First consideration was given, therefore, to those factors that place theoretical limits on performance in each of these areas. This section concludes with a review of some of the displacement techniques considered during the research phase and discusses the reasons that lead to the selection of the laser technique for the feasibility-design study phase.

2.1 MINIMUM DETECTABLE SIGNAL

A measurement system designed to detect minute displacements should be free of such small signal nonlinearities as threshold, hysteresis, and backlash. In the absence of such nonlinearities, the magnitude of the minimum displacement that can be detected depends upon the system noise level.

As an example, consider the displacement sensor shown in Fig. 1. For sufficiently large signals, the output voltage, E, may depend linearly on the input displacement X, as:

$$E = kX, \; X \gg 0 \qquad (1)$$

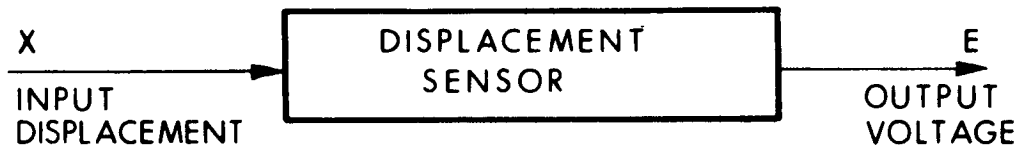

Figure 1. Displacement Sensor Elementary Block Diagram

However, if the input is removed (X = 0) the output will not be zero. In fact, it will consist of random noise due to sources within the displacement sensor itself. If this noise has a mean value of zero, and a standard deviation of σ_E, then small signals for which

$$kX \ll \sigma_E \tag{2}$$

will be difficult to detect, and large signals for which

$$kX \gg \sigma_E \tag{3}$$

will be quite easy to detect. The practical Minimum Detectable Signal (MDS) will be at some intermediate value.

A signal X is said to be detectable if it is observed with a probability $\geq \alpha$ when present, and "no signal" condition will be observed with a probability $\geq \beta$ when it is absent. These conditions may be written in the form:

$$P\ (E > kX_o \mid S) \geq \alpha \tag{4}$$

$$P\ (E < kX_o \mid NS) \geq \beta \tag{5}$$

where X_o is the MDS, S indicates there is an input signal X_o present, NS indicates that there is no signal present, and α and β are preassigned probabilities. The term $P(E > kX_o \mid S)$ is then read "the probability that E is greater than kX_o, given that an input signal is present," and similarly for Eq. 5.

With the above definition of detectability, and assuming Gaussian noise, it can be shown (Ref. 5) that

$$\frac{E_o}{\sigma_E} = \frac{kX_o}{\sigma_E} = \sqrt{2}\left[\text{erf}^{-1}(2\alpha - 1) + \text{erf}^{-1}(2\beta - 1)\right] \qquad (6)$$

where erf^{-1} is the inverse error function or probability integral. The ratio E_o/σ_E is plotted in Fig. 2 (Ref. 6) for the case $\alpha = \beta$. The relation $E_o = 2\sigma_E$ is sometimes used as a criterion for the MDS. Under these conditions,

$$X_o = \frac{2\sigma_E}{k} \qquad (7)$$

which is the result when $\alpha = \beta = 0.84$. Some of the fundamental processes that produce the noise and that place a lower limit on the MDS are outlined in Subsections 2.2 and 2.3.

2.2 MECHANICAL CIRCUIT

In considering noise sources that arise in the measurement of displacement, it will be useful to treat the sensor as a four-terminal network, as shown in Fig. 3. In this case, the velocity to be measured is applied across the input to the sensor. To the extent that the sensor loads the velocity source, a force will flow from the source into the sensor. The sensor develops a voltage across its output. To the extent that the electrical readout device loads the sensor, current will flow from the sensor into the readout device.

For the purposes of this analysis, velocity was chosen in preference to displacement as the input quantity. This choice permits certain analogies to be drawn between mechanical and electrical quantities. These are presented in Table I. Voltage and velocity are sometimes called "across" variables because the value of the variable at one

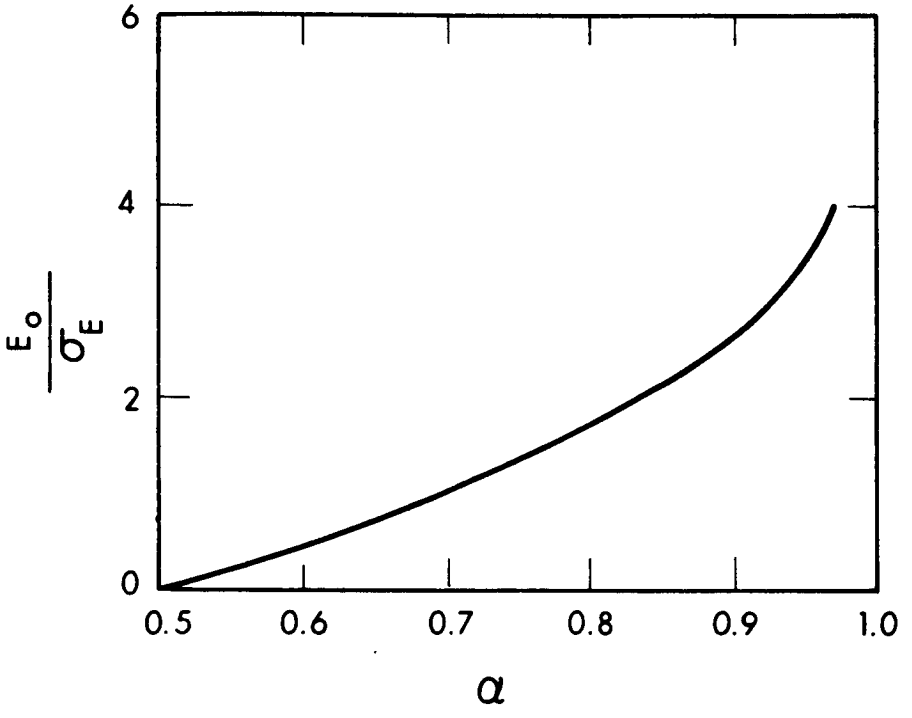

Figure 2. Ratio of E_o to σ_E versus α

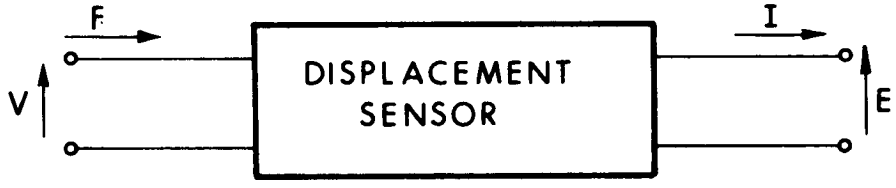

Figure 3. Displacement Sensor as a Four-Terminal Network

TABLE I

MOBILITY ANALOGY BETWEEN ELECTRICAL AND MECHANICAL QUANTITIES

Electrical			Mechanical		
Quantity	Unit	Sym	Quantity	Unit	Sym
Electromotive Force	Volt	E	Velocity	Meters Per Second	V
Charge	Coulomb	Q	Impulse or Momentum	Kilogram-Meters Per Second	Q_M
Current	Ampere	I	Force	Newton	F
Impedance	Ohm	Z	Mobility	Meters Per Second-Newton	z_M
Resistance	Ohm	R	Responsivity	Meters Per Second-Newton	$\frac{1}{D}$
Reactance	Ohm	X	Excitability	Meters Per Second-Newton	x_M
Inductance	Henry	L	Compliance	Meters Per Newton	C_M
Capacitance	Farad	C	Mass	Kilograms	M
Power	Watt	P	Power	Watt	P

point must be measured using a second point as a reference; thus they can be considered to be measured across the two points in question. Current and force are sometimes called "through" variables because their measurement normally requires that a wire or a piece of structure be cut and the measuring device inserted in series. For both electrical and mechanical circuits, the product of the "across" and "through" variables is power in watts. Furthermore, in both cases, the dissipative circuit elements (electrical resistance and mechanical responsivity) are defined by the ratio of the "across" to the "through" variable. These formal analogies will be important in Subsection 2.3 when both mechanical and electrical equivalent noise generators are considered.

Mechanically, the displacement source to be measured can be represented as a velocity source in series with a mechanical mobility, as shown in Fig. 4. To measure this velocity, both the source and the sensor must be referenced to the same point. Practically, this might be done by attaching the mechanism that provides the source of displacement to a large metal plate and attaching the displacement sensor to the same metal plate. The result is shown schematically in Fig. 5. If the temperature of the plate varies, so will its dimensions. This will cause an error in the reference between the source and sensor, as shown in Fig. 6. As an example of the magnitude of this effect consider the source and sensor to be mounted 10.0 inches apart on an Invar plate. If the Invar has a coefficient of expansion of 1.5×10^{-6} inch per inch per ^{o}C, the plate will exhibit 1.5×10^{-5} inch/^{o}C. A sensor with a sensitivity of from 10^{-6} to 10^{-9} inch would then be able to detect changes in temperature of from 10^{-1} to $10^{-4}{}^{o}C$. This effect may be minimized by making the plate massive so as to slow the temperature variations, and by mounting the source and sensor as close to each other as possible.

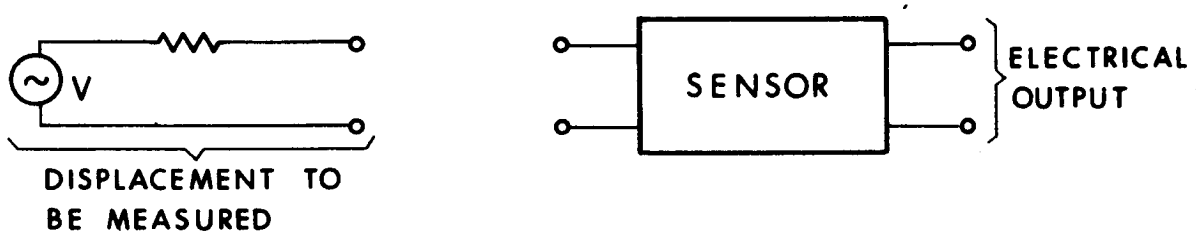

Figure 4. Displacement Source and Sensor

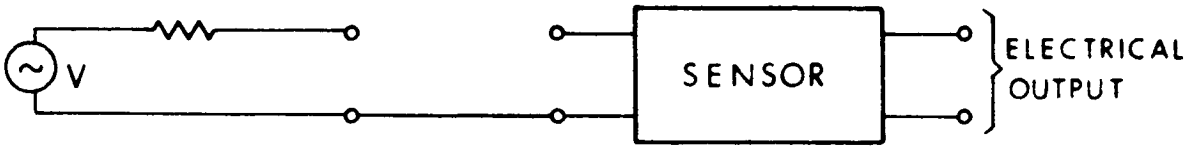

Figure 5. Displacement Source and Sensor with Common Reference

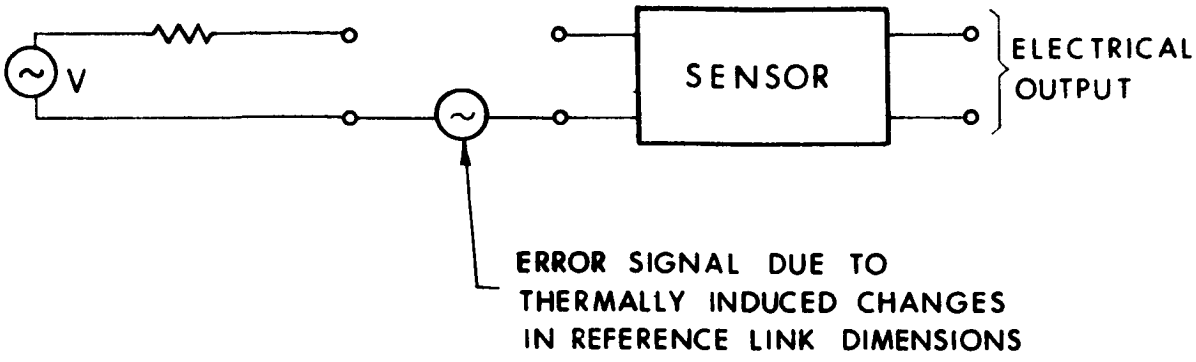

Figure 6. Displacement Source and Sensor with Reference Error

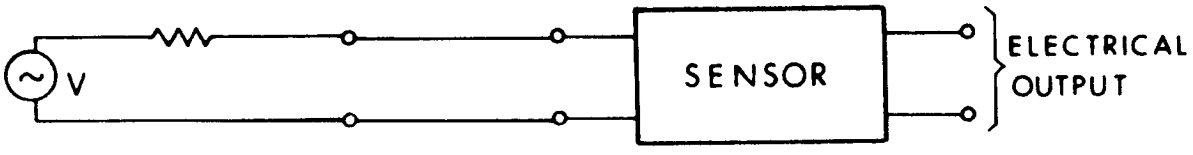

Figure 7. Displacement Source and Sensor, Completed Circuit

After a suitable reference has been provided between the source and sensor, the connection may be completed and the displacement measured as shown in Fig. 7. For a contact type of displacement transducer this connection would be made by a rod or other structural member. This inserts an additional mixed mass and compliance in series with the source. For a noncontact displacement transducer, the measurement is made at the source and no additional elements are inserted.

When the displacement sensor is remote, a reference surface may be placed near the surface whose displacement is to be measured. In this way it may be possible to sense differential displacement between the two surfaces. The static, thermal, reference error considered in this section then appears as a common mode signal in series with each leg of the measurement, as shown in Fig. 8.

2.3 SYSTEM NOISE

Noise in electrical circuits can originate internally or externally. External noise sources can be coupled to the circuit either electromagnetically or electrostatically. Such coupling can be reduced to a negligible amount by proper design of the system and its environment. The ultimate limit on the noise in a passive electrical circuit is set by the small random currents produced by the thermal agitation of electrons in the conductors. This noise is present in all resistors. It is present in inductors and capacitors only to the extent that they depart from ideal performance and exhibit dissipation.

Johnson (Ref. 7) observed such noise experimentally in 1928, and showed that it followed the relation:

$$E = \sqrt{4kTR\Delta f} \qquad (8)$$

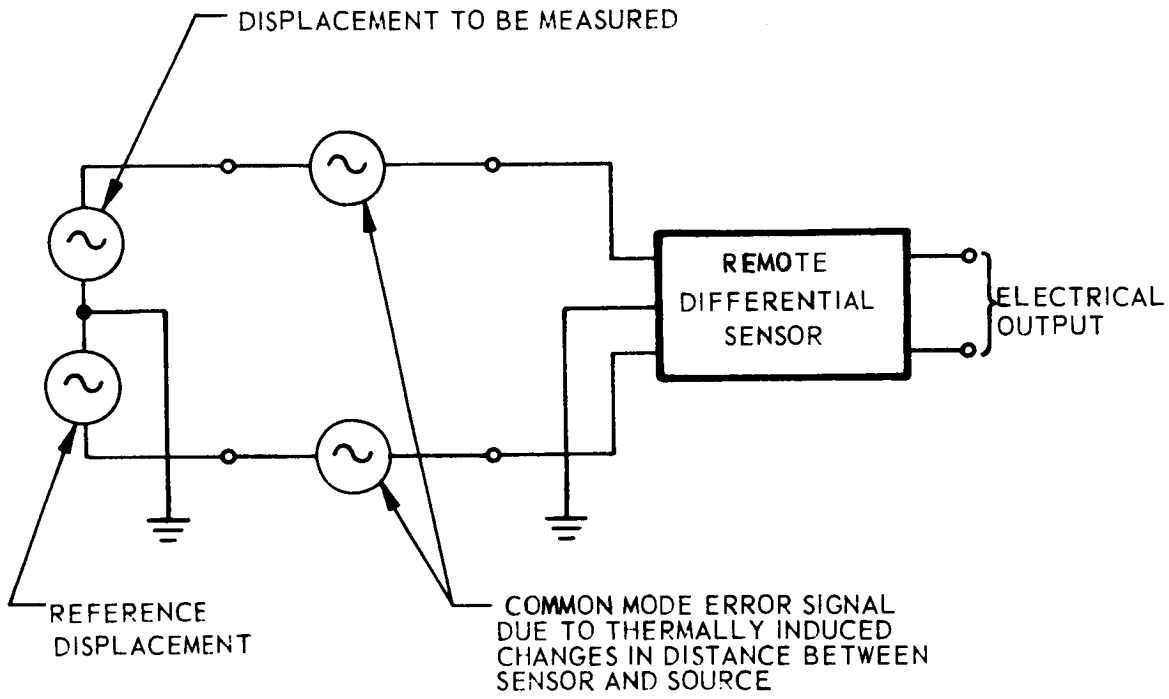

Figure 8. Remote Differential Sensor

where

k = Boltzmann's constant, 1.38×10^{-23} joule/^{o}K

T = absolute temperature in ^{o}K

R = resistance of conductor in ohms

Δf = bandwidth in which noise is to be measured, in hertz

Johnson determined that this formula predicted the noise in such varied conductors as carbon filaments, resistors wound from Advance wire, and a number of electrolytic solutions. Nyquist (Ref. 8) supplied a theoretical proof using thermodynamic arguments that are independent of the nature of the conductor. In fact, his argument is sufficiently general to apply to any system described by variables that are thermodynamically analogous (Ref. 9) to voltage, current, resistance, etc. One such system is the mechanical mobility analogy presented in Table I. It has been pointed out (Ref. 10) that relations similar to Eq. 8 serve to predict the acoustical noise due to thermal agitation of air molecules, and the mechanical noise due to thermal agitation of molecules in structural elements.

2.3.1 MECHANICAL NOISE

As an example of the level of mechanical noise that might arise from purely dissipative elements, consider the system shown in Fig. 9a. In this figure a block of mass M rests on a thin sheet of rubber of reciprocal viscous coefficient 1/D, which in turn rests on a massive base. The mechanical circuit is shown schematically in Fig. 9b, where V_1 is the equivalent velocity noise generator associated with 1/D, and V_o is the velocity of M with respect to the massive base.

The coefficient of friction of rubber is almost entirely viscous at sufficiently low velocities. A thin sheet, supporting a mass of one kilogram might exhibit a reciprocal viscous coefficient of

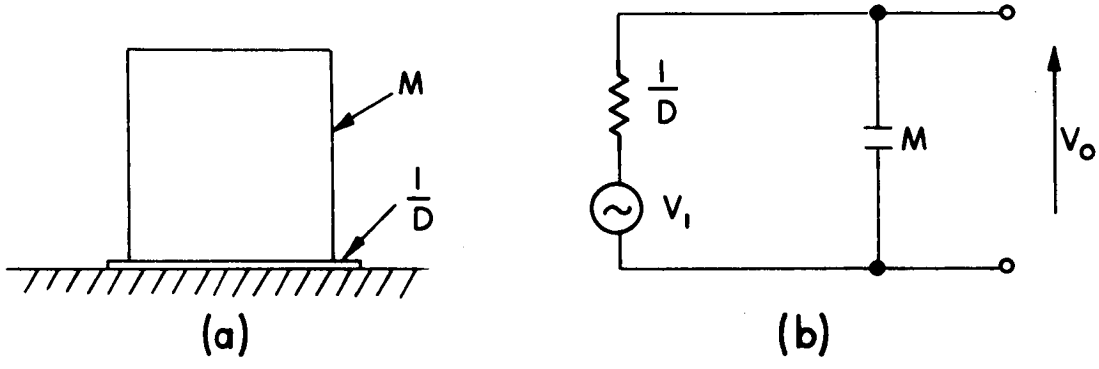

Figure 9. Mass Restrained by Viscous Mounting

$$\frac{1}{D} = 2.5 \times 10^{-3} \text{ meter/newton-second}$$

It would produce an equivalent noise velocity of

$$V = \sqrt{\frac{4kT\Delta f}{D}} = 6.4 \times 10^{-12} \text{ meter/sec} \qquad (9)$$

if $\Delta f = 1$ Hz. If $\Delta f = 1000$ Hz, the noise velocity would be about 32 times greater. The smaller value is typical of many conventional D'arsonval meter movements, such as might be used for visual readout of static or slowly varying displacements.

The Laplace transform of the velocity of the mass with respect to the support upon which it rests is

$$V_o(s) = \frac{1}{\frac{M}{D} s + 1} V_1(s) \qquad (10)$$

where $V_o(s)$ and $V_1(s)$ are the Laplace transforms of $V_o(t)$ and $V_1(t)$. This noise velocity would contribute an error to the measurement of the displacement of M. The Laplace transform of an ideal displacement sensor (such as described in Eq. 1, Subsection 2.1) would be

$$\begin{aligned} E(s) &= k\, X(s) \\ E(s) &= \frac{k}{s} V(s) \end{aligned} \qquad (11)$$

Combining Eqs. 10 and 11 gives

$$E(s) = \frac{k}{s\left(\frac{M}{D} s + 1\right)} V_1(s) \qquad (12)$$

In the example being discussed, the time constant M/D is 2.5×10^{-3} second, which corresponds to a corner frequency of 64 Hz. For frequencies much lower than 64 Hz, Eq. 12 reduces to

$$E(s) \cong \frac{k}{s} V_1(s) \tag{13}$$

The noise power due to V_1 is uniform over a wide bandwidth; i.e., V_1^2 per unit bandwidth is "flat" as shown in Fig. 10a. Equation 13 indicates, however, that the output voltage for constant input velocity slopes downward at the rate of -20 dB per decade. This in turn means that the spectral distribution of E^2 slopes downward at the rate of -40 dB per decade as shown in Fig. 10b.

The preceding argument indicates that mechanical noise due to thermal agitation of the molecules in structural elements exhibiting dissipation becomes more pronounced as attempts are made to extend the lower limit of frequency response closer to zero frequency. A sine wave with a peak velocity of 6.4×10^{-12} meter/sec would have an amplitude of 2.5×10^{-11} meter (10^{-9} inch) if its frequency were 0.04 Hz. This corresponds to a period of 25 seconds. On an order-of-magnitude basis, this means that if the system of Fig. 9a is observed with a 1 Hz bandwidth displacement transducer for periods in excess of 25 seconds, the uncertainties due to thermally generated mechanical noise will exceed 10^{-9} inch. Such effects may be minimized by careful attention to the method of attachment of the displacement source and the displacement sensor to their common reference. All contacting surfaces should be metal-to-metal, and carefully "fitted up." Such precautions, together with a light, stiff structure, will also help reduce the magnitude of mechanical noise coupled from such external sources as microseismic disturbances in the earth's crust, the apparent change in local gravity produced by lunar motion, acoustic disturbances, etc.

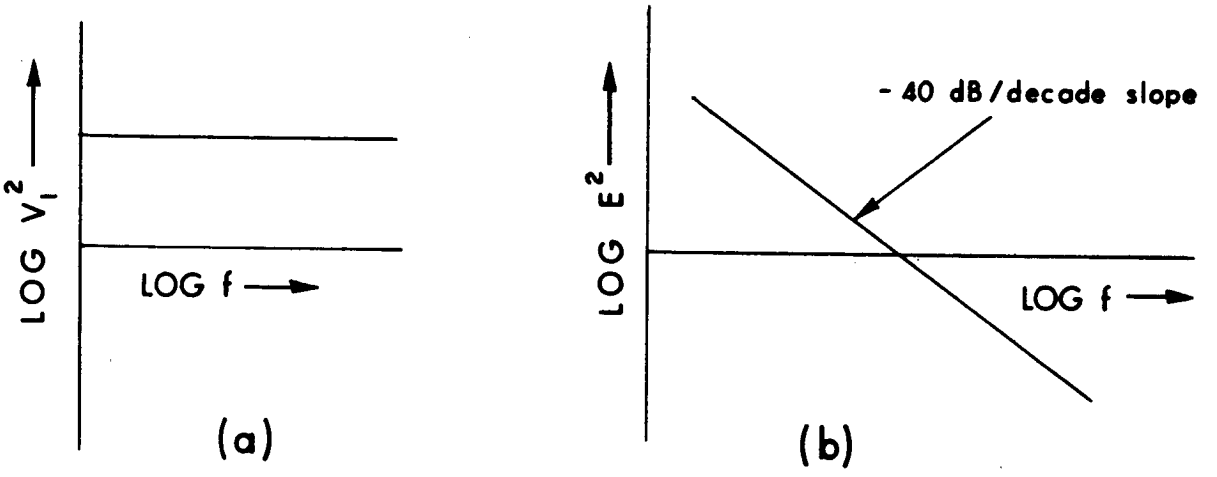

Figure 10. Spectral Power Densities

2.3.2 ELECTRICAL NOISE

To briefly assess the constraints placed on displacement measurement by electrical noise, assume that the output impedance of the transducer shown in Fig. 3 has a resistive component of 100 ohms. If observed with a 1000 Hz bandwidth voltmeter, such a resistor will be found to be equivalent to a noise voltage of about 4×10^{-8} volt. If 10^{-9} inch is the desired MDS, then it must produce 8×10^{-8} volt at the output of the displacement transducer. This sets the lower limit of transducer scale factor as

$$k = \frac{8 \times 10^{-8} V}{10^{-9} \text{ in.}} = 80 \text{ volts/inch}$$

For the particular example considered, if k is less than 80 V/in., 10^{-9} inch could not be detected unless the bandwidth is decreased to less than 1000 Hz. The electrical noise level and scale factor depends on the type of transducer selected and was one of the more important factors considered in the research phase study.

2.4 DISPLACEMENT MEASUREMENT TECHNIQUES

Only those techniques that received major emphasis during the research phase (Ref. 2) are reviewed in this section.

2.4.1 CAPACITIVE DISPLACEMENT SENSORS

When a voltage is applied across two conductors (or one conductor and ground) a current will flow until the net charge on each conductor is sufficient to create an electric field that just balances the applied voltage. The ratio of charge to voltage is defined as the capacitance

of the two conductors. A system of conductors may be designed so that its capacitance is a function of the displacement of some part of the system. Sensitive, small-displacement capacitive sensors usually rely on the variation of the spacing between plates of a condenser. At constant frequency, and neglecting fringing effects around the edges of the plates, the impedance of a parallel plate capacitor is directly proportional to plate spacing. Fringing may generally be neglected in small displacement applications.

The sensitivity of a capacitive sensor can be increased by increasing the applied voltage. The limit on applied voltage occurs when the field between the plates reaches the breakdown value. This value may be extended by the use of extremely clean, smooth plate surfaces. Another effect of increased applied voltage is an increased attractive force between the plates. If one of the plates is attached to the displacing member, this force will have the effect of a small, negative, nonlinear spring constant.

Dissipation is present in capacitive sensors as a result of losses in the dielectric material supporting the plates. This dissipation contributes electrical noise. A typical 1.0 picofard sensor with a plate spacing of 0.005 cm and excited by a 100 MHz current, might exhibit losses corresponding to a 1000 MΩ resistance. If the excitation current is sufficient to produce 100V across the plates, this value of shunt resistance would have self-noise that would make the minimum detectable change in plate spacing on the order of 10^{-13} inches. If the electrical signal is read with an rf voltmeter with a 2000 Hz bandwidth (10 MHz ±1000 Hz) and a noise level of 10^{-7} volt referred to the input, the minimum detectable change in plate spacing would be increased to on the order of 0.5×10^{-9} inch. The attraction between the plates in this case is on the order of 10 dynes.

2.4.2 INDUCTIVE DISPLACEMENT SENSORS

When a voltage is applied to the terminals of a coil, current of increasing magnitude will flow. The resulting magnetic field increases at a rate proportional to the rate of change of current, and generates a counter emf as it cuts the turns of the coil. The current rises at a rate just sufficient to produce a counter emf that balances the applied voltage. An inductor may be designed so that its impedance is a function of a physical displacement of one of its elements. Sensitive, small-displacement inductive sensors usually depend on the variation in thickness of one or more air gaps inserted in its magnetic core. Most such sensors and the accompanying read-out electronics are reasonably linear only when the displacement, or change in gap thickness, is small in comparison to the total gap thickness.

At low frequencies the principal losses in inductors are due to winding resistance and eddy current losses. A typical 10 mH sensor with a gap thickness of 0.005 cm and excited by a 10 kHz source, might exhibit losses corresponding to a 5Ω series resistance. If the excitation is a 30V series source, this value of series resistance would imply a minimum detectable displacement on the order of 10^{-12} inch. Practically available 10 kHz detectors with the required 2000 Hz passband might increase this level to on the order of 5×10^{-9} inch. The attractive force between the faces of the air gap would be on the order of 0.5 newton, or about 0.1 pound. To the movable face this would appear as an appreciable negative spring constant, and might result in mechanical instability in some instances.

2.4.3 INTERFEROMETRIC DISPLACEMENT SENSORS

When two beams of light are sufficiently coherent, they may interfere in such a way as to give rise to periodic variations in intensity. These

variations, which may have the visual appearance of alternate bright and dark bands, are interference fringes. Interferometry is a method of experimental optics that has been used for the measurement of index of refraction, lens testing, microscopy, and interference spectroscopy. In metrology, interferometers have been used for the precise measurement of lengths. In the last application resolution and speed of measurement are secondary to absolute accuracy. By means of known techniques (Ref. 11), the required resolution of 10^{-9} can be attained. Mechanical movement of one of the mirrors at amplitudes and rates sufficient to meet the 0-1000 Hz response requirement appears feasible using piezoelectric or similar transducers.

2.4.4 LASER FREQUENCY DISPLACEMENT SENSORS

The spectrum of a gas laser not operating in a single mode has a fine structure. This fine structure arises because the laser can oscillate in more than one mode simultaneously. The origin of the various transverse and axial modes is discussed in somewhat greater detail in Section 3. The principal modes are the transverse modes determined by the distance between the mirrors that form the optical cavity. If this distance is about one meter, the spacing between transverse modes is on the order of 150 MHz. It is possible to use the fine structure as the basis for a laser displacement sensor requiring only one optical path.

A sensor based on such an arrangement is shown in Fig. 11. M1 is a totally reflecting mirror, L is the laser discharge tube, M2 is a partially reflecting mirror (e.g., 98 percent reflection, 2 percent transmission), and D is a broadband photodetector. Since visible light has such a high frequency (about 5×10^{14} Hz in the case of 0.6 μm, visible, light) presently available photodetectors cannot respond to the amplitude of either the electric or magnetic waves of light incident upon

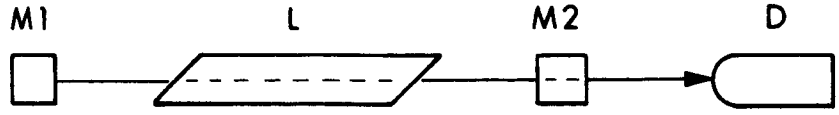

Figure 11. Single-Path, Fine-Structure, Laser Displacement Sensor

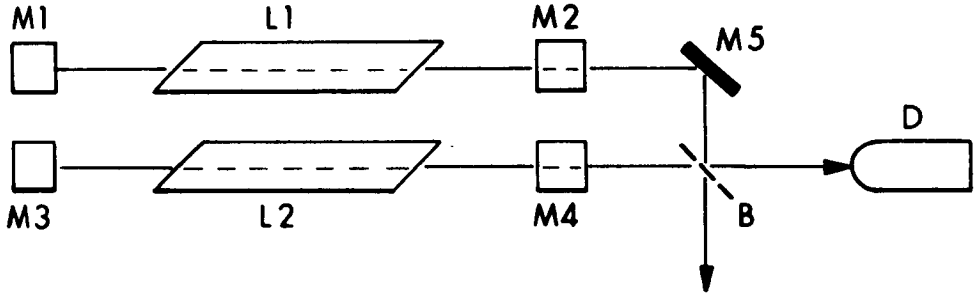

Figure 12. Heterodyne Laser Displacement Sensor

them. Instead, the response is proportional to power; that is, the square of the incident wave amplitude. Such square-law detectors have outputs that contain terms that are proportional to the product of the amplitudes of incident modes, and have frequencies equal to the difference of the mode frequencies.

Since this difference frequency depends on the distance between mirrors, it provides a measure of the optical cavity length, or mirror spacing. If one mirror is attached to a deflecting structure, and the second mirror is held fixed, the change in frequency output from the photodetector will be closely proportional to the incremental change in displacement. The basic limitation of this approach is that the displacement to be measured is small in comparison to the length of the laser, so that changes in the total laser length due to temperature variations, etc., will introduce significant efforts.

A configuration that overcomes this limitation is shown in Fig. 12. There are two lasers, M1-L1-M2 and M3-L2-M4. The optical output of one laser is reflected through a spacial angle of 90^{o} by a totally reflecting mirror, M5. It is then combined with the optical output of the second laser by the beam splitter, B. A photodetector, D, senses half of the combined optical output of the two lasers. If one mirror (say, M1) is displaced while the remaining mirrors (M2, M3, and M4) are held fixed, the difference frequency observed at the output of the photodetector will be proportional to the displacement of the displaced mirror.

A similar configuration (Ref. 12) in which the lasers were supported on a massive shock-mounted table in the wine-cellar of an isolated building indicated a short-term (tens of milliseconds) stability of equivalent to 2.4×10^{-12} inch and a long-term (2 minutes) stability equivalent to 0.3×10^{-9} inch. Such a system (Ref. 13) has been used to measure

strains in the earth's crust. In this latter system a noise level corresponding to strains of 4×10^{-10} was observed over a one-meter gage length. This is equivalent to a minimum detectable displacement of 1.6×10^{-8} inch.

2.5 TECHNIQUE SELECTION

It appears that by careful engineering design any of the techniques discussed in Subsection 2.4 could exceed, or substantially equal, the goals of 10^{-6} to 10^{-9} inch sensitivity and 0-1000 Hz frequency response. On the bases of the research phase conclusions the ultimate potential of each technique is ranked in Table II. In this table resolution is synonymous with sensitivity, or minimum detectable displacement, and is based on presently projectable signal-to-noise ratios. Frequency response is similarly based on ultimate capabilities. The performance criteria rankings made at the end of the research phase, and summarized in Table II, were made on the assumption of relatively simple, idealized configurations. Practically achievable configurations might result in a different order of ranking. For example, if the laser technique required closed-loop control similar to that of the interferometer, then its frequency response would be comparable to that of the interferometer.

TABLE II

RELATIVE RANKING OF FOUR DISPLACEMENT MEASUREMENT TECHNIQUES

Technique	Resolution	Frequency Response	Reaction Force
Laser	1	1	1
Interferometric	1	4	1
Capacitive	2	2	2
Inductive	3	3	3

Economy and practicability are influenced by a variety of factors. Broadly, the more economical techniques are those that allow the sensor to be in proximity to the member the displacement of which it is desired to measure. Practicability depends on set-up time, mechanical loading or reaction on the displacing member, and development costs.

If the sensor must be located remotely and/or if the reaction force must be as small as possible, then one of the optical techniques is indicated. The interferometer presents, perhaps, the most straightforward engineering design task. The laser displacement sensor requires a bolder design effort, but one that promises to yield an instrument that is simpler and less expensive. For these reasons the laser technique was selected for the feasibility-design study phase.

SECTION 3

GAS LASER OPERATION

As outlined in Subsection 1.3, the laser is an optical oscillator that consists of an optically resonant cavity containing an optical medium with gain. The frequency of oscillation is determined largely by the dimensions of the resonator; for example, by the distance between the two mirrors. If the resonator is strained (e.g., if the mirror spacing is varied), the oscillation frequency changes. A displacement sensor that relies on such frequency changes will have a resolution that depends on the coherence and stability of the laser output.

One of the most important factors that determines coherence and stability is the choice of the laser itself. Lasers may be broadly grouped into three classes: crystalline and glass solid lasers, gas lasers, and semiconductor lasers. For the most widely studied semiconductor laser, gallium arsenide, the lowest reported linewidth (Ref. 14, Ref. 15) is 150 kHz at $77^{\circ}K$ for 250 mW. One of the few crystalline solid lasers that can be operated in a single mode (Ref. 16), dysprosium doped calcium fluoride, has exhibited linewidths reported (Ref. 17) to be less than a few kHz when cooled to liquid nitrogen temperatures. Glass lasers generally have greater linewidths than crystalline lasers (Ref. 18). The first helium-neon laser is reported (Ref. 19) to have a short-term stability of better than 2 Hz. In addition to being able to provide a highly coherent output, the operation of gas lasers is well understood, at least from an engineering-design point of view. These two factors make the gas

laser in general, and the helium-neon laser in particular, the logical choice for the feasibility-design study. This section will present a qualitative review of the operation of helium-neon lasers and a quantitative review of factors that affect their use as displacement sensors.

3.1 OPTICAL AMPLIFICATION

The laser is an oscillator that produces coherent electro-magnetic radiation. The resonator that determines the frequency of oscillation has losses, and some radiation is deliberately allowed to escape at the output. In order for oscillation to persist, these losses must be overcome by amplification at the frequency of the oscillation, i.e., optical amplification. This section provides a general outline of how such amplification can occur, and points out those features that are important in the design of a laser displacement sensor.

3.1.1 ABSORPTION AND EMISSION

If a region containing an active optical medium exhibits amplification, a beam of light with an intensity, I, entering this region may emerge with an increased intensity, $I + \Delta I$. The increment of power, ΔI, is supplied by the active medium itself. This is not the usual experience. In fact, in the case of most media, the emergent beam is of reduced intensity, $I - \Delta I$. Such a reduction in intensity may be the result of a number of mechanisms. One of these mechanisms, absorption, is closely related to amplification.

When a photon is absorbed by an atom, that atom is raised from one energy level to a higher level. In the case of an unexcited gas the lower level is usually the lowest energy, or ground, state. In any case the difference between the two levels is equal to the energy of

the absorbed photon. The ways in which the excited atom can decay to the original, lower, energy level include collision with other atoms as well as reemission of a photon.

The excited atom may return to ground state as a result of a collision with a second atom that is initially in the ground state. In general the second atom will be excited to some higher energy by the collision. The energy available as a result of the decay of the first atom may be different from that required to excite the second atom. Such a difference will result in a change in kinetic energy of the two particles. This type of collision is more probable when the required change in kinetic energy is small. They are called collisions of the second kind.

The excited atom may also return to the ground state by the emission of a photon of the same energy as the originally absorbed photon. The emission may occur either spontaneously or as the result of stimulation. The time that a particular atom remains excited before spontaneous emission and decay cannot be predicted because the process is random. The average time, called the lifetime of the transition, can be predicted and measured. For allowed transitions in the visible range, lifetimes are typically on the order of 10 nanoseconds.

An excited atom can also be stimulated to decay and emit before the time it would ordinarily do so spontaneously. This can happen as a result of interaction with radiation, the photons of which are of the same energy as the one that originally excited the atom. Since the emitted quantum is added to the radiation, the occurrence is called stimulated emission of radiation. Stimulated emission of radiation and absorption of radiation are two faces of the same coin. For a given radiation density there is some probability that, in unit time, a particular atom in its lowest energy level will be excited to a

higher level, removing a quantum of radiation in the process. For the same radiation density there is also a probability that, in unit time, another atom, already excited to the higher level, will decay to its lowest energy level, adding a quantum of radiation in the process. Neglecting degenerate levels, these two probabilities are equal (Ref. 20, and, for a more available treatment, Ref. 21). The rate of absorption is equal to this probability times the density of atoms at the lowest energy level. The rate of stimulated emission is equal to this probability times the density of atoms at the higher level.

For media in thermal equilibrium at room temperature, almost all the atoms will be in the lower level, and virtually none at the higher level. Under these conditions, the rate of absorption exceeds the rate of stimulated emission and there is a net absorption. In order to obtain amplification, stimulated emission must predominate. This can occur if there are more atoms at the higher level than there are at the lower level. Such a condition is sometimes called a population inversion.

3.1.2 POPULATION INVERSION

Historically, Einstein (Ref. 20) was the first to predict the existence of stimulated emission. Tolman (Ref. 22) explicitly stated that such emission would reinforce the primary beam that caused the stimulation. In this way, it is quite different from spontaneous emission which is radiated in all directions and provides very little reinforcement of the primary beam. Subsequently, various proposals were made for schemes that would result in a population inversion, and so cause the reinforcement to give way to actual amplification. One of these schemes was Javan's suggestion (Ref. 23) of discharge excitation of a helium-neon mixture. It was this method that he and co-workers (Ref. 24) subsequently used when they demonstrated the first continuous

laser oscillation. This first gas laser operated in the infrared, but a helium-neon laser operating in the visible region quickly followed (Ref. 25).

The wavelengths at which gain, or amplification, can be obtained from the gas discharge tube of a helium-neon laser is determined by the energy levels of neon. However, the amount of gain obtained is strongly influenced by the presence of helium. In fact, laser operation at the visible, 632.8 nanometer, wavelength is not possible with neon alone (Ref. 26). The role of helium is illustrated by the simplified energy-level diagram shown in Fig. 13. In this diagram the levels of singly ionized helium and neon (identified He^+ and Ne^+) are shown for reference. In addition to these, only the desired levels that contribute to 632.8 nm laser operation are shown. There exists a large number of levels intermediate to, and greater than, the levels shown (Ref. 27). Transitions can occur in both directions between all of these levels. In addition to decreasing the efficiency of the process, this complexity has prevented construction of a quantitative theory of helium-neon laser operation.

For convenience, the levels in Fig. 13 have been identified by the numbers 1, 2, and 3. These numbers are placed at the heads and tails of the arrows that denote transitions. The electronic configuration of each level is enclosed in parentheses. Thus, in the ground state, helium has two 1s electrons. Electron collision may excite an individual atom so as to raise one of these two electrons to a 2s level. A sufficiently energetic collision may remove one electron completely, leaving singly ionized helium, He^+, with only a 1s electron. For the ground state of neon, the complete electronic configuration is given. For the excited levels of neon, only the configuration of the outer six electrons is indicated, since the configuration of the inner four remains unaltered.

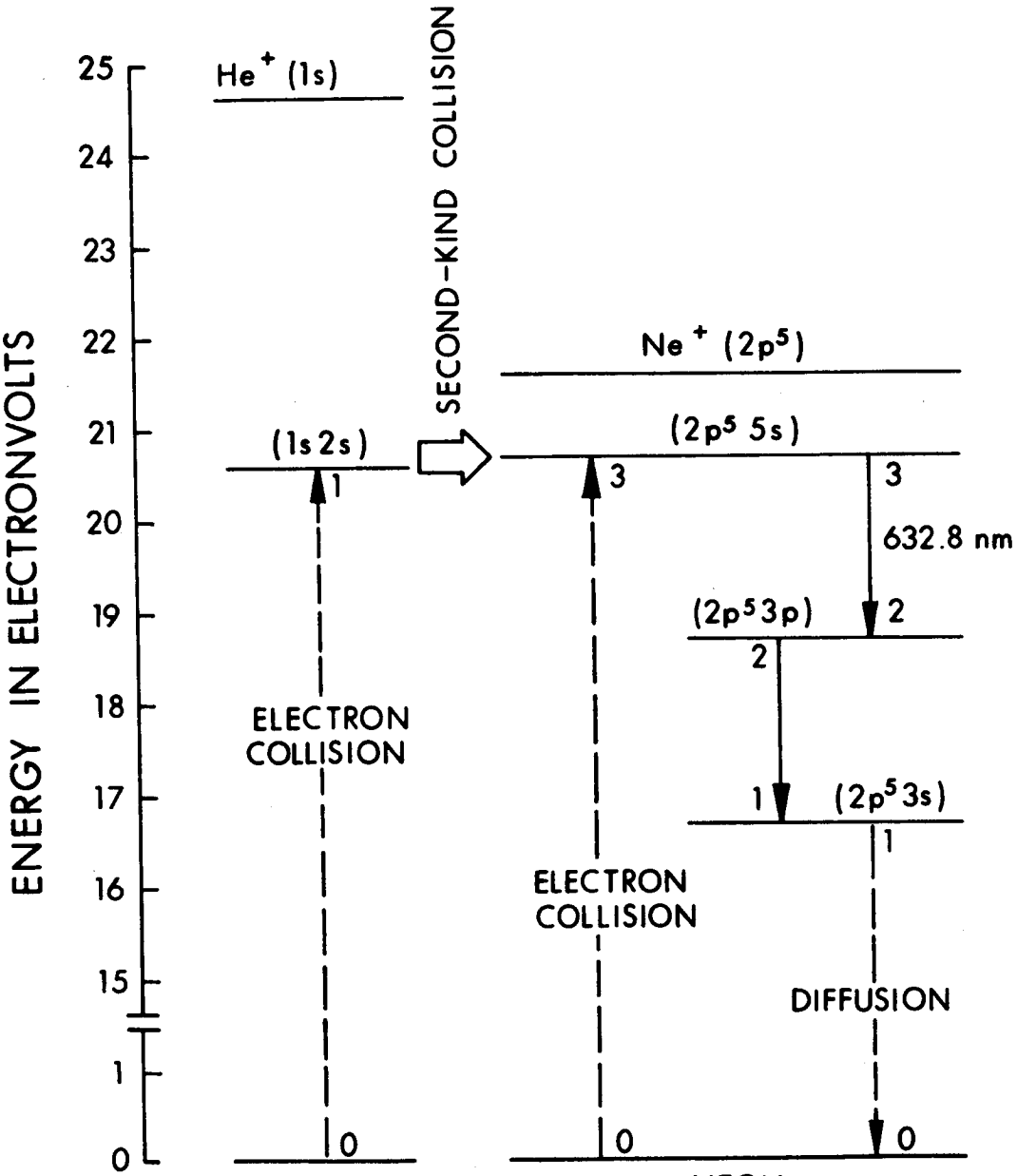

Figure 13. Energy-Level Diagram of Desired Levels and Transitions Involved in 632.8 nm Laser Operation

Tracing, through the processes illustrated in Fig. 13, conveniently starts when a helium atom is excited by an electron according to the reaction

$$e + He(0) \rightarrow He(1) + e \qquad (14)$$

Helium can have the 1s 2s electronic configuration with two different values of spin angular momentum. In one case, the energy is He(1) as shown in Fig. 13; the other case (not shown) has an energy level of 19.8 eV. In both cases the orbital angular momentum has the same value as that of the ground state; i.e., zero. Quantum mechanical selection rules allow radiative decay between states only when the quantum number for orbital angular momentum changes by ±1. Since this is impossible for helium atoms at the He(1) level, they cannot return to the ground state by emission of radiation, and are said to be metastable.

Helium atoms excited to the He(1) energy-level can return to the ground state by means of second-kind collisions, described earlier. For second-kind collisions with unexcited neon, the reaction is

$$He(1) + Ne(0) \rightarrow He(0) + Ne(3) + \Delta E \qquad (15)$$

where ΔE is the energy difference between the initial and final states. Neon can have the electronic configuration shown for level 3 in Fig. 13 at any of ten closely spaced energy levels. The level that is top of the 632.8 nm laser transition is only about 0.05 eV higher than the He(1) level. Thus ΔE is the same order as KT/e (about 0.03 eV at room temperature) and the reaction of Eq. 15 has a good chance of proceeding.

Neon atoms can also be excited to level 3 by collision with electrons in accordance with the reaction

$$e + Ne(0) \rightarrow Ne(3) + e \qquad (16)$$

Neon atoms excited to level 3 by either process (reactions of Eq. 14 and Eq. 15, or the reaction of Eq. 16) are said to have been pumped to that level.

The downward transition from level 3 to level 2 can be made by emitting 632.8 nm radiation either spontaneously or as a result of stimulation. Neon at level 2 decays to level 1 by the spontaneous emission of radiation. The radiative decay time from level 2 is on the order of 20 nanoseconds (Ref. 28). Thus, this level is rapidly emptied. If the rate of pumping to level 3 is sufficiently great, this rapid emptying of level 2 will result in a population inversion. Under these conditions, if the helium-neon mixture is illuminated with a beam of coherent 632.8 nm radiation, the rate of stimulated emission may exceed the rate of absorption with the result that the emerging beam is amplified rather than attenuated.

The tracing of the processes illustrated in Fig. 13 can be concluded by noting that the neon atoms emptied into level 1 decay to level 0 by what has been described as diffusion. Neon can have the electronic configuration shown for level 1 at any of four closely spaced energy levels. Not all of these levels have allowed transitions to the ground state. However, thermalization among these levels is probably rapid enough to distribute the population over all four (Ref. 29). Under actual operating conditions in a helium-neon laser, radiation emitted by a transition from level 1 to the ground state will be substantially absorbed by other neon atoms. The atoms that absorb the radiation will be excited from the ground state to level 1. This entrapment of radiation tends to keep level 1 full, thus greatly increasing its radiative

decay time. In the free state this level would have a decay time of on the order of 1 nanosecond. Entrapment increases it to the order of 1000 nanoseconds (Ref. 30).

Such a long lifetime tends to allow level 1 to fill, which in turn reduces the rate at which level 2 is emptied. The net effect is to reduce the extent of population inversion, and hence reduce gain. Fortunately, transitions from level 1 to the ground state can also be induced by collisions with the walls of the discharge tube. For a cylinderical tube, the ratio of curved surface area to enclosed volume is inversely proportional to the radius. On this basis it might be expected that the gain varies inversely as the radius. This has been observed for the 632.8 nm helium-neon laser (Ref. 31).

3.1.3 GAIN BANDWIDTH CHARACTERISTICS

The frequency of the 632.8 nm laser output is 4.74×10^{14} Hz. A laser displacement sensor that depends on sensing changes in output frequency must be capable of operating over a frequency interval. The medium providing optical amplification must have sufficient gain to sustain oscillation over at least this interval. Fortunately, the discharge tube of a helium-neon laser can provide useful gain over a band of frequencies.

Even a single atom, isolated in free space, and fixed with respect to the observer does not emit entirely at one frequency. This is a consequence of the fact that it does not emit continuously. In classical terms, each quantum of radiation that it emits can be thought of as a sine wave that begins to decay exponentially from the instant it is initiated. The frequency of the sine wave is determined by the energy levels of the transition involved. If the excited electron is imagined to be oscillating at this frequency, then damping arises as the outgoing radiation removes energy from the oscillation.

The exponentially decaying sinusoid has been described, above, in the time domain. It is nonperiodic. The Fourier spectrum of such a function is continuous in the frequency domain. It can be shown (Ref. 32) that this spectrum is sharply peaked at the frequency of the sinusoid. The frequencies, on either side of the peak, at which the power of the spectrum is reduced to half that of the peak, are separated by $1/2\pi\tau$ Hz, where τ is the time required for the power of the sinusoid itself to decrease by the fraction 1/e. For example, the intensity (power) of the radiation may be reduced by the factor 1/e in 10 nanoseconds. This is typical for transitions at the red end of the visible range. In this case, the total width of the spectrum between half-power points is about 16 MHz. This is the natural linewidth.

In this example, that of natural linewidth, it was assumed that the radiating atom was isolated and at rest with respect to the observer. Real atoms are neither isolated nor at rest, and, as consequence, have broader than natural linewidths. In solids and gases at high pressures, broadening occurs principally as a result of collisions between atoms. In gases, at pressures as low as those commonly used in lasers, broadening results principally from Doppler shifts caused by thermal motion of the atoms.

For a large group of particles subject to thermal agitation, the velocity components in one direction, say that of the observer, are such that, on the average, half are positive and half are negative. The component of energy in that direction has the Boltzmann distribution. The density of particles per unit increment of velocity component is highest for the velocity increment at zero. For higher or lower velocity components, the particle density is less. The frequency of radiation emitted by particles with low velocity component in the observer's direction will not be shifted appreciably. Radiation emitted from particles moving rapidly toward or away from the observer will appear to him to have higher or lower frequencies due

to the Doppler effect. This causes the frequency spectrum of the radiation emitted by the group of particles to be symmetrically broadened on either side of the natural line frequency.

Under the conditions that exist during actual laser operation, the 4.74×10^{14} Hz line of neon has a full width between the half-power points of 1.7×10^{9} Hz, or 1700 MHz (Ref. 33). If a laser displacement sensor is designed with sufficient gain to sustain oscillation at the half-power points, the output frequency can be allowed to vary over a total range of 1700 MHz, or ±850 MHz from the natural line center.

3.2 OPTICAL RESONATORS

As pointed out in the previous section, a laser gas discharge system can provide optical gain over a band of frequencies. In order to insure oscillation at some frequency within this band, an optical resonator is used. In the case of some simple electrical and mechanical resonators, the components used exhibit nearly ideal behavior, and dynamic behavior can be described adequately by a linear, second-order differential equation. Such resonators effectively have only one mode, or resonant frequency. Because of the short wavelength of electromagnetic radiation in the visible range, and because of the high losses of small optical components, analogous single-mode optical resonators are ruled out. Instead, multi-mode resonators must be used. They may be compared, roughly, to such distributed-parameter mechanical and electrical oscillators as beams, organ pipes, and transmission lines. Multi-mode optical resonators exhibit a similarly wide variety of forms and characteristics.

3.2.1 FABRY-PEROT RESONATOR

A Fabry-Perot resonator consisting of two, facing, plane-parallel mirrors is shown in Fig. 14. If a beam of light were somehow trapped between the two mirrors, it would travel back and forth, undergoing multiple reflections. If the cavity length, d, is close to some integral number of half-wavelengths of the light, then the waves produced by successive reflections would be substantially in phase. If the cavity length is close to some odd number of quarter-wavelength, then the waves due to successive reflections will be substantially out of phase. It is a reasonable guess that, if this structure has resonant modes, the modes will have to satisfy an equation of the form

$$f = \frac{(q + 1)c}{2d}$$
$$q = 0, 1, 2, \ldots \qquad (17)$$

where f is the resonant frequency in Hz, c is the velocity of light in meters/sec, d is the cavity length in meters, and (q + 1) is the number of half-wavelengths between the mirrors. The longitudinal mode number, q, measures the number of field zeros between the mirrors. This equation may also be written as

$$\frac{f}{f_o} = q + 1$$
$$f_o = \frac{c}{2d} \qquad (18)$$

where f_o is the frequency spacing between the resonances of two modes that differ by $\Delta q = 1$.

The questions of whether the structure shown in Fig. 14 has resonant modes, and if it does, whether they satisfy Eq. 18 are not simple.

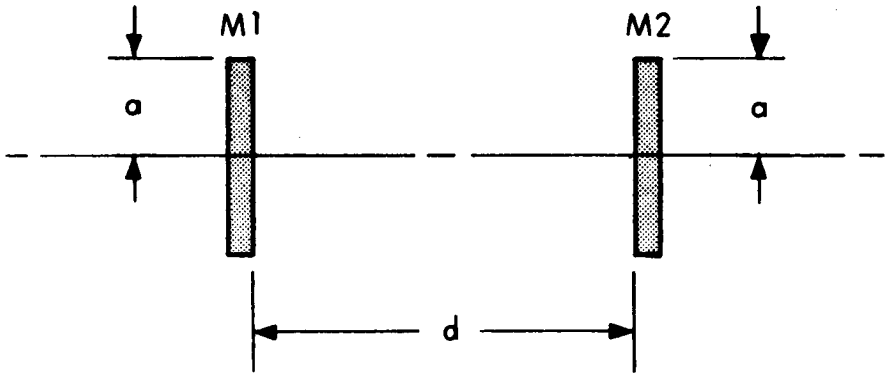

Figure 14. Fabry-Perot Resonator Using Two Facing, Plane-Parallel Mirrors

If such resonances exist, each will represent a three-dimensional distribution of electric and magnetic fields, the intensities of which vary sinusoidally at the mode frequency, and each will be a solution to Maxwell's equations. This is somewhat analogous to saying that standing waves of sound that are known to be able to exist at a variety of frequencies within a rectangular enclosure, must be solutions to the three-dimensional wave equations that describe the propagation of sound in air.

There is one great difference between standing electromagnetic waves in a Fabry-Perot resonator and standing sound waves in a room. The room is completely enclosed whereas the Fabry-Perot is an open structure with only two "walls." Radiation can leak out at the sides. One way this can happen can be illustrated by imagining that a single mirror is illuminated by an infinite, plane wave of coherent light as shown in Fig. 15. For clarity, the reflected light is shown on separate figures. Near the mirror, the reflected beam will be approximately the same size as the mirror as shown in Fig. 16. However, even in this region, the edges will be fuzzy and will trail out beyond the main beam. This is due to diffraction. Since light is an electromagnetic wave, it cannot have a particular intensity in a region and then discontinuously drop to zero at the boundary of that region.

At a great distance from the mirror, most of the light will appear to be contained within a cone as shown in Fig. 17. Since, in this example, the mirror was illuminated with a plane wave, the far field distribution can be obtained from Fraunhofer diffraction theory. If the mirror is circular, with radius a, the bright central portion of the cone will be surrounded by a dark shell (region of minimum intensity) at an angle of $0.61\ \lambda/a$ radians from the axis of the cone. About 85 percent of the energy will be contained within this cone (Ref. 34).

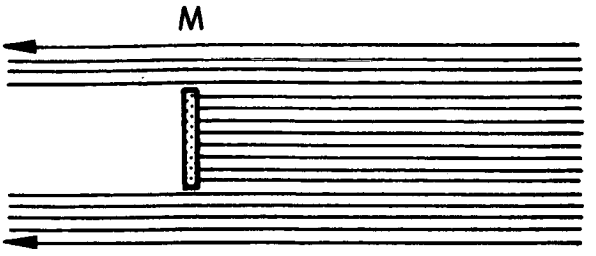

Figure 15. Mirror Illuminated by Plane Wave of Coherent Light Propagating from Right to Left

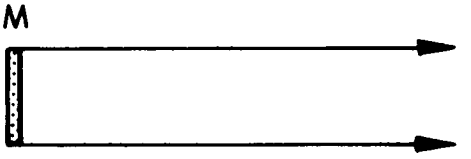

Figure 16. Reflected Beam Shape Near the Mirror

Figure 17. Reflected Beam Shape Far from the Mirror

If the near-field cylinder of Fig. 16 and the far-field cone of Fig. 17 are combined on one drawing with a greatly compressed horizontal scale, a beam contour of the sort shown in Fig. 18 will result. The cross sectional area of the cylindrical part is πa^2. The area of the cone at a distance d is $\pi(\theta d)^2$ since θ is a small angle. Adding these two areas together permits the value of an effective beam radius, a_e, to be calculated.

$$a_e = \left[1 + \left(\frac{0.61\ \lambda d}{a^2}\right)^2\right]^{\frac{1}{2}}$$
$$= \left(1 + \frac{0.37}{N^2}\right)^{\frac{1}{2}} \qquad (19)$$

where

$$N = \frac{a^2}{\lambda d} \qquad (20)$$

N is the Fresnel number and is an important measure of the diffraction loss of the system.

If a second mirror of radius a is placed in the beam as shown in Fig. 19, it is clear that part of the beam will spill over the edges. If the field intensity is uniform across the section of the beam at M2, the fraction of the energy lost at this reflection, α, is simply

$$\alpha = \frac{0.37}{N^2} \qquad (21)$$

But the field intensity is not uniform over the section, and, moreover, it changes at each succeeding reflection. Fox and Li (Ref. 35) programmed a digital computer to calculate the field distribution across the mirrors of a Fabry-Perot resonator after each successive reflection

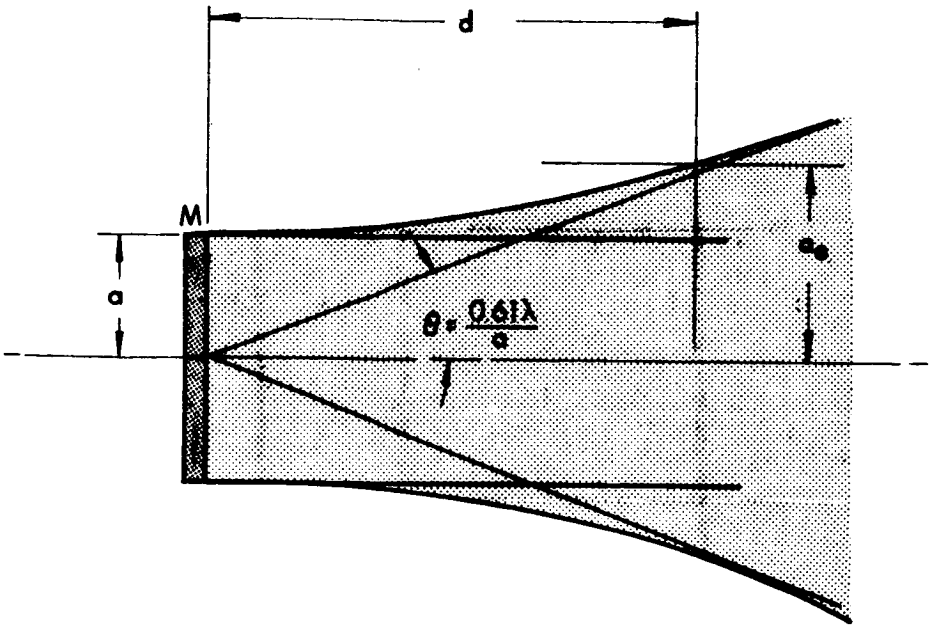

Figure 18. Beam Contour with Greatly Compressed Horizontal Scale

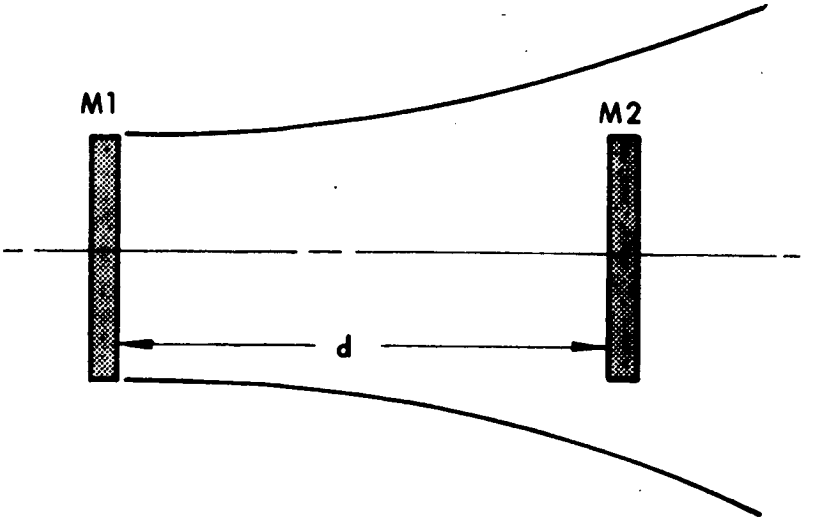

Figure 19. Beam Contour with Second Mirror Inserted at Distance d

following an initially given field distribution. It was found that after a number of transits (on the order of 300) each field became essentially identical to the one immediately preceding it, except for multiplication by a complex constant. The value of this complex constant determines the power loss and phase shift per transit. Their results for the fractional power loss per transit can be approximately represented by the expression

$$\alpha = \frac{0.2}{N^{1.4}} \qquad (22)$$

$$0.5 \leq N \leq 20$$

Although there has still not been an analytical derivation of the values of the resonant frequencies of the Fabry-Perot resonator with plane circular mirrors, the various numerical (e.g., Ref. 35) and experimental (e.g., Ref. 25) results are convincing evidence of the existence. More recently, there have been mathematical proofs of the existence of eigenvalues for resonators with plane-parallel mirrors (Ref. 36).

Practical difficulties involved in the use of plane-parallel resonators are the result of high diffraction losses and difficulty of adjustment. If the Fresnel number is less than 9, the loss given by Eq. 22 is greater than 1.0 percent. For a 1.0 meter long 632.8 nm laser, a Fresnel number of 9 implies a mirror (and hence discharge tube) diameter of about 5 mm. Because of the inverse dependence of gain on tube diameter mentioned in Subsection 3.1.2, 5 mm is about the order of, or even greater than, the desired diamenter. In the case of the first helium-neon laser, it was found that the loss increased about 1 percent per second of angular misalignment of the mirrors (Ref. 37).

3.2.2 TRANSVERSE MODES

In the previous section, the standing waves of sound that can exist in a closed rectangular room were mentioned. It can be shown (Ref. 38) that the resonant frequencies of a room with perfectly reflecting walls are given by

$$f = \frac{c}{2}\left[\left(\frac{q}{\ell_x}\right)^2 + \left(\frac{r}{\ell_y}\right)^2 + \left(\frac{s}{\ell_z}\right)^2\right]^{\frac{1}{2}} \tag{23}$$

where

f = frequency in Hz
c = velocity of sound in meter/sec
ℓ_x = length of room in meters
ℓ_y = width of room in meters
ℓ_z = height of room in meters

and q, r, and s are discrete variables that can assume the values 1, 2, 3, ..., to infinity.

The box can be made to look somewhat like the resonator discussed in the previous section by setting $\ell_x = d$ and $\ell_y = \ell_z = 2a$. If this is done, and some rearrangements made, the result is

$$\left(\frac{f}{f_o}\right)^2 = q^2 + (r^2 + s^2)\left(\frac{d}{2a}\right)^2 \tag{24}$$

where f_o is as previously defined by Eq. 18. If q^2 is much larger than the term to the right, then it is approximately true that

$$\frac{f}{f_o} = q + \frac{r^2 + s^2}{16N} \tag{25}$$

where N is the Fresnel number as defined by Eq. 20. Equation 25 bears

some resemblance to Eq. 18 except for the presence of r and s. These terms describe the pressure distribution across the width and height of the room. If both are zero, the sound intensity is constant across any particular section.

If the floor, ceiling, and two long walls are removed, there remain two square walls separated by a distance, d. If Eq. 25 can predict anything about the modes of the new structure, it can only do so if r and s are both one or more. If either is zero, there will be large diffraction losses because of the high intensity where the walls had been. The condition described by r = s = 1 is possible because it can be satisfied by an intensity distribution that is maximum along the center line and trails off to zero on either side. A schematic of this possible intensity distribution is shown at a Y-Z section of the resonant structure in Fig. 20. The X axis (the long, or d, direction) is perpendicular to the paper.

In order to show the meaning of cases where either r, or s, or both, are greater than 1, a particular case is shown in Fig. 21. Here there is a node along the center of the Y direction. This is indicated by the dashed line. The maxima on either side of the line have opposite phases. There are many other combinations. Any particular combination could be designated by a trio of numbers of the form qrs. Thus, Fig. 20 is the q11 mode, and Fig. 21 is the q21. Only the cases of the form qrs, qsr, will have the same resonant frequency. The others will generally be different.

Such modes exist in optical resonators. For example, in the computer study by Fox and Li (Ref. 35) that was described in the last section, such modes were simulated. Instead of starting with a uniform field distribution, it was assumed that one-half had a uniform field of one phase, and the other side had the opposite phase. This led to a

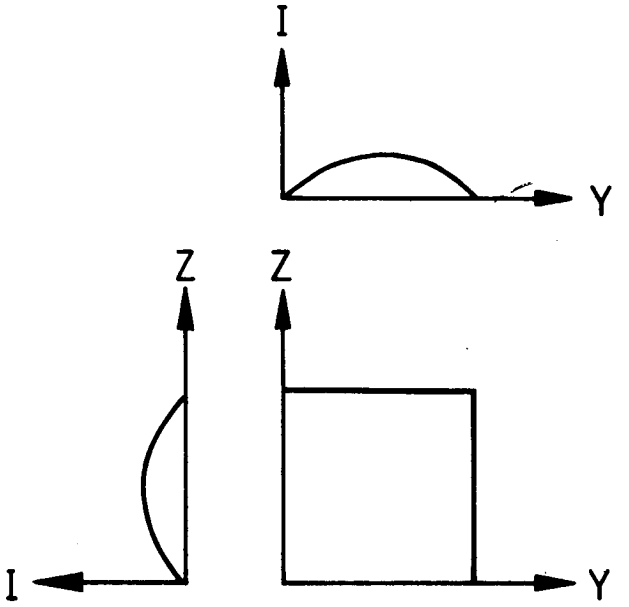

Figure 20. Intensity Distribution Across a Y-Z Section for the Case r = s = 1

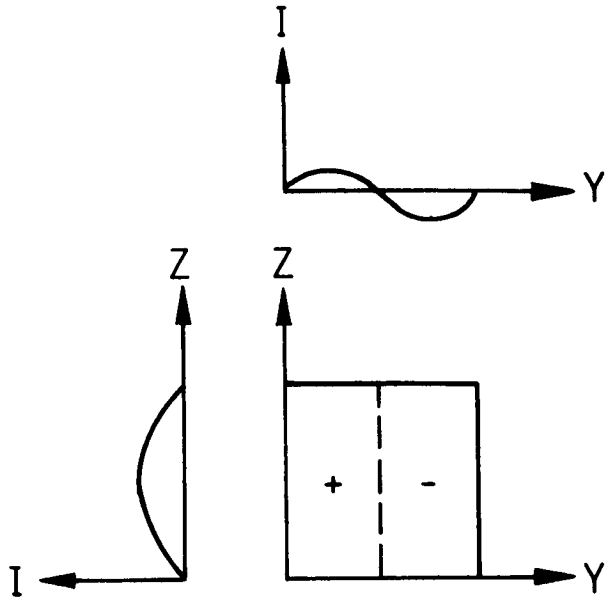

Figure 21. Intensity Distribution Across a Y-Z Section for the Case r = 2, s = 1

stable field distribution after a number of transits, but one with a higher power loss per transit, and a slightly different resonant frequency.

Optical resonator modes are specified in a different way than previously described. Since neither r nor s can be zero, it is convenient to define to new discrete variables as follows

$$\left.\begin{aligned} m &= r - 1 \\ n &= s - 1 \end{aligned}\right\} \text{ for square mirrors}$$

$$\left.\begin{aligned} p &= r - 1 \\ \ell &= s - 1 \end{aligned}\right\} \text{ for circular mirrors}$$

The mode will be completely specified by the numbers qmn for square mirrors, and qpℓ for circular mirrors. Since the optical modes are transverse electromagnetic modes, they are sometimes called TEM modes. The specific mode would be completely described by the symbol $TEM_{qp\ell}$. Because the cavities are long, q is large. When loses are low it has little effect on the shape of the field distribution. For this reason, it is usually dropped from the mode designation, which then becomes $TEM_{p\ell}$. Using this notation, Fig. 20 would correspond to a TEM_{00} mode, and Fig. 21 to a TEM_{10} mode.

The mode patterns of visible-light lasers may be seen and photographed (Ref. 39). As might be expected, the TEM_{00} has a single bright spot, the TEM_{10} has two, and higher modes similarly correspond to their expected field distributions. For most purposes, when single mode operation is desired, the TEM_{00} mode is selected.

3.2.3 SPHERICAL-MIRROR RESONATORS

An examination of Fig. 19 might suggest that if M1 was made slightly concave toward M2, the beam would be narrowed and diffraction losses reduced. In a very rough sense this is true. A variety of resonators with nonplane mirrors have been studied. The case of circular mirrors with equal diameters is illustrated in Fig. 22.

For the confocal system, $R_1 = R_2 = d$. Its modes may be calculated exactly (Ref. 40), and are given by

$$\frac{f}{f_o} = (q + 1) + \frac{1}{2}(m + n + 1) \qquad (26)$$

The practical advantages of the confocal resonator are low losses and easy alignment. The loss per transit, α, for the confocal cavity is shown in Fig. 23 for several modes. It will be recalled from Subsection 3.2.1 that for plane-parallel mirrors, the loss per transit reached 1 percent for Fresnel numbers below 9. The TEM_{00} mode of the confocal resonator has losses less than 1 percent for Fresnel numbers down to about 0.7, and the losses decrease quite rapidly for higher numbers. The higher losses of the other modes permits the resonator to be designed to suppress oscillation at their frequencies. The increase in loss as a result of angular misalignment of the mirrors is several orders of magnitude lower than the plane-parallel (Ref. 42).

If the mirrors do not have the correct radii, or spacing, losses may be substantially higher. A stability diagram, or Boyd-Kogelnik (Ref. 43) diagram, that serves to define the problem is shown in Fig. 24. The confocal system is located at point δ on this diagram. In order to avoid the high loss regions, it is customary to operate the resonator slightly shorter (point ϵ, say) or slightly longer (point γ, say) than optimum.

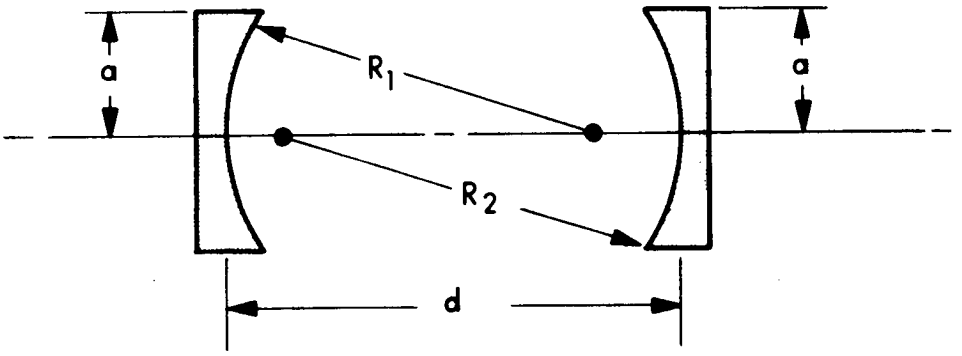

Figure 22. Resonator with Circular, Spherical Mirrors of Equal Diameters

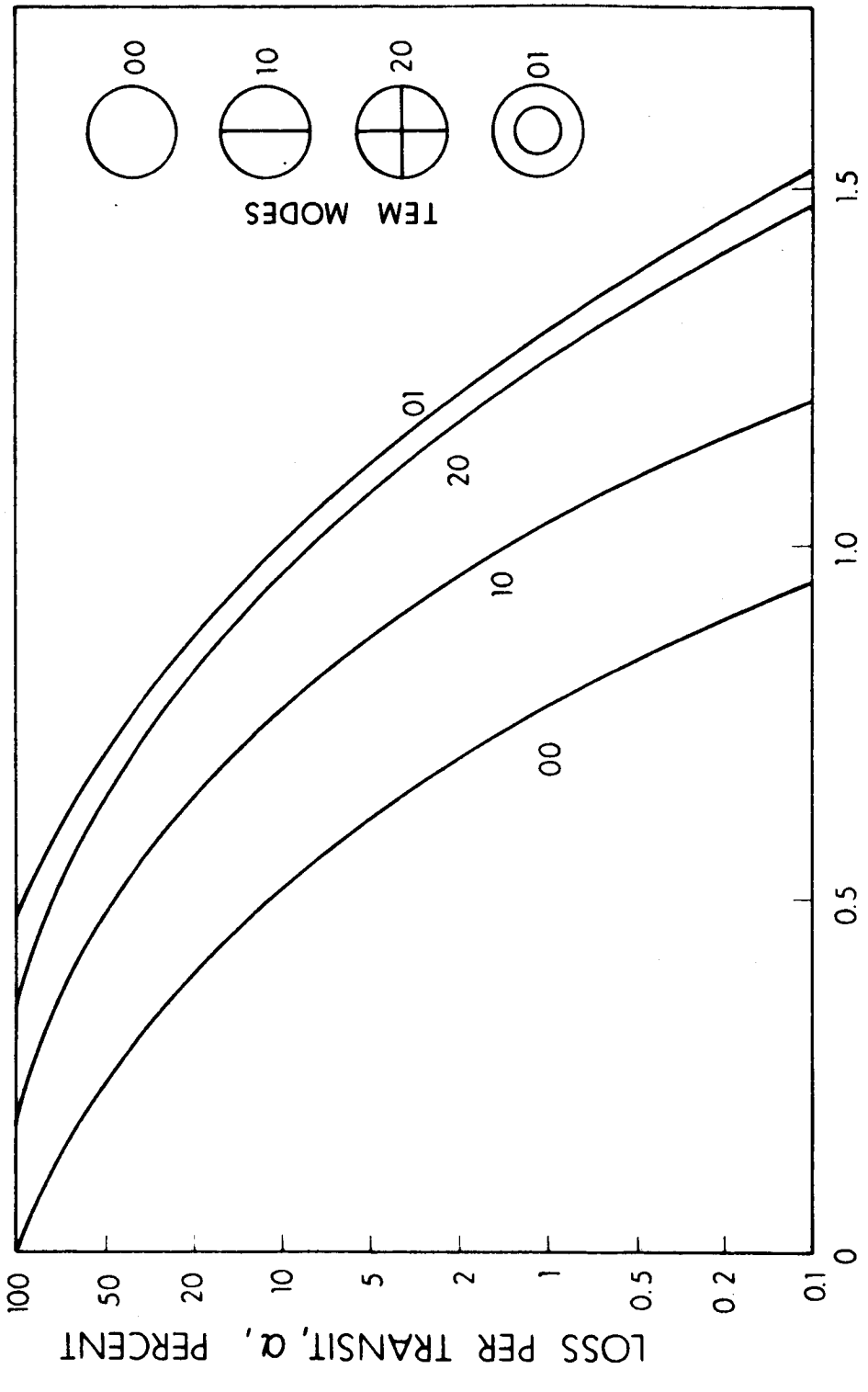

Figure 23. Confocal Resonator Loss as a Function of Fresnel Member (Ref. 41)

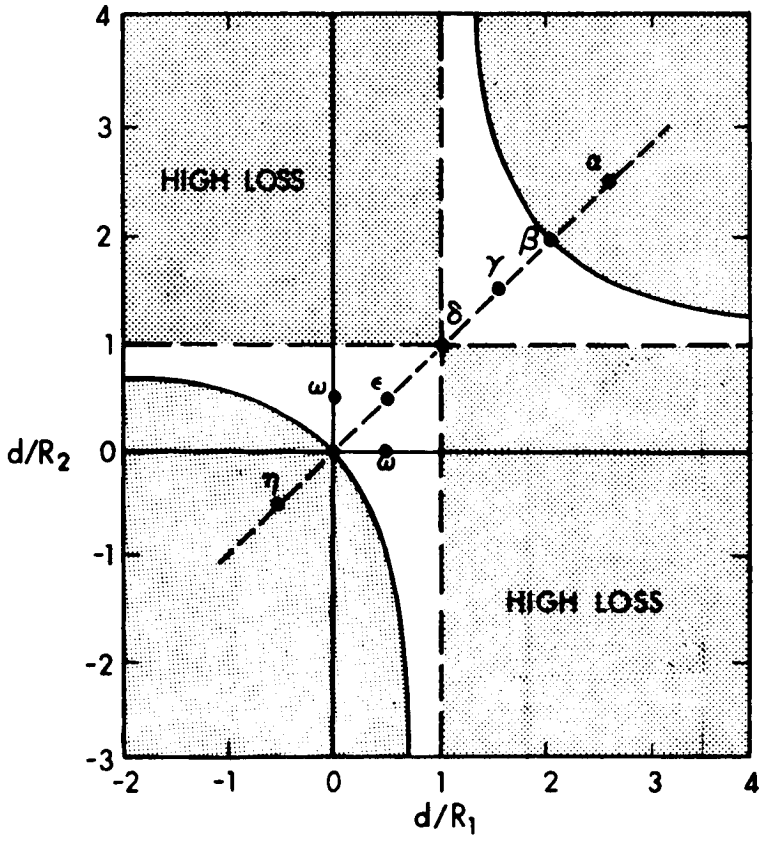

Figure 24. Stability Diagram, R_1 and R_2 are Mirror Radii, and d is the Cavity Length (Ref. 45)

A related resonator is the half-confocal. In this system one mirror is flat ($R_1 = \infty$) and one mirror is spherical ($R_2 = 2d$). This system is located a point ω on Fig. 24. In the case of a laser that must be capable of being set up to operate at different lengths (different d) provisions must be made to insure that operation will take place in a stable region of Fig. 24. This can be done by using mirrors of selectable radii, or by inserting selectable lenses into the cavity (Ref. 44) in such a way as to alter its optical configuration.

3.3 SINGLE MODE OPERATION

The basic spacing of axial (longitudinal) mode frequency of the resonator is

$$f_o = \frac{c}{2d}$$

For a 1.0 meter laser this is about 150 MHz. In an earlier section it was pointed out that gain may be available from a helium-neon discharge tube over a range of 1700 MHz. It is clear that some precautions must be taken to insure single mode operation. If the gain were sufficient to permit oscillation anywhere between the half-power frequencies of the Doppler-broadened neon line, as many as 11 frequencies might occur at 150 MHz intervals. One way of avoiding this is to reduce the excitation to the discharge, and hence lower the gain, until one mode is in a region that has sufficient gain to oscillate. This approach is not practical for the present use because it would require frequent readjustment of excitation level to maintain oscillation, and it would have a severely restricted range over which the frequency could be varied.

A second, and more generally used, approach is to use a quite short cavity. For example, an 0.1 meter laser would have axial modes spaced

every 1500 MHz. The likelihood of single mode operation is greatly improved in this case. This approach is not applicable to the design of a laser to measure displacements at a meter, or more, distance.

A third general approach is to make the optical properties of the cavity selective. If one mode has high Q (low losses) and all nearby modes have substantially lower Q, then single mode operation is comparatively easy. The end windows of the discharge tube can be coated so as to transmit only a desired band of radiation. The two mirrors that define the cavity can be coated so as to reflect only a desired band of radiation. A dispersive prism can be inserted in the cavity so as to cause radiation of undesired wavelengths to be deflected out of the cavity. Selective windows and mirrors, and dispersive prisms, can be used to discriminate against widely spaced modes. For example, in the case of a helium-neon laser intended to operate in the visible range, these means can be used to prevent simultaneous infra-red oscillation. They are not suitable for discriminating between the closely spaced (e.g., 150 MHz) modes of a laser cavity of conventional length.

One arrangement that can discriminate between closely spaced, neighboring modes (Ref. 46) is shown in Fig. 25. In Appendix I it is shown that L_1 and L_3 can be adjusted so that mirror pairs M1-M2 and M3-M4 will strongly reflect light from the discharge. Strong reflections occur at frequencies separated by

$$\Delta f = \frac{c}{2L}$$

$$\text{if } L_1 = L_2 = L$$

If L_1 and L_3 are sufficiently short, Δf may be comparable to, or greater than, the Doppler width. Under these conditions, even if L_2 is long enough to have many resonant frequencies within the Doppler width, only

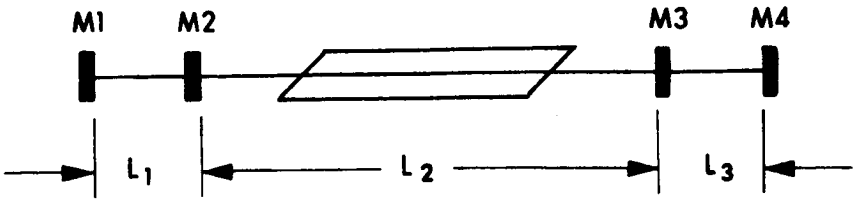

Figure 25. Composite Fabry-Perot Cavity for Discrimination Against Unwanted Modes

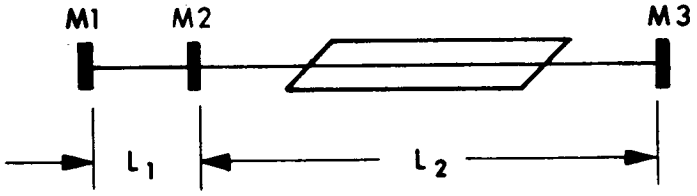

Figure 26. Three-Mirror Composite Fabry-Perot Cavity for Discrimination Against Unwanted Modes

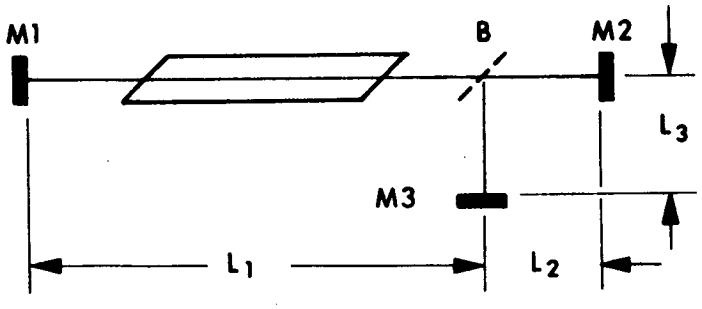

Figure 27. Laser with Three-Mirror (B, M2, M3) End Reflector

those that coincide with the reflective modes of L_1 and L_3 will have low losses. Successful single mode operation was obtained (Ref. 47) with the similar arrangement shown in Fig. 26. These schemes for mode selection have also received consideration from a design standpoint (Ref. 48).

Generally, discrimination against unwanted modes by means of Fabry-Perot end reflectors requires a very high degree of mechanical and thermal stability and appears to have been successful only at low power levels. A more recent optical resonator with improved mode selectivity (Ref. 49) is shown in Fig. 27. One might, intuitively, look upon this arrangement as two coupled optical resonators, one (M1, B, M2) of length, $L_1 + L_2$, and another (M3, B, M2) of length, $L_3 + L_2$. The passive cavity does, in fact, behave this way as demonstrated in Appendix II. If the lengths of these two cavities are properly selected, widely spaced low-loss modes will be separated by modes of substantially higher loss as previously described in the case of Fig. 25 and Fig. 26.

A similar, but independently developed (Ref. 50, Ref. 51) arrangement is shown in Fig. 28. In this case a laser discharge tube is located in each of two arms of the resonator. The passive cavity (both discharge tubes removed) has the same resonant frequencies as Fig. 27. In practice if the difference in length between L_1 and L_2 is on the order of the length that corresponds to the Doppler width (say 10 cm, as in the case of single mode operation obtained by means of a short cavity), this structure is reported to operate consistently in a single axial mode (Ref. 51).

3.4 FREQUENCY ERRORS

This design-feasibility study of a displacement transducer is based on the use of a laser technique in which the displacement to be measured

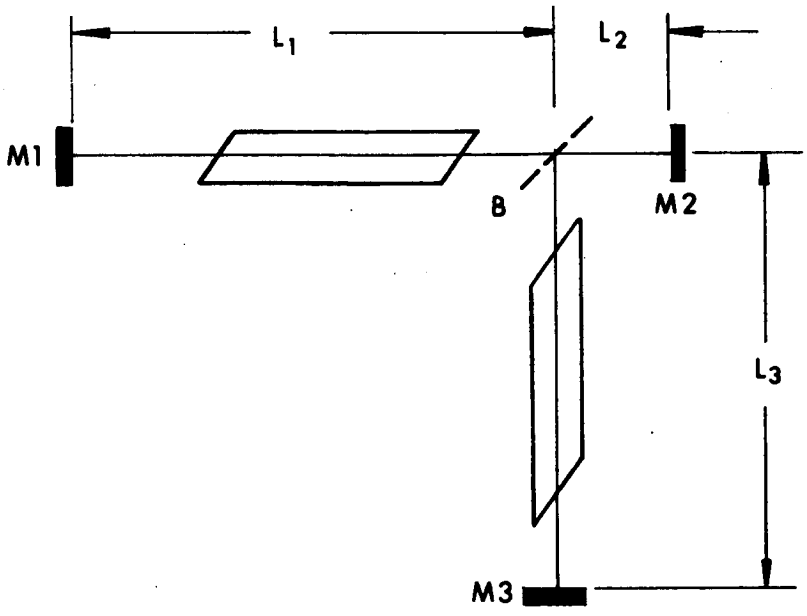

Figure 28. Michelson-Type Single Frequency Laser

causes a change in the operating frequency of the laser. Frequency stability in the presence of environmental disturbances is of the greatest importance. Further, if two lasers (e.g., Fig. 12) or two discharge tubes (e.g., Fig. 28) are used, any factors that affect the frequency of one should be arranged to affect the other to an equal extent. For gas lasers operated in the visible region, frequency depends principally on the cavity and secondarily on the discharge.

Changes in cavity length will produce frequency changes given by

$$\Delta f = -f_o \frac{\Delta d}{d} \tag{27}$$

For a 1.0 meter laser operating at 4.74×10^{14} Hz, this gives

$$\Delta f = -(4.74 \times 10^{14})\ \Delta d$$

Thus a change of 3.6×10^{-6} meter, or 1.4×10^{-4} inch, would use the entire 1700 MHz bandwidth of the discharge. Changes of this magnitude are easily produced by small temperature variations (Subsection 2.2). It seems likely that in practical laboratory use, the cavity length of a laser displacement sensor would require frequent readjustment in order to maintain oscillation. Continuous, closed-loop readjustment of the cavity appears to be an operating necessity.

Changes in atmospheric pressure affect the refractive index of air. The resulting frequency variation (Ref. 52) is given by

$$\Delta f = f_o(3.63 \times 10^{-7}) \frac{D\Delta p}{d} \tag{28}$$

where D/d is the fraction of the optical path exposed to the atmosphere, and Δp is the pressure change in torr. For a laser displacement sensor

with one remote mirror, D/d may be appreciable, say 0.5. Then Δf may be on the order of 100 MHz per torr. Without a closed-loop cavity control it appears that pressure fluctuations resulting from opening and closing doors (even interior doors) in an air-conditioned structure might be enough to stop oscillation.

Frequency shifts in the output of 632.8 nm helium-neon laser have been observed as a result of variation in discharge gas pressure (Ref. 53). Total shifts on the order of 40 MHz in the region between 2 and 4 torr occurred. Errors from this source can be minimized by providing a gas reservoir, and if two discharge tubes are used, an equalizing path between them.

SECTION 4

SYSTEM DESIGN

Following a statement of the target specifications and a brief description of overall system operation, each functional block is described on the basis of its input-output characteristics. These characteristics then form the basis of stability and error analyses.

4.1 TARGET DESIGN SPECIFICATIONS

The goal of this feasibility study is a displacement sensor that will be capable of meeting the following target design specifications:

a. Displacement Sensitivity: 10^{-6} to 10^{-9} inch.

b. Frequency Response: Flat, ±1 dB, from 0 to 1000 Hz, minimum. Attenuation slope beyond the flat portion shall be approximately 20 dB per octave.

c. Resolution: 1 percent or better.

d. Tracking Error: 1 percent or lower.

e. Overall System Accuracy: 5 percent or better.

f. Self-Resonance Frequency: Greater than twice the response band width.

The overall system is to be free of spurious or parasitic resonances and be insensitive to harmonics of externally induced vibration and electrical noise signals. The system should meet the requirements of the target specifications when making measurements in the following environment:

a. Pressure: 10^{-6} torr to one atmosphere.

b. Temperature: Ambients from 60°F.

c. Vibration: Seismic and artificial vibrations typically in the range 0 to 0.4g, 5 to 80 Hz.

d. Atmosphere: May contain ammonia, helium, hydrogen, or nitrogen.

Pressure, temperature, and atmosphere environments may be ignored for those portions of the measuring system that can be located outside of a vacuum chamber that contains the displacement of interest.

4.2 OVERALL SYSTEM OPERATION

As discussed in Section 2.2, a noncontacting, remote sensing, displacement transducer may be presented with common mode error signals (Fig. 8) due to thermal and other environmental effects. The displacement that it is desired to measure may have components as high as 1000 Hz and is of quite small magnitude, on the order of 10^{-6} to 10^{-9} inch (Section 4.1). The common mode error signals due to thermal effects will change relatively slowly, but their magnitude, on the order of 10^{-3} inch, may be large compared to the desired signal.

Upon first consideration it appears that a continuous, closed-loop readjustment of the laser cavity will require mirrors that will be able to displace 10^{-3} inch and follow the desired signal at rates of 1000 Hz. In order to obtain a closed-loop response of 0-1000 Hz, it is necessary to control the open-loop response over a much wider band, say, 0-10,000 Hz. A mirror displacement transducer capable of smooth response to 10 kHz, and displacements of 10^{-3} inch is not impossible. The production of the force levels required to deflect such a stiff structure by 10^{-3} inch do not, however, seem compatible with an optimum instrument.

If the requirement to follow the relatively slow 10^{-3} inch common mode error could be separated from that of following the relatively rapid 10^{-6} inch displacement signal, the probability of successfully meeting

all of the design goals would be greatly increased. An approach to the optical resonator design that will separate these requirements is shown in Fig. 29. With the exception of the additional, totally-reflecting mirror, M4, this arrangement is identical to the passive resonators of the lasers shown in Fig. 27 and Fig. 28, and further described in Appendix II. Since resonant frequencies are determined by $L_1 + L_2$, and $L_1 + \Delta L + L_2$, a common mode error that changes both M1 and M3 can be compensated by a movement of M2 alone. If the desired signal moves only M3, this can be compensated by a change in ΔL alone. The scheme for implementing this approach is shown in Fig. 30.

For the transducer of Fig. 30, the laser resonator is that of Fig. 29, with discharge tubes in two arms as shown in Fig. 28. A low-frequency length control (conventional electro-mechanical servo) moves M2 to compensate for common mode error signals. A high-frequency length control (piezoelectric transducer) moves M4 to compensate for movements of M3 that result from the displacement signal that it is desired to measure. The optical output of the laser oscillator passes through M2 to a frequency selective cavity of adjustable length. This cavity is tuned to the frequency of the laser oscillation. Its length is modulated at 52.5 kHz. This in turn causes the intensity of the light emerging from the cavity and falling on the photocell to be modulated at 52.5 kHz.

If the laser output frequency is below the center frequency of the cavity, the intensity modulation will be opposite in phase to that resulting when the laser output frequency is above that of the cavity. By applying this signal successively to a photodetector, an amplifier, and a phase sensitive detector, an error signal is obtained. The polarity of the error signal depends on whether the laser oscillation frequency is too high or too low. The error signal is amplified and

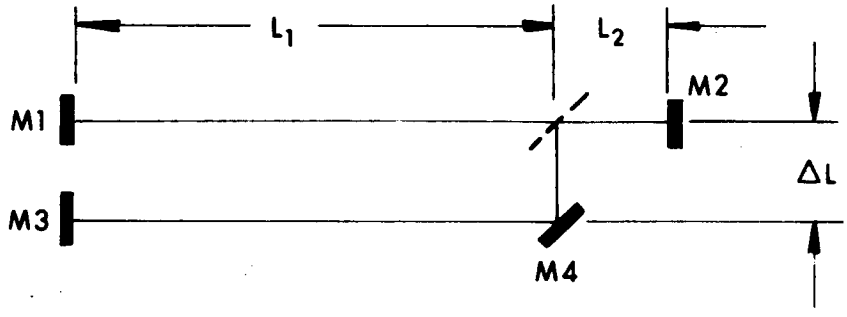

Figure 29. Passive Resonator with Two Parallel Arms

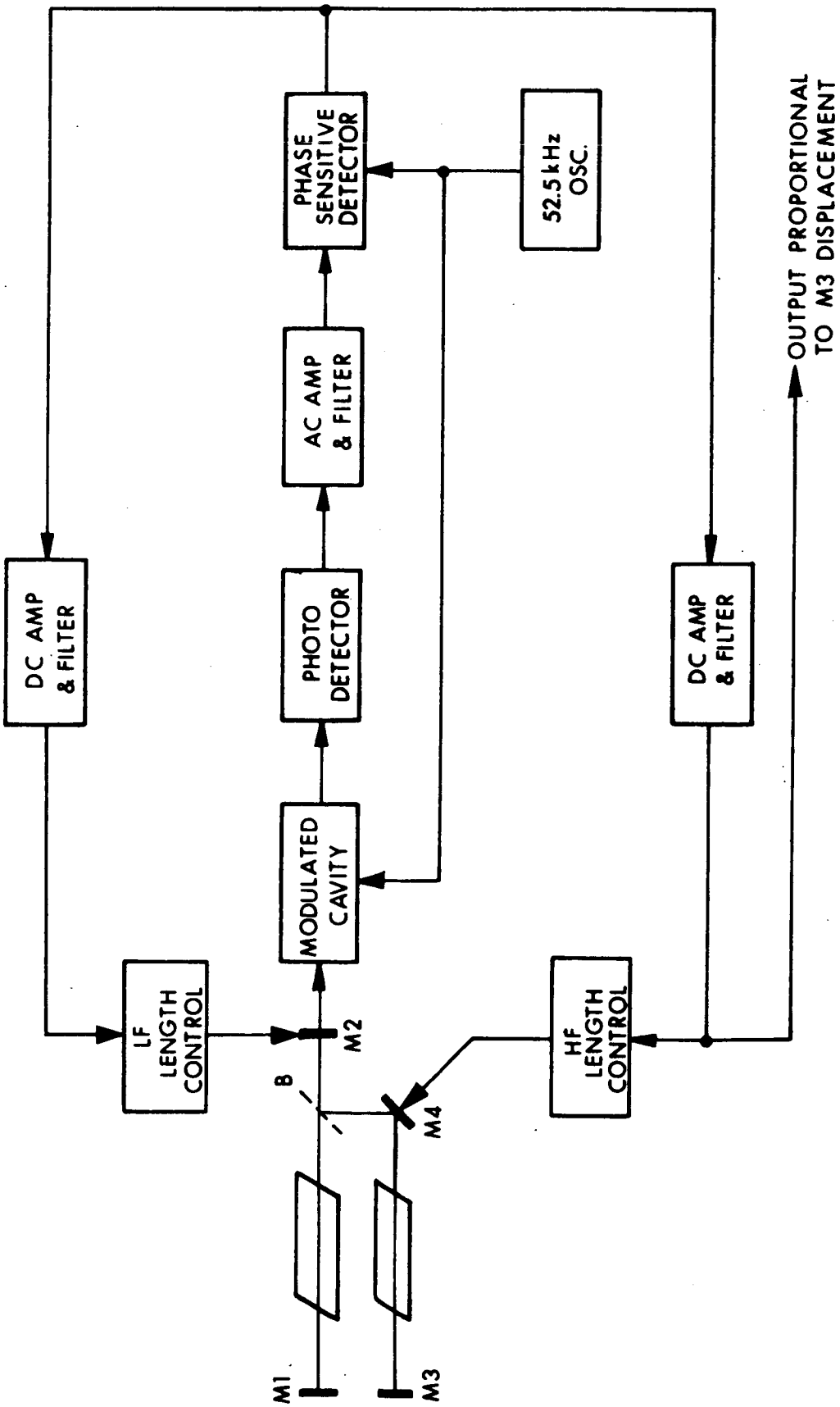

Figure 30. Simplified Block Diagram of Laser Displacement Transfer

applied to both the high-frequency and low-frequency length controls. If the dc amplifiers have sufficient gain, the error signal at their inputs will be small. If, now, M3 is moved this closed loop servo will reposition M4 to maintain the correct cavity length and frequency. The input to HF Length Control (again assuming sufficient open-loop gain) will be an accurate measure of the required movement, and hence the movement of M3.

4.3 FUNCTIONAL BLOCKS

This section defines each functional block in terms of its input-output characteristics. Figure 31 is a block diagram of the system. This diagram identifies many of the symbols used in subsequent sections. Locations on the diagram are by reference to row (B, C, D,...) and column (2,3,4,...) designations. For example, the photodetector (E-7) is located in Row E, Column 7. Its output current, ΔI, is related to the input power, ΔP, by the relation, $\Delta I = K_5 \Delta P$. Generally, sources of power and excitation have been omitted. The exception is the 52.5 kHz oscillator that drives the modulated cavity and the phase-sensitive demodulator. This was included to clarify operation.

4.3.1 OPTICAL RESONATOR

The three-mirror, Michelson-type resonator has been shown schematically in Fig. 28. In normal operation only the common-mode signal, X_2, affects the position of mirror M1, so that

$$\Delta L_1 = X_2$$

The sum (F-2) of the input signal, X_1, and the common-mode signal cause incremental displacements, X_3, of mirror M3. The net change in path length, ΔL_3, depends on the difference (F-3) between X_3 and the incremental changes in path length, X_4, produced by movements of mirror, M4.

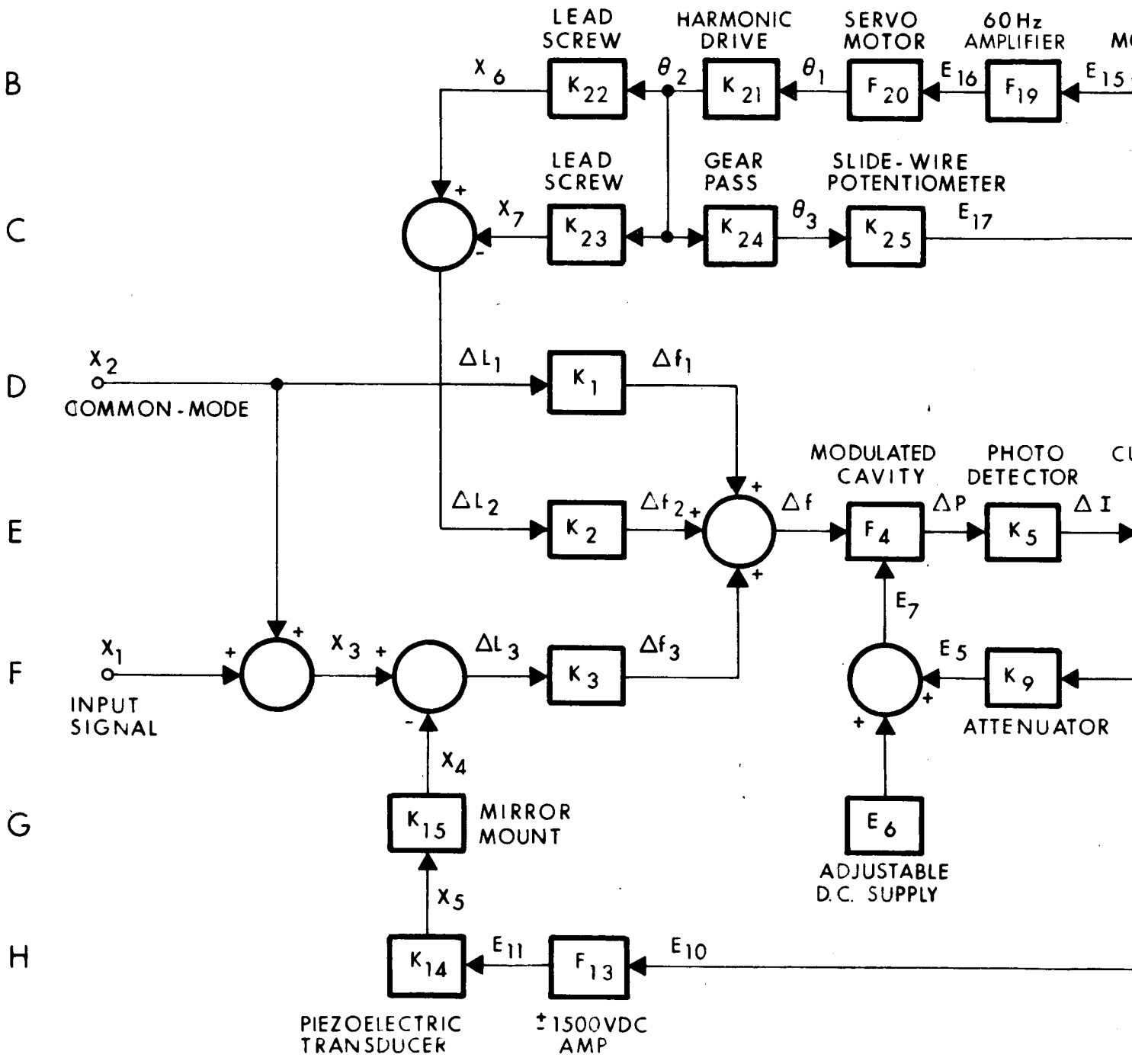
2
3
4
5
6
7
B
C
D
E
F
G
H
LEAD SCREW
HARMONIC DRIVE
SERVO MOTOR
60 Hz AMPLIFIER
X_6
θ_2
θ_1
E_{16}
E_{15}
K_{22}
K_{21}
F_{20}
F_{19}
LEAD SCREW
GEAR PASS
SLIDE-WIRE POTENTIOMETER
X_7
θ_3
E_{17}
K_{23}
K_{24}
K_{25}
X_2
COMMON-MODE
ΔL_1
Δf_1
K_1
MODULATED CAVITY
PHOTO DETECTOR
ΔL_2
Δf_2
Δf
ΔP
ΔI
K_2
F_4
K_5
E_7
X_1
INPUT SIGNAL
X_3
ΔL_3
Δf_3
K_3
E_5
K_9
ATTENUATOR
X_4
K_{15}
MIRROR MOUNT
E_6
ADJUSTABLE D.C. SUPPLY
X_5
K_{14}
E_{11}
F_{13}
E_{10}
PIEZOELECTRIC TRANSDUCER
±1500VDC AMP

FIG 3/- A
71- A

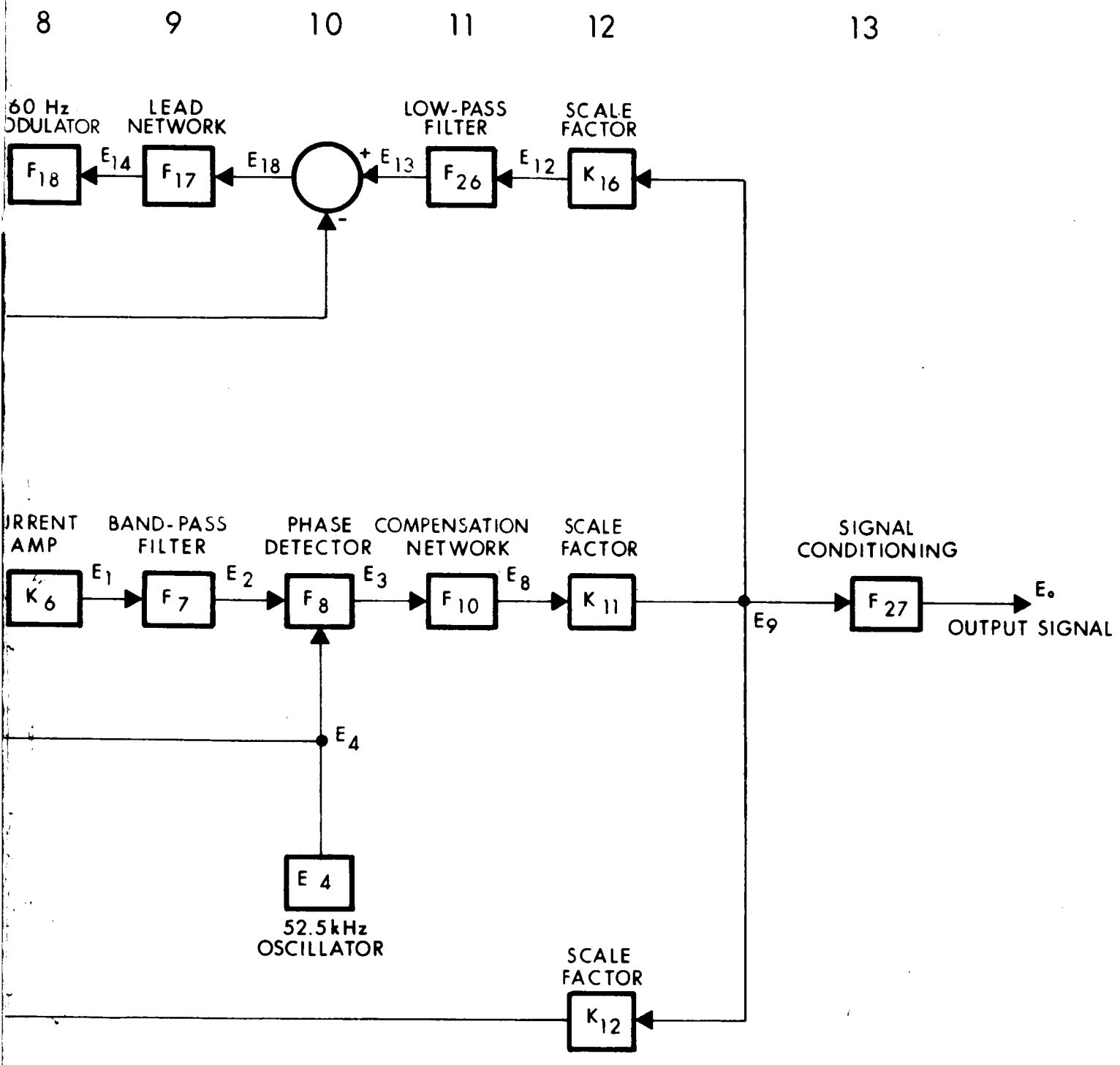

Figure 31.B System Block Diagram

Mirror M4 is moved by a piezoelectric transducer whose output displacement, X_5, is at an angle of 45^o with the two perpendicular segments of L_3. For this reason, $K_{15} = \sqrt{2}/2$. Because M4 is at an angle to the optical path, its movement causes a lateral shift in the path as well as a change in length. Such a lateral shift is equivalent to a slight tilting of the end mirrors. For a 1 meter path length, a 10^{-6} m lateral displacement is equivalent to a tilt of only a few tenths of a second. As pointed out in Section 3.2.3, such angular misalignments do not significantly affect the loss of a confocal resonator. The total change in the path length, L_3, is given by

$$\Delta L_3 = X_1 + X_2 - K_{15}X_5$$

Each incremental change of one of the path lengths, ΔL_i, produces a corresponding change in frequency Δf_i, which is related (D-4, E-4, F-4) by

$$\Delta f_i = K_i \Delta L_i \tag{29}$$

The individual increments of frequency are summed (E-5) to give

$$\Delta f = \Delta f_1 + \Delta f_2 + \Delta f_3 \tag{30}$$

This result is strictly correct only for the passive resonator, and the existence of gain (laser discharge tubes) in paths L_1 and L_3 will result in mode-pulling (Ref. 51) that will somewhat alter the magnitude of the frequency shift.

The values of K_i for Eq. 29 are given by Eq. III-8 of Appendix III. For the case where the paths' lengths are

$L_1 = 1.000$ m

$L_2 = 0.057$ m

$L_3 = 1.100$ m

then the average cavity length, L, is found from Eq. III-10 to be 1.107 m. This value together with the fact that $f = 4.74 \times 10^{14}$ Hz permits K_1, K_2, and K_3 to be calculated. The results of such calculations are given below in units of hertz/meter as well as megahertz/microinch.

	Hz/m	MHz/μ in.
K_1	-2.14×10^{14}	-5.44
K_2	-4.28×10^{14}	-10.87
K_3	-2.14×10^{14}	-5.44

It was pointed out in the concluding paragraph of Appendix III that in order to assure reasonably low losses, Δf_1 and Δf_3 should not exceed about f/2Q. If resonator losses are about 2% ($t^2 = .02$), and L is as previously given, then Eq. III.14 yields a Q of 5.5×10^8, and it follows that f/2Q is about 0.43 MHz. It should be emphasized that this limitation applies only to dynamic errors and not to larger displacements that occur at rates with the capability of the closed-loop control system. Its effect on system operation will be considered in greater detail in Section 4.5.

4.3.2 ERROR DETECTOR

The previous section described how the input signal, X_1, the common-mode error signal, X_2, and the feedback signals, X_5 and ΔL_3, each

contribute to the production of an incremental frequency change Δf, at the optical output of the laser resonator. This section will describe the arrangement for developing a dc voltage analog of Δf. The optical output of laser resonator is passed through a Fabry-Perot cavity (E-6) the length of which is modulated at 52.5 kHz. It is shown in Appendix IV that such a modulated cavity produces an output that, when properly filtered, is equivalent to balanced, full-wave modulation. In order to accomplish the required filtering, the power output of the cavity is first collected by diffused, silicon photodiode (E-7). The output current from the diode is amplified (E-8) and applied to an electrical band pass filter (E-9). The filter passes frequencies in the range from 42.5 kHz to 62.5 kHz. It rejects both undesired harmonics of signal frequencies below 20 kHz and the undesired harmonic of the carrier at 105 kHz, but retains the desired components centered about the carrier frequency at 52.5 kHz. The filter output is applied to a phase-sensitive demodulator (E-10) that is driven by the same 52.5 kHz oscillator (G-10) that modulates the cavity. The demodulator output is a dc voltage proportional to Δf.

From Eq. IV-8 the transfer function, F_4, of the modulated cavity is found to be

$$F_4 = \frac{\Delta P}{\Delta F} = \frac{8r^2}{t^2} \left(\frac{2\pi}{c}\right)^2 P_o L f \delta L \sin \omega_c t \qquad (31)$$

for the values

$$r^2 = 0.985$$

$$t^2 = 0.015$$

$$P_o = 2 \text{ mW}$$

$$L = 2.54 \times 10^{-2} \text{ m}$$

$$\delta L = 2.67 \times 10^{-10} \text{ m}$$

it will be found that

$$F_4 = -0.1 \sin \omega_c t \text{ mW per MHz} \quad (32)$$

It will be shown in Section 6.3 that required value of δL will be obtained when the 52.5 kHz voltage, E_5, that drives the cavity has a peak value of about 0.2V. This value will be set by an attenuator (F-7). A dc power supply (G-6) with an output voltage, E_6, that is adjustable over the range from -10V to +10V will allow the cavity to be manually tuned through a ±250 MHz range. This feature will be used during preliminary setup as described in Section 9.

The photodetector (E-7) is an EG&G, Inc. type SGD-100 (Ref. 54). It has a peak sensitivity of 0.5 mA/mW for 900 nm radiation, and about 0.4 mA/mW for 632.8 nm light. The maximum steady-state photocurrent is limited to 1.0 mA. This implies a maximum input power of 2.5 mW at 632.8 nm. The active region is circular with an area of 5.1 mm^2. The cross-sectional area of the laser discharge tube bore is 3.14 mm^2, and the average effective cross-sectional area of the laser beam is about 1/5 that of the tube (Ref. 55), or 0.6 mm^2. Proper optical design and mechanical positioning will allow the detector to collect substantially all of the output from the laser.

The amplifier (E-8) following the photodetector will be designed to have a gain, K_6, of 25 V/mA. The photodetector bias and amplifier input circuits block the signal due to the steady-state intensity of the laser beam (e.g., the first, or unity, term in Eq. IV.6). The remaining undesired signal frequency and carrier frequency harmonics are removed by a combination (E-9) of a band pass filter and a band-reject filter. The band pass portion is a fourth-order Butterworth filter with cut-off (3dB) frequencies of 36.6 kHz and 72.5 kHz. The attenuation at 20 kHz (second harmonic of highest expected signal frequency) is 20 dB. The attenuation at 42.5 kHz and 62.5 kHz (the

limits of the passband required for the suppressed-carrier modulated signal) is less than 0.5 dB. The phase lag in the passband is approximately linear with frequency and varies from a 48^{o} lead at 42.5 kHz to a 48^{o} lag at 62.5 kHz. In combination with the essentially constant, unity gain in the passband, this linear phase characteristic can be considered as equivalent to a uniform delay of the modulating signal (Ref. 56). Since the curve has a slope of about -1.35×10^{-5} radians per radian/second, the effective delay is 13.5 μs.

The attenuation of this portion of the filter at 105 kHz (the second harmonic of the carrier frequency) is 8 dB. The magnitude of this harmonic, even after an 8 dB loss, is on the order of magnitude of the modulated signal that results when Δf = 1 MHz. Theoretically the only effect of such harmonics is an increase in the harmonic content of the output of the phase sensitive detector. Practically, it appears desirable to keep the output filter that is internal to the detector relatively simple and suppress the 105 kHz component at its input. This is done by adding a passive parallel-T filter to the output of the band pass filter. The theoretical attenuation at the notch frequency is infinite. For practical values of input and output impedances and component values, attenuations as high as 60 dB can be obtained. The notch is sharp enough that the effect on the magnitude and phase in the 42.5 to 62.5 kHz passband is negligible.

The phase sensitive detector (E-10) is a balanced, full-wave demodulator. Demodulation is accomplished by effectively multiplying the signal, E_2, by the reference, E_4, from the 52.5 kHz carrier oscillator. From Fig. 31, E_2 is seen to be

$$E_2 = F_4 K_5 K_6 K_7 \Delta f \qquad (33)$$

substituting the actual value of F_4 from Eq. 32 gives

$$E_2(t) = -0.1\, K_5K_6F_7\, \Delta f \sin \omega_c t \tag{34}$$

The reference carrier signal may be assumed to be of unit amplitude,

$$E_4(t) = \sin \omega_c t$$

since the sample and hold technique used to implement the multiplication is relatively insensitive to the absolute magnitude of E_4. The product of E_2 and E_4 is

$$E_2(t) \cdot E_4(t) = -0.05\, K_5K_6F_7\, \Delta f\, (1 - \cos 2\, \omega_c t) \tag{35}$$

It has been assumed that the maximum frequency at which Δf will vary is 10 kHz. Because of the filtering at the input to the detector there are no harmonics lower than the cos 2 $\omega_c t$ component generated by the detector itself. A simple output filter removes this component without substantially affecting the low (0 - 10 kHz) frequency signals. Under these conditions the output of the phase sensitive detector is

$$E_3 = -0.05\, K_5K_6F_7F_8\, \Delta f \tag{36}$$

The expression is the outcome of the chain that included optical modulation, conversion to an electrical signal, and electrical demodulation. Since the carrier frequency no longer appears in Eq. 36, E and Δf are sometimes said to be dc or low-frequency variables even though in this case their spectra may extend from 0 to 10 kHz.

Now that return has been made to the "signal domain," it is possible to take explicite note of the 13.5 μs signal delay associated with the

fourth-order Butterworth filter. If this is done, the Laplace transform of Eq. 36 becomes

$$E_3(s) = -0.05\ K_5K_6K_8\ e^{-1.35 \times 10^{-5}s}\ \Delta f \qquad (37)$$

remembering that $|F_7| = 1$ in the passband, and assuming that $F_8(s) = K_8$.

4.3.3. HIGH-FREQUENCY LENGTH CONTROL

The displacement of mirror M4 is produced by a piezoelectric transducer (H-3). As pointed out in the opening portion of Section 4.3.1, this mirror is mounted (G-3) at an angle of 45^o with respect to the optical paths. As a result its effective displacement is modified in accordance with

$$K_{15} = \frac{X_4}{X_5} = \frac{\sqrt{2}}{2} \qquad (38)$$

The piezoelectric transducer is a cylinder, the end of which displaces 36.4 μin. when the applied voltage, E_{11}, is 1500V, hence

$$K_{14} = \frac{X_5}{E_{11}} = 24.3 \times 10^{-3}\ \mu in/V \qquad (39)$$

The total range of the change in optical path length, X_4, for the ±1500V range of E_{11} is approximately 50 μin. The natural frequency of the transducer is on the order of 50 kHz, so that the phase lag in the desired 0-10 kHz passband of the open loop response will be negligible.

The amplifier (H-4) that drives the piezoelectric transducer has a gain of 200. Its amplitude response within the linear range is substantially flat, and its phase lag substantially zero, over the desired 0-10 kHz passband, so that it can be assumed

$$F_{13} = K_{13} = 200 \qquad (40)$$

4.3.4 LOW-FREQUENCY LENGTH CONTROL

The displacement of mirror M2 is the difference of the displacements of two lead screws. One screw (C-4) has a pitch of 0.025 inch (40 threads/in.) and the second (B-4) has a pitch of 0.0246063 inch (16 threads/cm).

When the output shaft of the harmonic drive makes one turn ΔL_2 changes by the difference of the pitches, or 0.0003937 inch, so that

$$K_{22} - K_{23} = \frac{\Delta L_2}{\theta_2} = -62.66 \ \mu\text{in/rad} \tag{41}$$

The harmonic drive also rotates a slide-wire potentiometer through a one-stage gear pass (C-5). The gear on the harmonic drive has 170 teeth, and that on the potentiometer, 180 teeth, so that

$$K_{24} = \frac{\theta_3}{\theta_2} = \frac{170}{180} \tag{42}$$

In order to produce a 1000 μin. displacement of M2 the shaft of the harmonic drive makes 2.54 revolutions and the potentiometer makes 2.4 revolutions. The potentiometer is a 3 turn, or 1080° unit. However, because of end resistance the effective rotation is decreased 35° to 1045°. If the potentiometer is excited by 20V (±10V, symmetrically with respect to ground), then

$$K_{25} = \frac{E_{17}}{\theta_3} = 1.096 \ \text{V/rad} \tag{43}$$

The harmonic drive has a 370:1 reduction, so that

$$K_{21} = \frac{\theta_2}{\theta_1} = \frac{1}{370} \tag{44}$$

The transfer function of the servo motor (B-6) that powers the harmonic drive is approximately (Ref. 57) given by

$$F_{20}(s) = \frac{\theta_1(s)}{E_{16}(s)} = \frac{K_T/K_F}{s\left(\frac{J}{K_F}s + 1\right)} \qquad (45)$$

The motor has a stall torque of 3.1 oz.-in for a 40V rms input to the control phase. The torque constant, K_T, is the ratio of these quantities, or

$$K_T = 5.46 \times 10^{-4} \text{ N-m/V}$$

The synchronous speed of the motor is 60 rps. The damping constant, K_F, is approximately one-half of the ratio of the stall torque to the synchronous speed, or

$$K_F = 2.9 \times 10^{-5} \text{ N-m per rad/s}$$

The combined inertia of the motor (4 g-cm^2) and the input to the harmonic drive (13 g-cm^2) is 17 g-cm^2, or

$$J = 1.7 \times 10^{-6} \text{ kg-m}^2$$

The gain of the motor is

$$\frac{K_T}{K_F} = 18.85 \text{ rad/s per V}$$

and its time constant is

$$\frac{J}{K_F} = 0.0586 \text{ s}$$

A time constant of 0.0586 seconds corresponds to a corner frequency of about 17.1 rad/s, or 2.82 Hz.

The amplifier (B-7) that drives the motor has a gain of 1750. Its amplitude response is substantially flat, and its phase lag is substantially zero, over the passband of the servo, so that it can be assumed that

$$F_{19} = K_{19} = 1750 \tag{46}$$

The modulator (B-8) has similar amplitude and phase characteristics. It has been designed so that

$$F_{18} = K_{18} = 1 \tag{47}$$

The modulator receives its input from the output of a lead network (B-9). The transfer function of the lead network is given by

$$F_{17}(s) = \frac{1 + sT_1}{1 + sT_2} \tag{48}$$

It has been designed so that $T_1 = 0.0586$ seconds and $T_2 = 0.00586$ seconds. In the total open-loop transfer function of the low-frequency length-control servo, the numerator of the lead circuit transfer function cancels with the corresponding term in the denominator of the motor transfer function. A time constant, T_2, of 0.00586 corresponds to a corner frequency of 171 rad/s, or 28.2 Hz. Thus, the effect of the lead circuit is to move the first corner frequency of the open-loop transfer function from 2.82 Hz out to 28.2 Hz.

From the block diagram, the closed-loop response of the low-frequency length control is found to be

$$\frac{\Delta L_2(s)}{E_{13}(s)} = \frac{(K_{22} - K_{23})\, K_{21}F_{20}F_{19}F_{18}F_{17}}{1 + K_{24}K_{25}K_{21}F_{20}F_{19}F_{18}F_{17}} \tag{49}$$

When the values of the various block transfer functions are substituted, the closed-loop response is found to be

$$\frac{\Delta L_2(s)}{E_{13}(s)} = \frac{-61.2}{\left(\frac{s}{125}\right)^2 + \frac{s}{91.3} + 1} \quad \mu in/V \tag{50}$$

It follows that the undamped natural frequency and damping ratio are

$$\omega_n = 125 \text{ rad/s}$$

$$f_n = 19.9 \text{ Hz}$$

$$\zeta = 0.685$$

The closed-loop response was obtained by neglecting nonlinearities. The most important nonlinearity is due to the frictional load at the motor output shaft. The "stiction," S, or starting torque of the harmonic drive is 0.8 oz.in., or 5.65×10^{-3} N-m. The value of the error voltage, E_{18}, required to overcome this torque may be found from the static gains of the blocks between E_{18} and θ_2. Its value is

$$\frac{S}{K_T K_{19} K_{18} K} = \frac{5.65 \times 10^{-3}}{.955} = 5.9 \times 10^{-3} V$$

The output circuit to be described in the next section causes E_{13} to have a level of 1V for an input of 1 μin. Thus the error voltage (above) required to start the motor is equivalent to about 6×10^{-9} inches. Below this range the high-frequency length-control will still be operational.

4.3.5 OUTPUT CIRCUIT

The output voltage, E_3, from the phase sensitive demodulator is applied to a compensation network (E-11).

The transfer function of this network is

$$F_{10}(s) = \frac{1 + T_2 s}{(1 + T_1 s)^2} \qquad (51)$$

It has been designed so that

$$T_1 = 5 \times 10^{-4} \text{ second}$$

$$T_2 = 5 \times 10^{-5} \text{ second}$$

The larger time constant, T_1, corresponds to a corner frequency of 2000 rad/s, or about 320 Hz. The smaller time constant, T_2, corresponds to a corner frequency of 20,000 rad/s, or 3.2 kHz. The effect of this forward loop compensation is discussed in the next section.

The output voltage, E_9, from the compensation network is scaled (E-12) in order to obtain E_9. The latter voltage is scaled (H-12, B-12) for feedback to both the high-frequency and low-frequency length controls. The products $K_{11}K_{12}$ and $K_{11}K_{16}$ are constant, so that regardless of the value of K_{11}, the loop gain is constant. By varying the three scale factors appropriately the overall scale factor between E_9 and X_1 can be varied. Three useful sets of values are

$\frac{E_9}{X_1}$, V/μin.	K_{11}	K_{12}	K_{16}
0.1	0.184	2.88	10
1.0	1.84	0.288	1
10.0	18.4	0.0288	0.1

The output voltage, E_{12}, from K_{16} is applied to a second order low-pass filter (B-11). This filter has unity gain at dc and an adjustable

break frequency. Its use and effect will be discussed in the next section. Voltage E_9 after being operated upon by signal conditioning (E-13) emerges as the output voltage, E_o. The signal conditioning function is discussed in Section 8.

4.4 STABILITY ANALYSIS

From the system block diagram, the following relations can be written

$$E_o(s) = F_{27}E_9(s) \tag{52}$$

$$\frac{E_9(s)}{\Delta f(s)} = A(s) = K_{11}F_{10}F_8F_7K_6K_5F_4 \tag{53}$$

$$\frac{\Delta L_2(s)}{E_9(s)} = B(s) = \frac{\Delta L_2(s)}{E_{13}(s)} F_{26}K_{16} \tag{54}$$

$$\frac{X_4(s)}{E_9(s)} = C(s) = K_{15}K_{14}F_{13}K_{12} \tag{55}$$

$$\Delta f = K_3X_1 + (K_1 + K_3) + K_2 \Delta L_2 - K_3X_4 \tag{56}$$

From the functional descriptions in the preceding sections

$$A(s) = -\frac{1 + T_2s}{(1 + T_1s)^2} 10K_{11} \quad \text{V/MHz} \tag{53'}$$

$$B(s) = \frac{-61.2\ F_{26}K_{16}}{\left(\frac{s}{125}\right)^2 + \frac{s}{91.3} + 1} \quad \mu\text{in./V} \tag{54'}$$

$$C(s) = 3.44\ K_{12} \quad \mu\text{in./V} \tag{55'}$$

$$\Delta f = -5.44\ X_1 - 10.87\ X_2 - 10.87\ \Delta L_2 + 5.44\ X_4 \quad \text{MHz} \tag{56'}$$

In the case of Eq. 53, the phase-shift due to the band pass filter has been neglected.

4.4.1 HIGH-FREQUENCY OPERATION

It is useful to examine the operation with the low-frequency length control turned off, i.e., $\Delta L_2 = 0$. The transfer function between the output voltage, E_o, and the input displacement, X_1, is given by

$$\frac{E_o(s)}{X_1(s)} = \frac{F_{27}K_3A(s)}{1 + K_3A(s)C(s)} = D(s) \tag{57}$$

If the actual values of K_3, A, and C are substituted, the transfer function simplifies to

$$\frac{E_o(s)}{X_1(s)} = \frac{0.544\ F_{27}K_{11}\left(1 + \frac{s}{2x10^4}\right)}{\left(\frac{s}{2x10^4}\right)^2 + (0.595 \times 10^{-4})s + 1} \tag{57'}$$

from which it follows that the undamped natural frequency is 2×10^4 rad/sec, or 3.18 kHz, and the damping ratio is 0.6. The presence of the $1 + s/2 \times 10^4$ term in the numerator and a quadratic with $\omega_n = 2 \times 10^4$ in the denominator means that the asymptotic response above 3.2 kHz decreases at the rate of -6 dB per octave or -20 dB per decade.

The static (low-frequency) loop gain is on the order of 100. This has decreased to on the order of 10 at 1000 Hz. Lowering the closed-loop corner frequency much below 3.2 kHz would decrease the loop gain at 1000 Hz even further, resulting in excessive errors. If it is desired to reduce the instrument band width to 1000 Hz, this should be done by external filtering; for example, by signal conditioning at F_{27}.

4.4.2 LOW-FREQUENCY OPERATION

When the low-frequency length control is still inoperative, a slowly varying common mode signal, X_2, produced by environmental effects will affect the output in accordance with

$$E_o(s) = D(s) \left[X_1(s) + 2\, X_2(s) \right] \tag{58}$$

The resulting errors will frequently be unacceptable. Discrimination against slowly varying signals can be achieved by the operation of the low-frequency length control servo. Under these conditions, the transfer function is given by

$$E_o(s) = \frac{F_{27} K_3 A(s) [X_1 + 2X_2]}{1 + K_3 A(s) C(s) - K_2 A(s) B(s)} \tag{59}$$

The addition of the new term in the denominator increases the static (low-frequency) feedback gain by a factor of about 120. The output voltage, E_o, is reduced by the same factor. However, this reduction only occurs at frequencies within the range of operation of the low-frequency servo. At frequencies much above its natural frequency of 20 Hz, this servo is effectively inoperative and the system operation is as described in Section 4.4.1. However, the slowly varying common mode effects due to temperature, etc., will occur at frequencies far below 20 Hz, and it appears that 20 Hz is needlessly high for the purpose of suppressing these effects. A low-pass filter (B-11; transfer function, F_{26}) is inserted ahead of servo for the purpose of lowering the frequency at which the gain of the servo become ineffective. The corner frequency of this filter is best determined after operating experience with system. It seems likely that a range of values selectable by a switch can be provided to accommodate a large variety of situations.

4.5 ERROR ANALYSIS

Referring to high frequency operation as described in Section 4.4.1, the dynamic error referred to the input can be shown to be

$$\frac{\epsilon(s)}{X_1(s)} = \frac{1}{1 + K_3A(s)C(s)} \tag{60}$$

For the values previously given, this becomes

$$\frac{\epsilon(s)}{X_1(s)} = \frac{1}{100} \cdot \frac{\left(1 + \frac{s}{2x10^3}\right)^2}{\left(\frac{s}{2x10^4}\right)^2 + (0.595x10^{-4})s + 1} \tag{60'}$$

The term in the numerator has a corner frequency of 2000 rad/s, or 320 Hz. For frequencies much below 320 Hz, the magnitude of E/X_1 will be about 1 percent. At 700 Hz it will be on the order of 5 percent, and at 1000 Hz, on the order of 10 percent. In Section 4.3.1 it was pointed out that Δf_3 should be held to about 0.43 MHz to keep cavity losses low. This corresponds to a displacement error of about 0.08 μin. Such an error could exist for an input displacement of 8 μin. if $\epsilon/X_1 = 0.01$. If this condition proves troublesome, it will be a simple matter to substantially reduce the error by changing the transfer function of the compensation network (E-11) and that of the immediately following scale factor (E-12). The transfer function of these combined blocks is

$$\frac{E_9(s)}{E_3(s)} = K_{11}F_{10}(s) = \frac{K_{11}(1 + T_2s)}{(1 + T_1s)^2} \tag{61}$$

If the scale factor gain is raised from K_{11} to KK_{11} and the time constant of the denominator is raised from T_1 to T_3, the transfer function becomes

$$\frac{KK_{11}(1 + T_2s)}{(1 + T_3s)^2}$$

If K and T_3 are selected so that $K = (T_3/T_1)^2$, then the low-frequency gain will be raised by the factor K, and the high-frequency characteristics (say, above $1/T_2$ rad/s) will remain about the same. Such a change would have relatively little effect on the undamped natural frequency of the system, and would produce a small reduction in damping factor. For example, if K = 10 the damping factor would be reduced from about 0.60 to 0.53, but ϵ/X_1 would be reduced from 1.0 percent to 0.1 percent.

The absolute error depends primarily on the gain stability of the piezoelectric transducer (H-3) and the amplifier (H-4) that drives it. The characteristics of the piezoelectric material depend on both time and temperature (Ref. 58). For the material chosen the coupling factor (square root of the ratio of mechanical energy out to electrical energy in) decreases at a rate of about 0.2 percent per decade of time after the original polarization. Thus, if the coupling factor were 0.344 100 hours after poling, it would only decrease to about 0.343 at 10,000 hours. At room temperature the thermal sensitivity of the piezoelectric constant of this material is about 0.15 percent per ^{o}F (Ref. 59). A detailed analysis of the gain stability of the driver amplifier has not been made; however, about 20 dB negative feedback should result in shifts of less than 1 percent for operating times on the order of 8 hours.

SECTION 5

ELECTRICAL DESIGN

This section presents circuit diagrams and discusses the electrical and electronic design considerations for each of the appropriate blocks described in Subsection 4.3.

5.1 ERROR DETECTOR

The functional characteristics of the error detector were described in Subsection 4.3.2. It converts the incremental frequency change, Δf, to an error voltage, E_3. The change in length of the modulated cavity in response to applied voltage, E_7, will be discussed in Subsection 6.3.

5.1.1 CURRENT AMPLIFIER

The current amplifier (E-8) receives the output current, ΔI, from the photodetector (E-7) and converts it to a voltage. A schematic is shown in Fig. 32. The silicon photodiode has a guard ring (D2) and an active area (D1). Back bias of the guard ring at the same potential as the active area minimizes electrical noise due to leakage. The 100 μF input condenser blocks the rather large dc component that exists due to the steady state output of the laser, yet provides a low impedance path to the amplifier at signal frequencies. The 25 kΩ feedback resistor sets the gain at 25 V/mA. The parallel 100 pF condenser prevents high frequency instability. A fixed 50 kΩ resistor sets the dc level of the output near zero. The amplifier is a Philbrick P45A. It was chosen because of its high gain in the passband and its ability to deliver full output at the signal frequency.

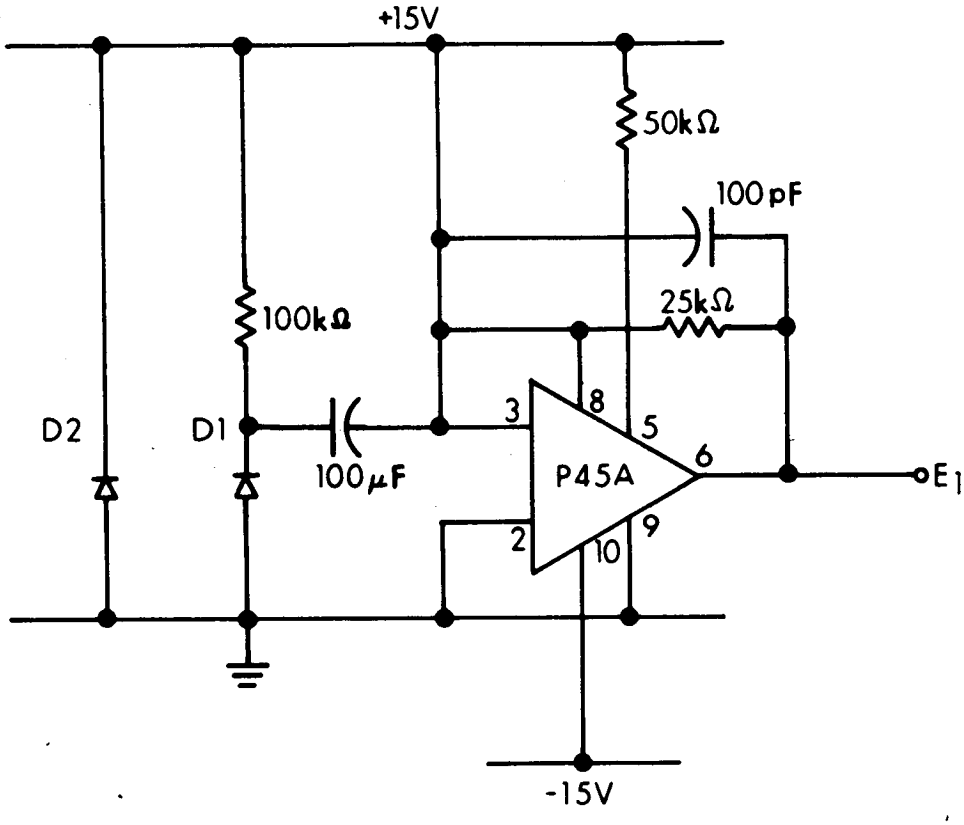

Figure 32. Current Amplifier Schematic

5.1.2 BAND PASS FILTER

The band-pass filter (E-9) removes unwanted harmonics of the signal and carrier. A schematic is shown in Fig. 33. The amplifiers are both Philbrick P45A's and may be provided with power and grounds as shown in Fig. 32. Each amplifier behaves as a narrow band-pass filter with a transfer function given (Ref. 60) by

$$\frac{2BRCs}{1 + 2\zeta RCs + R^2C^2s^2}$$

The required fourth order Butterworth characteristic described in Subsection 4.3.2 will be obtained if component values for the first amplifier are selected so that

$$\zeta = 0.707$$
$$B = 0.355$$
$$RC = 3.80 \times 10^{-6} \text{ seconds}$$

and for the second amplifier so that

$$\zeta = 0.707$$
$$B = 0.355$$
$$RC = 2.67 \times 10^{-6} \text{ seconds}$$

At the output of the second amplifier is a parallel - T filter tuned to suppress the 105 kHz second harmonic of the carrier. If the expression (Ref. 61)

$$\frac{n_1}{n_2(1 - n_1)} = \frac{1 + m_1}{m_2} = k$$

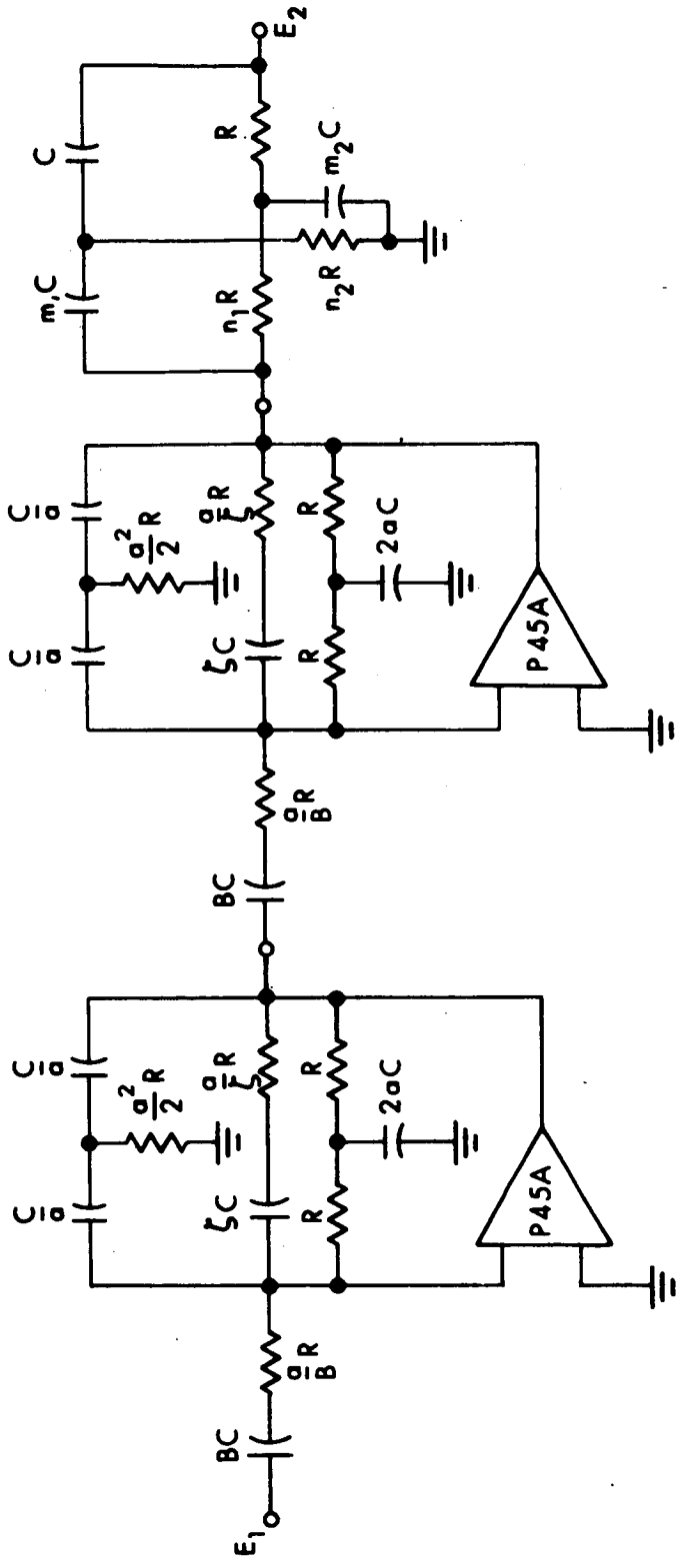

Figure 33. Band Pass Filter Schematic

is satisfied, the transfer function of the parallel - T will be

$$\frac{1 + \left(\frac{s}{\omega_o}\right)^2}{1 + K\left(\frac{s}{\omega_o}\right)^2 + \left(\frac{s}{\omega_o}\right)^2}$$

where

$$K = \frac{n_1 (1+m_1) + k (1+n_1)}{\sqrt{k n_1 m_1}}$$

The desired response will be obtained if the component values are selected so that

$$K = 0.1$$
$$\omega_o = 6.59 \times 10^5 \text{ rad/s}$$

The three resistors of the parallel - T will be adjustable so as to simplify tuning.

5.1.3 PHASE-SENSITIVE DEMODULATOR

The phase-sensitive demodulator (E-10) accepts the 52.5 MHz supressed-carrier modulated signal, E_2, and operates on it to obtain a dc error voltage, E_3. A schematic is shown in Fig. 34. All of the resistors, R, can be the same value, e.g., 10 kΩ The input signal, E_2, is applied to a pair of complementary current gates, Philbrick SPG-1, contained in a single module. These gates are switched by a square wave, (C), so that SPG-1a is on and SPG-1b is off for a half-cycle, and SPG-1a is off and SPG-1b is on for the following half-cycle. The result is a very precisely rectified full-wave signal, (A). This signal is applied to a Philbrick SPT&H track and hold module. A

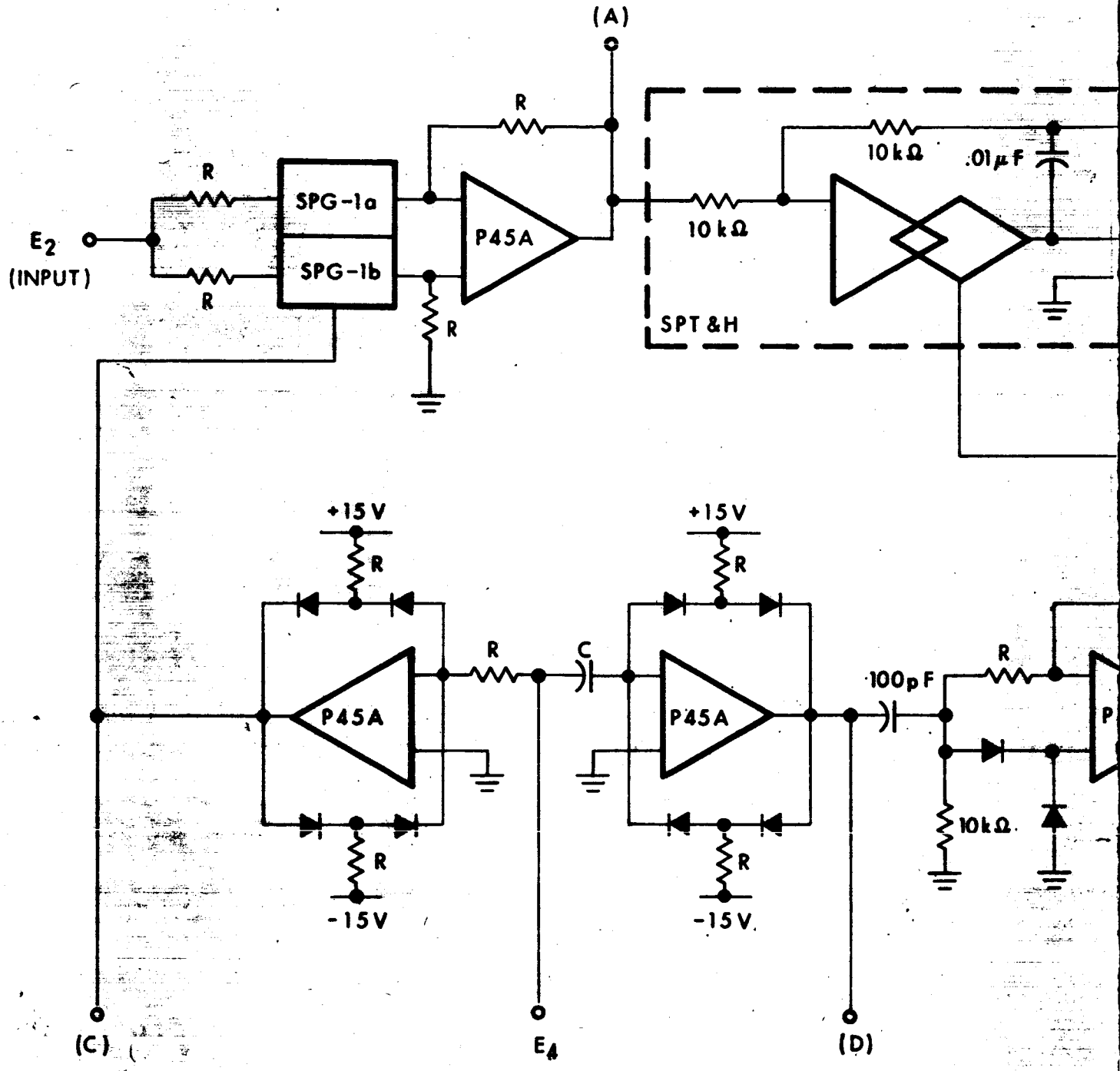

73629546

Fig. 34-A

97-A

7205-Final

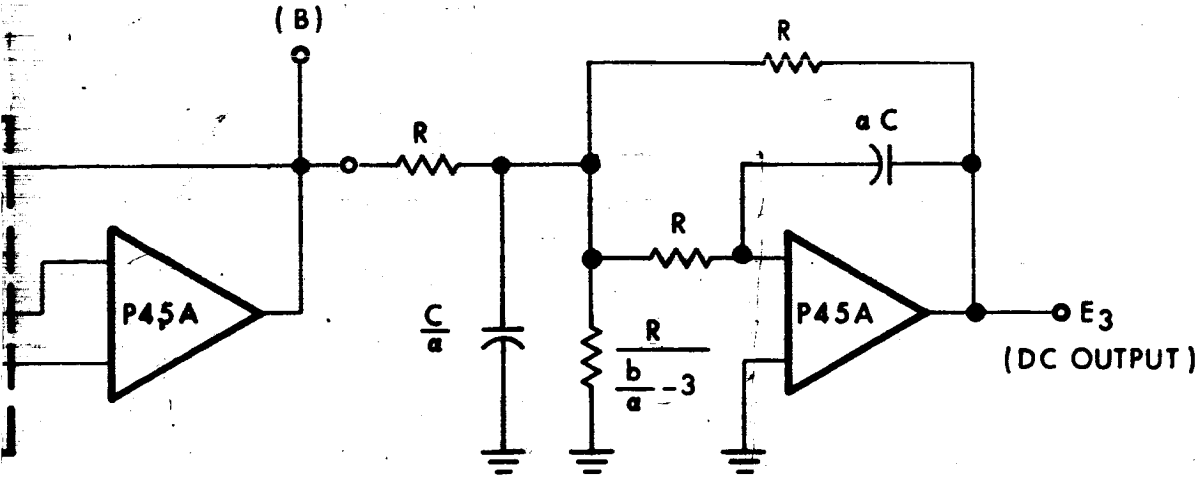
(B)
R
R
a C
P45A
C/a
R
R/(b/a - 3)
P45A
E3
(DC OUTPUT)

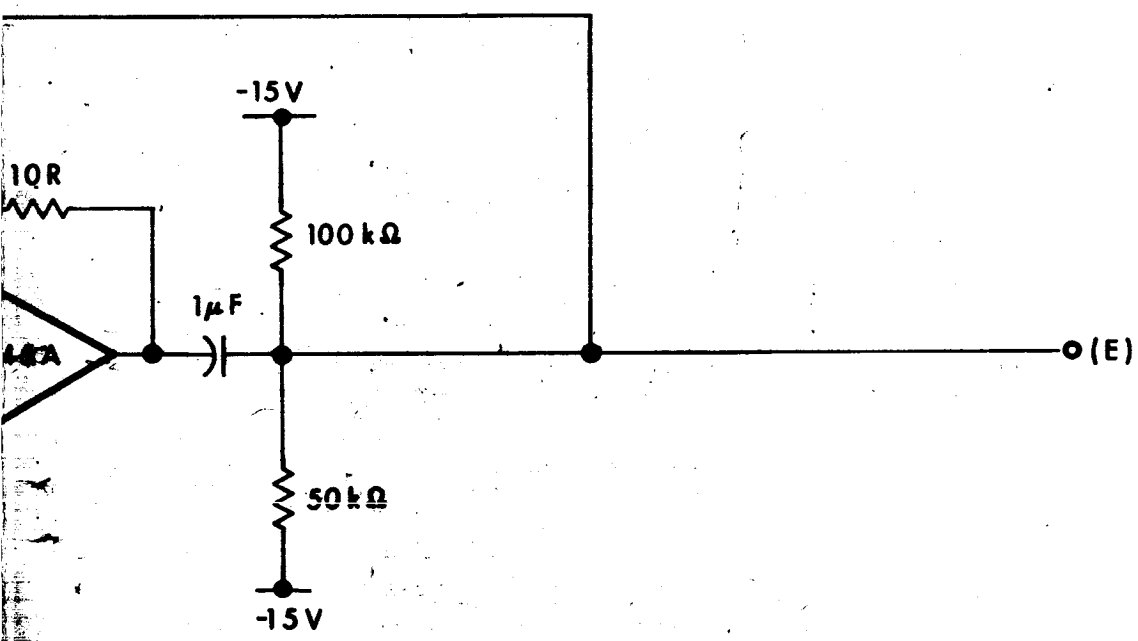
-15V
10R
100 kΩ
1μF
(E)
50 kΩ
-15V

Fig 34-A

97-B

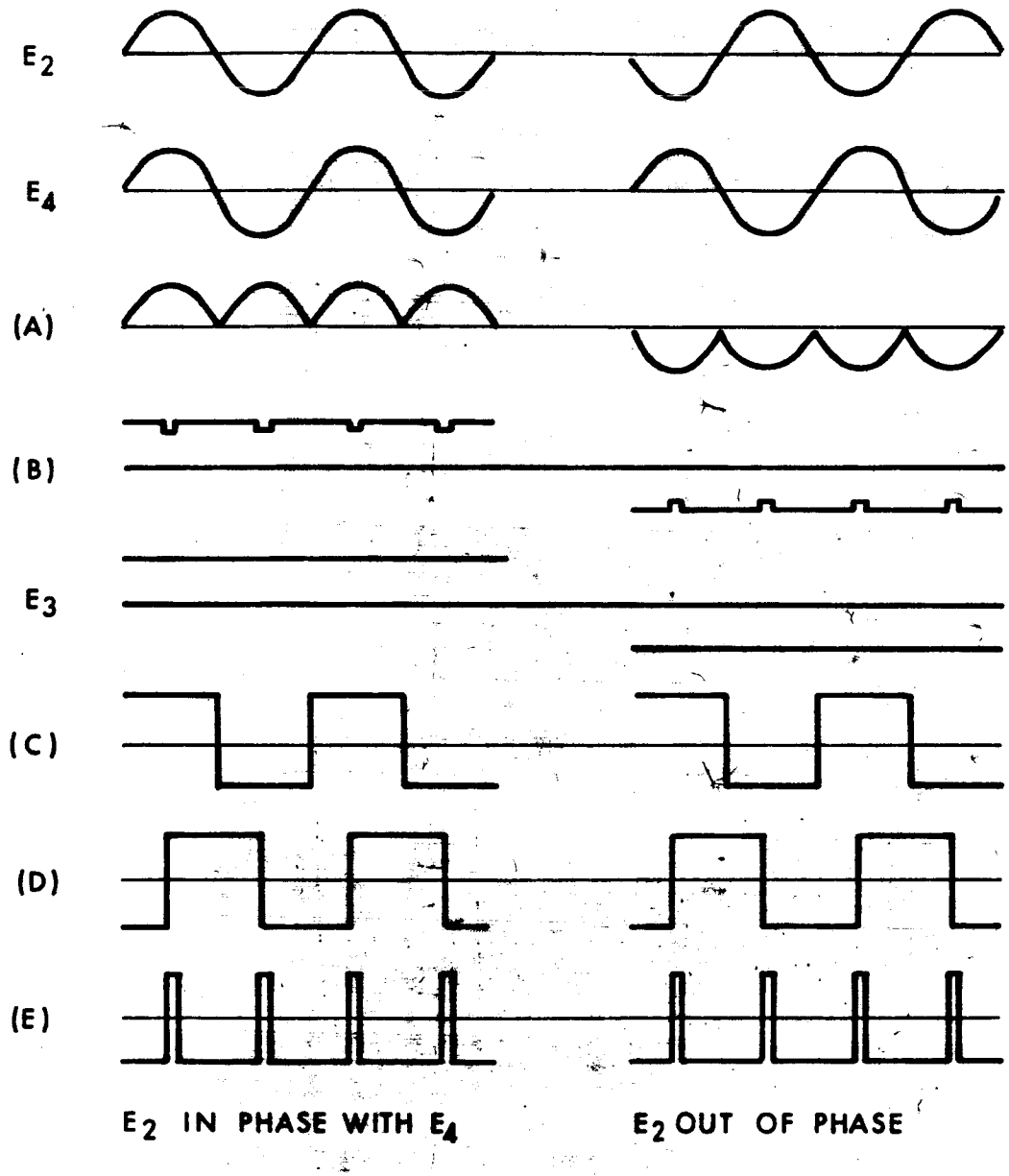

Figure 34.C Phase-Sensitive Demodulator Schematic and Wave Forms

logic signal, (E), causes the SPT&H to instantaneously assume and maintain the exact value of its input signal, (A), when (E) is positive, and remember or hold this value when (E) is negative. The resulting output signal, (B), has small transient disturbances that result at the time of the hold command. A filtered dc output signal, E_3, is obtained by means of a second-order, low-pass, Butterworth filter. Its transfer function (Ref. 62) is

$$\frac{1}{1 + bRCs + R^2C^2s^2}$$

the required response will be obtained if component values are selected so that

$$b = \sqrt{2}$$

$$RC = 3 \times 10^{-6} \text{ seconds}$$

The switching commands, (C) and (E) for SPG-1 and SPT&H are both derived from the carrier reference, E_4. A simple zero-crossing detector generates the (C) square wave. A similar circuit in which the input resistor is replaced by a condenser generates the (D) square wave, displaced from (C) by 90°. The displaced square wave, (D), is differentiated by the 100 pF - 10 kΩ coupling circuit. The result is a series of pulses of alternating polarity. There are converted to uniform positive-going pulses by an operational-amplifier, absolute-value circuit. Its output is coupled by a 1 μF condenser to a 50 kΩ - 100 kΩ voltage divider that sets the normal level of (E) at -5V. Positive-going pulses of 10V amplitude charge the level of (E) to +5V, resulting in the waveform required to switch SPT&H.

5.2 HIGH-FREQUENCY LENGTH CONTROL

The functional characteristics of the high-frequency length control were described in Subsection 4.3.3. It positions mirror M4 in response to error signals.

5.2.1 PIEZOELECTRIC TRANSDUCER

The transducer is a cylinder of lead zirconate - lead titanate ceramic. It is supplied with two metallic electrodes, one covering the entire outer cylindrical surface and one covering the entire inner cylindrical surface. During manufacture the material is poled by an electric field produced by applying a high dc voltage to these electrodes. The cylinder has an outside diameter of 0.50 inch (1.27×10^{-2} m), an inside diameter of 0.25 inch (0.635×10^{-2} m), and a length of one inch (2.54×10^{-2} m). The particular material selected, Clevite PZT-5A, (Ref. 58) has a density of 7.75×10^{3} kg/m^3. The lowest, longitudinal, natural frequency of the cylinder is given by (Ref. 63)

$$f_1 = \frac{1}{2L} \sqrt{\frac{1}{S_{11}^E \rho}}$$

where

L = length in m

ρ = density in kg/m^3

S_{11}^E = elastic compliance in m^2/N

The elastic compliance is the reciprocal of the stiffness, Young's modulus. For the symbol S_{11}^E, the superscript E indicates that the compliance is measured at constant voltage; for example, with the

electrodes shorted. The subscripts 1 and 1 indicate that both stress and strain are in the longitudinal direction and perpendicular to the electric field. For PTZ-5A, S_{11}^{E} is 16.4 x 10^{-12} m^2/N, and f_1 is found to be 55 kHz. If the mirror on one end and a similar glass blank on the opposite end increase the effective length by 10 percent, the natural frequency will be on the order of 50 kHz.

While 50 kHz is well above the nominal 10 kHz to which it is desired to control the passband, there may be lower resonances due to the mounting structure. The ideal structure would be infinitely massive and infinitely stiff. If it is not, energy from the transducer may be coupled into structural resonances that are within the passband. Such coupling will change the electrical impedance of the transducer and consequently affect the performance of the ±1500V dc amplifier (H-4) that drives it.

One method of successfully reducing such coupling (Ref. 64) is to support the cylinder in the plane of the node of its first natural resonance. Such a mounting is shown in Fig. 35. As a consequence of this method of mounting, only about 45 percent, or 0.45 inch, of the transducer length is available for producing mirror displacement. The longitudinal strain in the cylinder is related to the electric field by

$$d_{31} = \frac{\text{strain}}{\text{field}}$$

where the subscript 3 indicates the electric field is applied in the transverse direction, and the subscript 1 indicates that the strain is in the longitudinal direction. For PTZ-5A, d_{31} is 171 x 10^{-12} m/V. The strain is equal to the ratio of the incremental change in position of the mirror, X_5, divided by the active length, 0.45 in, so that E is 2.22 x X_5 x 10^{-6}, where X_5 is in microinches. The average electric

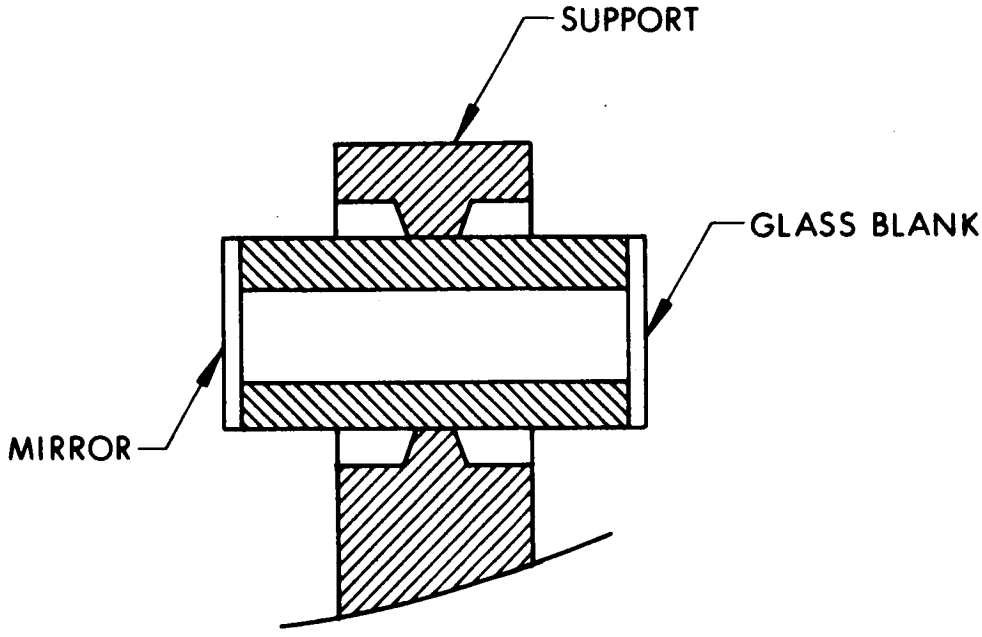

Figure 35. Section Through Piezoelectric Transducer Showing Nodal Plane Support

field is the ratio of the impressed voltage, E_{11}, to the wall thickness of the cylinder, 0.3175×10^{-2} m. Finally,

$$d_{31} = (2.22 \times 10^{-6})\ (0.3175 \times 10^{-2})\ \frac{X_5}{E_{11}}$$

and

$$K_{14} = \frac{X_5}{E_{11}} = 2.43 \times 10^{-2}\ \mu\text{in./V}$$

The total range of X_5 for the ±1500V range of E_{11} is 72.8 μin.

When a voltage is applied to the electrodes, the highest electric field will be at the inner electrode. Its value can be shown (Ref. 65) to be

$$E_r = \frac{V}{r \ln \frac{b}{a}} \qquad (62)$$

where

E_r = electric field in V/m
V = potential difference across electrodes, V
r = radius at which field is calculated, m
b = outside diameter, m
a = inside diameter, m

For V = 1500V and r = 0.125 in (0.3175×10^{-2} m), it is found that $E_r = 6.8 \times 10^5$ V/m. The ac depoling field is 7×10^5 V/m. Electrical stops on the amplifier insure that this limit is not exceeded. The capacity per unit length of a cylindrical capacitor (Ref. 2) is

$$C = \frac{0.098\ \epsilon_v \left(\epsilon_3^T/\epsilon_v\right)}{\ln \frac{b}{a}} \qquad (63)$$

where the dielectric constant of free space, ϵ_v, is 8.85×10^{-12} F/m, and the relative dielectric constant, ϵ_3^T/ϵ_v, is 1700 for PZT-5A. In the case of the symbol ϵ^T_3 the superscript T indicates that dielectric constant is measured with the cylinder free (the length unrestrained). The subscript 3 indicates that the electric field is in the transverse direction. For the case at hand, it is found that C is 54 pF. It will be assumed that stray capacitance will increase the capacitance as seen by the amplifier to 65 pF. The low value of stray capacitance will be attained by locating the amplifier (exclusive of power supply) in the after portion of the complete displacement transducer housing.

5.2.2 HIGH VOLTAGE AMPLIFIER

A ±1500V dc amplifier (H-4) supplies the drive voltage, E_{11}, to the piezoelectric transducer described in the previous section. This amplifier is required to have a direct-coupled characteristic, an output-voltage capability of ±1500 volts, and a high-frequency response extending to 10 kHz. The key requirements of this amplifier are:

Output voltage full scale	±1500 volts
Voltage gain	200X
Frequency response	dc through 10 kHz
Load (reactive component)	65 pF nominal

Such an amplifier need might be satisfied by a transistor/vacuum tube hybrid, as shown in Fig. 36. This amplifier uses a differential

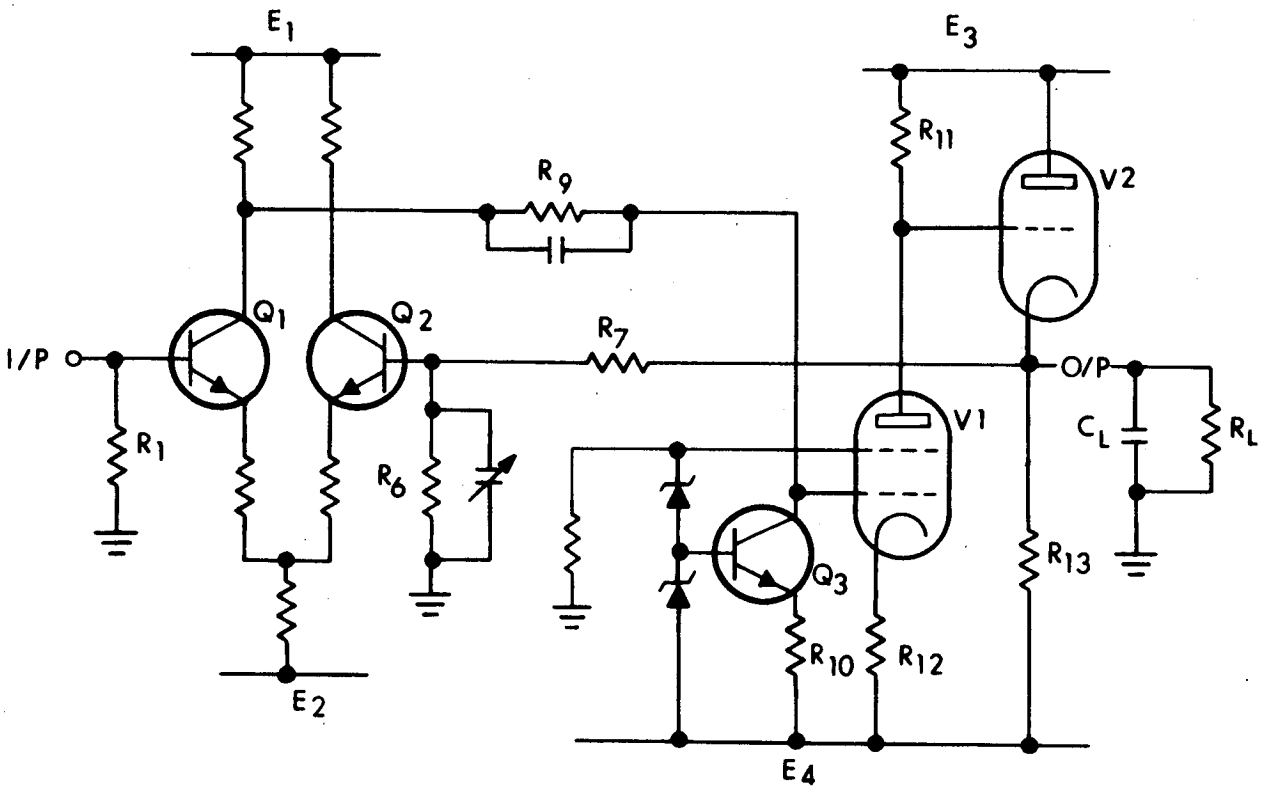

Figure 36. Hybrid Transistor/Vacuum Tube Amplifier

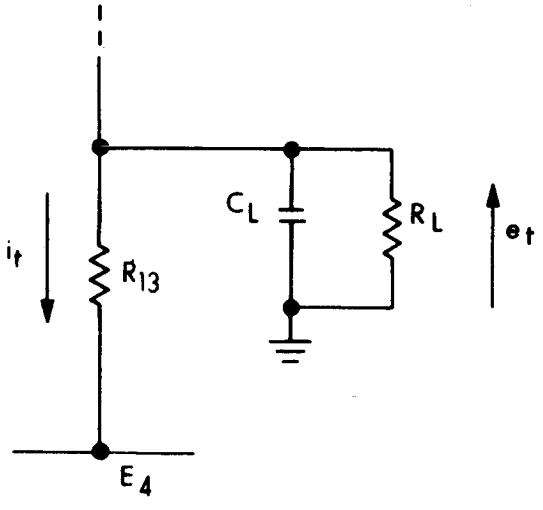

Figure 37. Output Circuit with V2 Cutoff

transistor amplifier to handle the input feeding via a constant current dc voltage drop to a high voltage pentode operating as a Class A amplifier. This amplifier then feeds a cathode follower to give output current driving capability.

5.2.2.1 Swing Rate Limitations

Simple ended output stages, such as the one considered here, suffer a swing rate limitation in one direction. In the particular configuration shown in Fig. 36, when the output is moving in a positive sense the load capacitor C_L is charged through V2 from the positive supply. As the rate of positive charging is increased, the dynamic resistance of V2 will be reduced until some limit dependent upon V2 and the power supply is reached. On the other hand, the extreme rate of negative swinging occurs when V2 is cut off; at this point the circuit effectively becomes that shown in Fig. 37. When V2 is cut off, the output voltage, e_t, is moving negatively at the maximum rate.

Since an upper frequency response is required to 10 kHz, the maximum rate of charge of voltage of this frequency is of interest. Consider the sine wave shown in Fig. 38. The slope of this waveform is given by the differential of the equation for e_t, viz,

$$e_t = E_p \sin \omega t$$

where E_p is the peak excursion of the output

$$\frac{de_t}{dt} = \omega \cdot E_p \cos \omega t$$

At $t = t_o$ shown in Fig. 38, the time rate of charge of output voltage is

$$\omega E_p(-1)$$

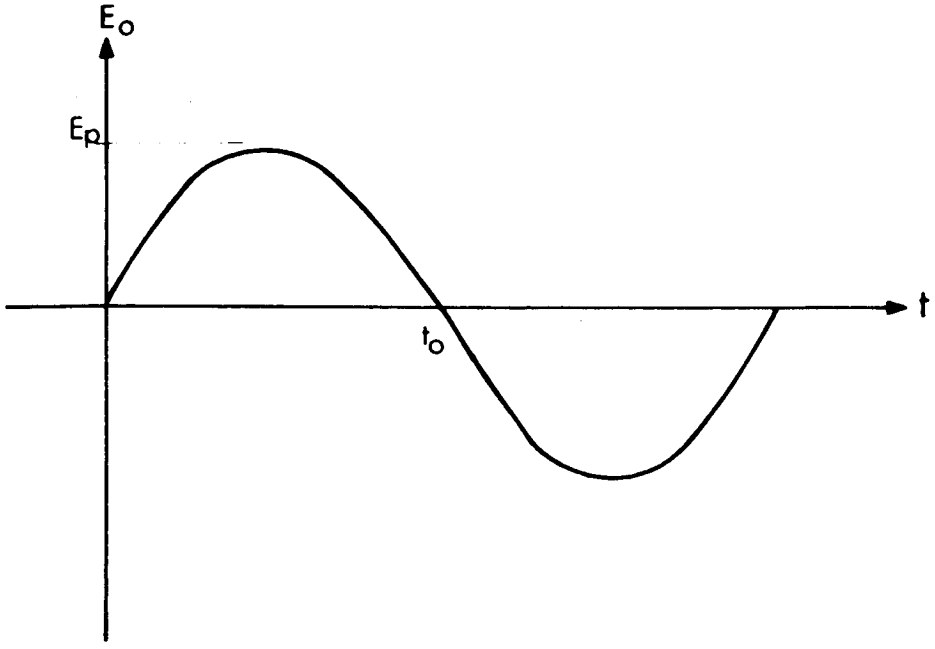

Figure 38. Output Sine Wave

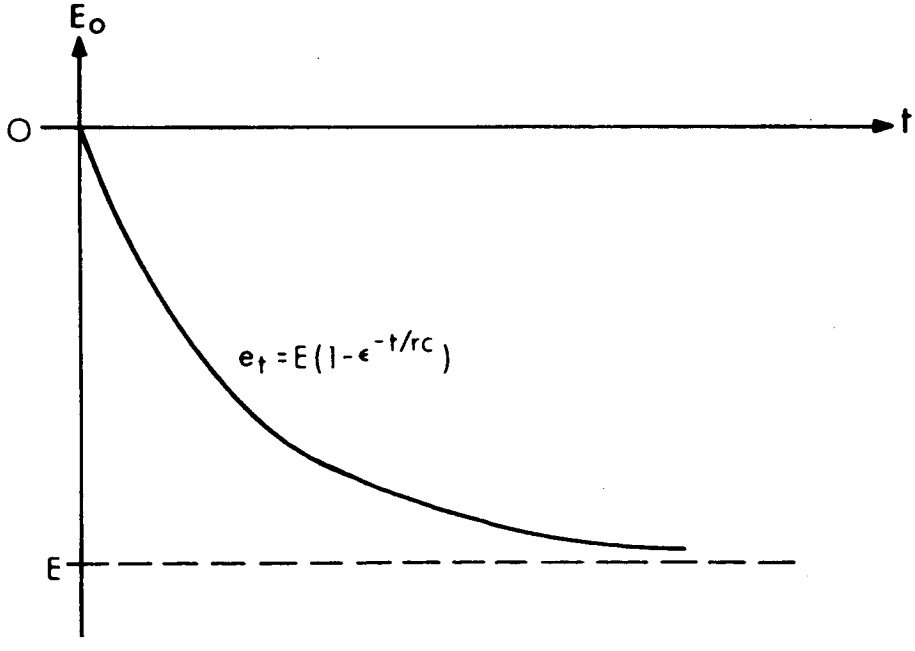

Figure 39. Response to Step Negative Input

If the frequency is 10 kHz and E_p is 1000 volts, the rate of charge is

$$-2\pi \cdot 10^4 \cdot 10^3 \text{ volt/sec}$$

$$= 63 \times 10^6 \text{ volt/sec}$$

Now consider a value for the cathode follower resistor, R13. If one selects E3 = -E4 = 2500, knowledge of the power dissipation limit of V2 will allow the choice of the lowest allowable value for R13. The maximum allowable plate dissipation is 12 watts; the maximum dissipation in V2 will occur when the plate resistance of V2 equals R13; i.e., when the output voltage is midway between the two power supplies.

$$P = \frac{E^2}{R}$$

$$R_{13} = \frac{2500^2}{12} = \frac{6.25 \times 10^6}{12}$$

$$= 0.52 \text{ M}\Omega$$

There is, however, a current limitation of 5 mA average on this triode. Maximum current will flow at an output of +1500 volts, i.e., maximum voltage across the load resistor. The maximum load current is given by

$$I_{max} = \frac{1500 \times 2500}{0.52 \times 10^6} \text{ A}$$

$$= 7.7 \text{ mA}$$

This maximum current may be reduced through reductions in the power supply voltages but, at this point, it is expedient to calculate the maximum rate of negative swing (Fig. 37).

The response of the output voltage to a step negative input will be a negative exponential shape asymptotic to the negative supply voltage, -E (Fig. 39). The output voltage is given by the equation

$$e_t = -E\left(1 - \epsilon^{-t/RC}\right)$$

where

e_t = the instantaneous voltage at time t
E = the negative supply potential
t = the time
R = R13
C = the load capacitor

Two things are now of interest: (1) the minimum time for the output voltage to reach, say, -1000 volts, and (2) the time rate of change of potential at t = 0, i.e., the initial slope.

The first of these may give a qualitative idea of the distortion to be expected on a sine wave of a given frequency The second may be used to calculate the maximum sine wave frequency on which there will be no detectable distortion.

The time for the output to reach -1000 volts may be calculated as follows.

$$e_t = -E\left(1 - \epsilon^{-t/RC}\right)$$

substitute

$e_t = -1000$

$E = 2500$

$R = 0.52 \times 10^6\ \Omega$

$C = 65\ pF$

$$-1000 = -2500\left(1 - \epsilon^{-t/RC}\right)$$

$$= -2500 + 2500\ \epsilon^{-t/RC}$$

$$\frac{3}{5} = \epsilon^{-t/0.52 \times 10^6 \times 65 \times 10^{-12}} = \epsilon^{-t/34 \times 10^{-6}}$$

$$\frac{5}{3} = \epsilon^{t/34 \times 10^{-6}}$$

$$34 \times 10^{-6} \log_\epsilon 1.667 = t$$

$$t = 17.4 \times 10^{-6} \text{ seconds}$$

One may show that the maximum frequency of undistorted sine wave that will be passed by a system is related to system rise time by the expression

$$f = \frac{1}{2\pi\ t_r}$$

If the rise time were 17.4 μsec as calculated above, this gives a frequency of 9.2 kHz.

The time rate of change of potential at t = 0 will correspond to the maximum rate.

At t = 0

$$\text{current } i_o = \frac{2500}{0.52 \times 10^6} \text{ A}$$

$$= \frac{d_V}{d_t}$$

With the capacitor, C,

$$\frac{dv}{dt} = \frac{1}{C} \frac{d_V}{dt}$$

$$= \frac{10^{12}}{65} \times \frac{2500}{0.52} \times 10^{-6}$$

$$= 74 \times 10^6 \text{ volt/sec}$$

It was previously calculated that the maximum time rate of change of potential of a 1000 volt single amplitude peak, 10 kHz, sine wave was 63×10^6 volt/sec. So, at least with a 2000V p-p sine wave, response to 10 kHz may be approached.

In order that the average current limitation of 5 mA for the Victoreen 7235 triode not be exceeded, either the power supply potential may be reduced or the cathode resistor may be increased. To simplify the design, as a first step the power supply will be reduced as much as possible. Inspection of the plate characteristic curves for both the 7234 pentode and 7235 diode indicates a minimum potential across the tube of 500 volts; since a peak output of 1500 volts is desired, the practicality of a ±2000 volt supply will be checked.

Recalculations for R13 based on 12 watt power limitation:

$$R13 = \frac{2000^2}{12} = 0.334\ M\Omega$$

Maximum anode current check:

$$I_{max} = \frac{1500 + 2000}{0.334 \times 10^6} = 10.5\ mA$$

Calculation of R13 based on 5 mA average current limitation

$$R13 = \frac{1500 + 2000}{5} = 0.6\ M\Omega$$

Calculation of time to reach -1000 volt from 0 volt with 2000 volt power supply and 0.6 MΩ cathode follower load resistor

$$e_t = -E\left(1 - \epsilon^{-t/RC}\right)$$

$$1000 = -2000 + 2000\ \epsilon^{-t/0.6 \times 10^6 \times 65 \times 10^{-12}}$$

$$0.6 \times 10^6 \times 65 \times 10^{-12} \log_\epsilon 2 = t$$

$$t = 39 \times 10^{-6} \times 0.69$$

$$= 27\ \mu sec$$

The frequency to which this corresponds is given by

$$f = \frac{10^6}{2\pi \times 27} = 5.9\ kHz$$

The maximum negative swing rate, with V2 cutoff, an 0.6 MΩ cathode resistor, and a -2000 volt supply potential is given by

$$i_o = \frac{2000}{0.6 \times 10^6}$$

$$\frac{dV}{dt} = \frac{1}{c}\frac{dq}{dt}$$

$$= \frac{10^{12}}{65} \times \frac{2000}{0.6} \times 10^{-6}$$

$$= 51 \times 10^6 \text{ volt/sec} \quad \text{(c.f. the required } 63 \times 10^6 \text{ volts/sec)}$$

These several foregoing calculations show that, as presently envisaged, this cathode follower output stage will not provide full power output at 10 kHz, at least if the signal is a 2000 volt p-p sine wave. Reduction of signal amplitude would raise the undistorted upper frequency response, and will provide satisfactory response during normal operation.

With a maximum slew rate of 51×10^6 volt/sec, the maximum amplitude of 10 kHz sine wave that may be passed without distortion is 810 volts single amplitude peak, i.e., 1620 volt p-p (c.f. 2 kV desired).

Since the maximum power dissipation of the output triode may be related to the cathode load resistor and the supply voltage, from which the maximum slew rate may be calculated, the minimum power supply voltage necessary to achieve response to 10 kHz for a 2000 volt p-p sine wave may be calculated. A supply voltage of 2.93 kV is indicated, which will give a load resistor of 0.72 MΩ and a maximum current of 6.1 mA at +1500V dc output.

The limitations exist, but may be modified in several ways. At this point they are accepted and the following values chosen

$$E3 = -E4 = 2000V \text{ dc}$$

$$R13 = 0.6\ M\Omega\ 12 \text{ watt.}$$

These values will allow satisfactory operation within the desired operating passband.

5.2.2.2 Calculation of Anode Load Resistor

The vacuum tube V1 was chosen to be a Victoreen 7234 pentode. From the plate characteristic (Fig. 40) a suitable load resistor may be chosen given that the supply voltage is about 4 kV and the maximum allowable current is 5 mA. It is necessary that this pentode operate with about 500V dc across it. This point, viz., 500V dc at 5 mA, and the cutoff point, viz., 4000V dc at 0 mA, enables an optimum load line to be drawn.

The load line so constructed represents a resistor value calculated as follows:

$$R11 = \frac{3500}{5 \times 10^{-3}} = 0.7\ M\Omega$$

5.2.2.3 Voltage Gain

The closed loop voltage gain was given as 200X. In order to maintain satisfactory stability an open loop gain of at least 2000X is desirable. The large signal voltage gain of the pentode V1 may be calculated from the plate characteristic and the load line for 0.6 MΩ. It

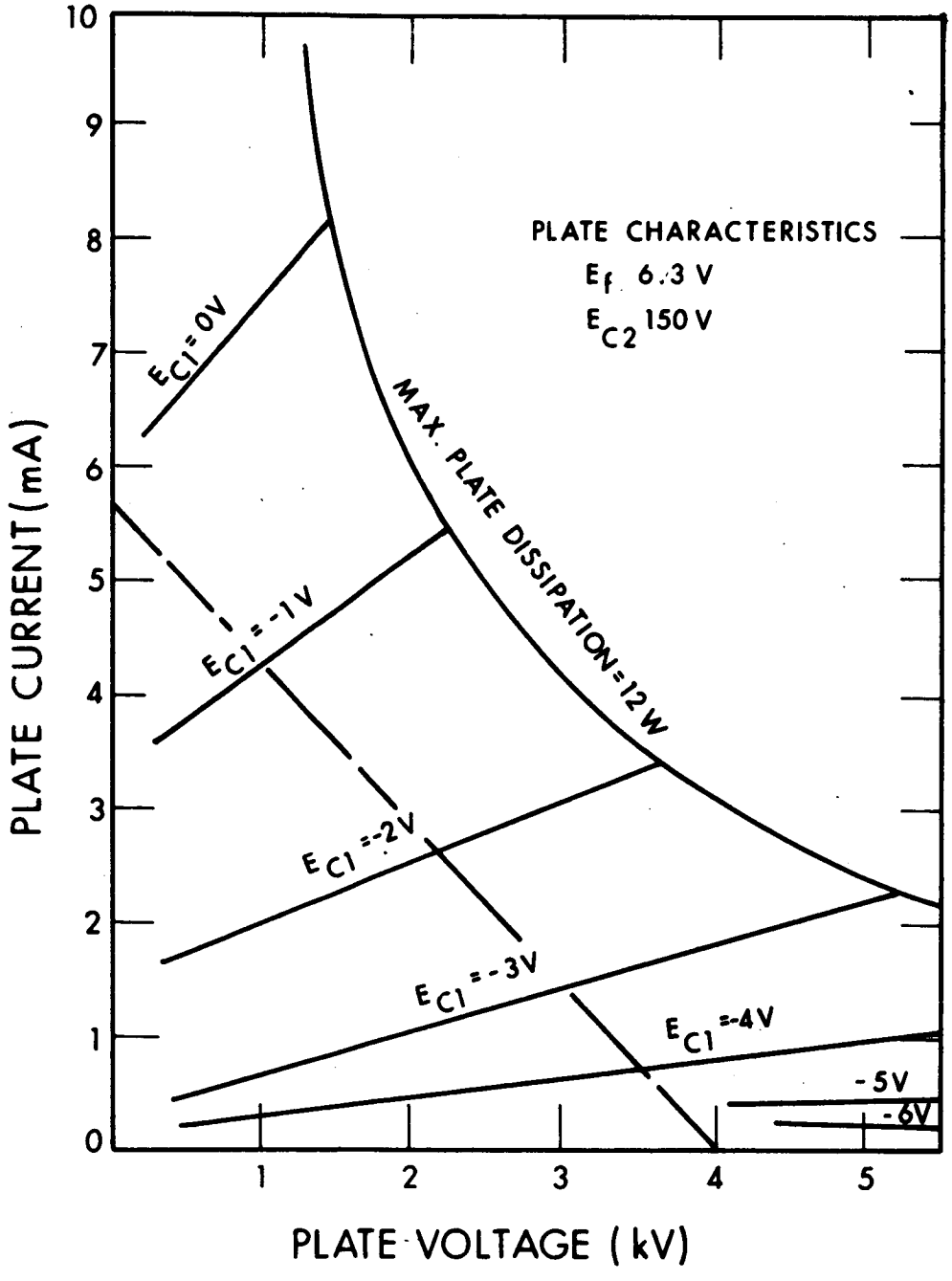

Figure 40. Plate Characteristic of the Victoreen 7234 High Voltage Pentode

will be seen that about the operating point (approximately 2 kV) a 1 volt change in either direction at the control grid will cause a change of about 1100 volts at the anode. The voltage gain of the stage is given by

$$A_v = \frac{\Delta E_o}{\Delta eg} = 1100X .$$

A voltage gain from the first stage of about 30X, has been selected allowing for some degeneration in that stage so that the second stage will provide a voltage gain of

$$\frac{2000}{30} \approx 67X.$$

In order to allow for losses in the cathode follower and voltage dropping circuit (Q3), a 10 percent allowance is added to this figure to give about 75X. Since ample gain may be obtained from V1, cathode degeneration will be added to improve stage stability and reduce the negative feedback in the overall loop in anticipation of improved closed loop stability.

The voltage gain, A_{vc}, of a vacuum tube is given by

$$A_v = - \frac{g_m R^1}{1 + g_m R_K}$$

where R^1 is the effective anode load, usually $r_p \| R_L$

R_K is the unbypassed cathode resistor

g_m is the tube transconductance (mhos)

Transconductance is given by the expression

$$g_m = \left| \frac{\partial i_a}{\partial e_g} \right|_{e_a}$$

i.e., the ratio of change in anode current produced by a change in control grid potential with the anode-to-cathode potential maintained constant.

Scrutiny of Fig. 40 allows an estimate of g_m to be made. For a change of about 1/2 volt about the operating point a current change of about ±1-1/4 mA results in anode current
hence

$$g_m = \frac{1\text{-}1/4 \times 10^{-3}}{1/2} = 2.5 \times 10^{-3}$$

The appropriate R_K, actually R12, for V1 is calculated as follows:

Voltage gain desired from V1, A_v, = 150X

Anode load resistor, R_L, $0.6 \times 10^6 \Omega$

Dynamic anode resistance, $r_p = \left| \frac{\partial e_a}{\partial i_a} \right|_{e_g}$

determined from Fig. 40 = $2 \times 10^6 \Omega$

$$A_v = - \frac{g_m R^1}{1 + g_m R_K}$$

$$R^1 = \frac{r_p R_L}{r_p + R_L} = \frac{2 \times 10^6 \times 0.6 \times 10^6}{(2 + 0.6) \times 10^6} = 0.46 \times 10^6$$

Rearranging the voltage gain expression to give R_K we obtain

$$R_K = \frac{R^1}{A_v} - \frac{1}{g_m}$$

Substituting the above values gives

$$R_K = \frac{0.46 \times 10^6}{150} - \frac{1}{2.5 \times 10^{-3}}$$

$$= 3.07 \times 10^3 - 0.4 \times 10^3 \approx 2.7 \text{ K}\Omega$$

Make R12 = 2.7 KΩ

At the operating point the anode current is 2.9 mA which will give a potential drop across R12 of 8 volts. Since the grid of V1 will be more positive than the base of Q3 (to allow an operating negative bias on Q3 collector-base diode) the cathode of V1 will require connection to a source of potential evaluated from the negative rail. The circuit of Fig. 36 has been modified to satisfy this need and is shown in Fig. 41.

A series of zener diodes may be readily chosen for the CR1, 2, and 3 string. Each diode, especially CR3, should have a modicum of temperature compensation; a wide variety of zeners are available so the selection is not made at this time. If a 10 mA standing current is selected, the dissipations of CR1, 2, and 3 are 1.5 watts, 60 mW, and 500 mW respectively; the diodes would be selected from groups of diodes, the dissipation of which matched the respective needs.

A current must be selected for the voltage dropping network of R9. If it is too low, e.g. 1 μA, resistor R9 is awkwardly high and it is difficult to design a good current regulator. If the current is

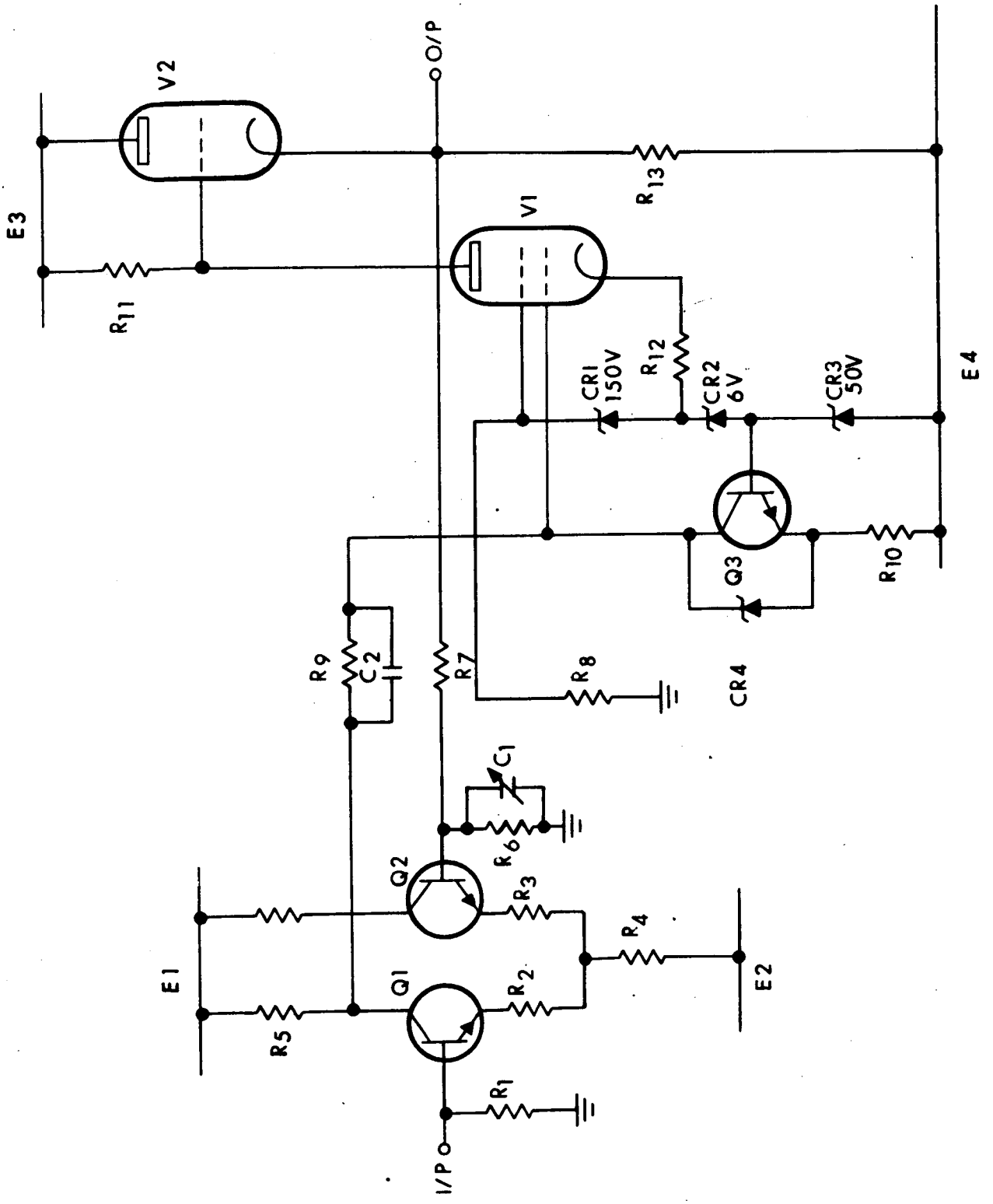

Figure 41. Modified Hybrid Amplifier

very high, e.g., 100 mA, excessive power is consumed. The current chosen is 1 mA. The collector of Q1 will be at some positive potential, e.g., +30 V, while the grid of V1 will be near the negative EHT supply rail, e.g., -1950V. The drop across R9 will be the difference between these two, viz., approximately 1980V dc. The value of R9 is given by

$$R9 = \frac{1980}{1 \times 10^{-3}} = 1.98\ M\Omega$$

Note that the power dissipation in R9 is $1980 \times 10^{-3} \approx 2$ watts.

Examine, now, the voltage transfer character of this network. The source impedance for the constant current regulator (CCR) is R9. The equivalent impedance of the CCR is RS (Fig. 42).

It is clear that the voltage transfer, ξ, is given by

$$\xi = \frac{e_o}{e_i} = \frac{RS}{R9 + RS}$$

$$= \frac{1}{1 + R9/RS}$$

The purpose of this network is to achieve a dc voltage transfer without loss, i.e., $\xi = 1$. In order that $\xi \rightarrow 1$ it is necessary that RS >> R9. R9 is chosen to be 1.98 MΩ so the effective impedance of the CCR should be at least 20 MΩ. If it was 20 MΩ, ξ would calculate to be

$$\xi = \frac{1}{1 + \frac{1.98}{20}} \approx 0.91$$

representing a loss of 9 percent.

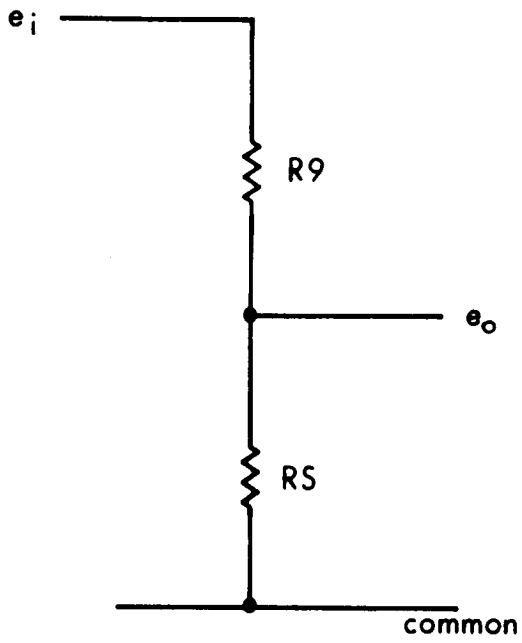

Figure 42. Equivalent Circuit of R9 and Current Regulator

A voltage gain of 150X was completed for the second stage. A full scale output voltage of ±1500 volts and a 0.95 gain for the emitter follower implies that the input at the grid of V1, and the swing on the input to the CCR, is

$$\frac{1500}{0.95 \times 150} = \pm 15.8 \text{ volts}$$

$$\approx 32 \text{ volt swing}$$

Assume that the 2N1711 transistor has been selected for the Q3 position. Collector to emitter breakdown is 50 volt minimum, so, for protection during turn-on transients, etc., a 40 volt zener diode, CR4, is placed across Q3 from collector to emitter.

Since a 1 mA collector current and a 50 volt bias at the base have been selected, the value of the emitter resistor, R10, may be chosen as follows:

$$R10 = \frac{V_B - V_{BE}}{I_e}$$

where V_B is the base potential 50V

V_{BE} is the base-emitter drop 0.6V

I_e is the emitter current

$$I_e = (1 + 1/\beta)\, I_c$$

$$R10 = \frac{50 - 0.6}{10^{-3}(1 + 1/70)} = 48.7 \text{ K}\Omega$$

Where a value of 70 is taken from the data sheet as being typical for a 1 mA collector current.

In the event that the effective impedance of the CCR using a single transistor is insufficient, i.e., introduces an excessive insertion loss, there are three other schemes available, one of which will certainly cure the situation. These alternatives are shown in Fig. 43.

5.2.2.4 Input Differential Pair

A voltage gain of 30X was allocated to this first stage. The input common mode level is to be at 0V dc nominal and the output full scale swing need not exceed ±15 volts. In order to allow sufficient potential to allow such a change at the collector, a supply for E1 and E2 of ±50 volts is selected. The operating point for the collector of Q1 is to be set at 30 volts; the collector may swing, therefore, to a high of 45 volts and a low of 15 volts.

For this position a matched dual transistor of moderate breakdown voltage should be used and the 2N2060 is selected. As a first approximation, the voltage gain of this shape may be written as

$$\frac{e_o}{e_i} = \frac{R5}{R2(1 + 1/\beta)}$$

Since $\beta >> 1$ typically, this may be further simplified to R5/R2. Consideration of the device collector characteristics indicates a 4 mA collector current as satisfactory. The collector load resistor, R5, is given by

$$R5 = \frac{60 - 30}{4}\ k\Omega$$

$$= 7.5\ k\Omega$$

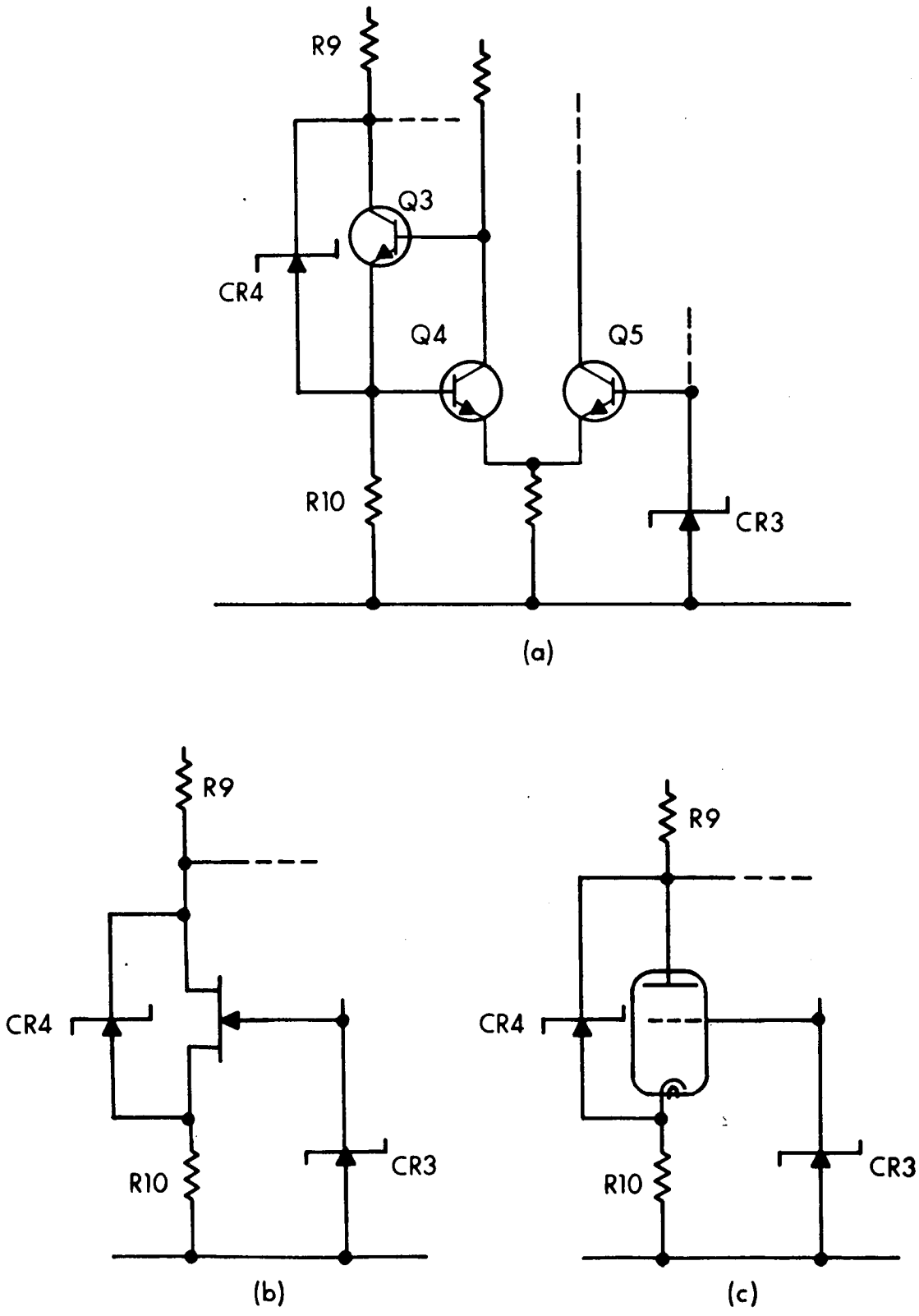

Figure 43. Alternative Current Regulators

At an output level of 30 volts plus 15 volts, the collector current would be 15/7.5 = 2 mA; and at the low output level the collector current would be 45/7.5 = 6 mA. The collector current will therefore swing ±2 mA about the nominal 4 mA balanced value.

The emitter resistor, R2, will be given approximately by

$$R2 = \frac{R5}{\text{voltage gain}}$$

$$R2 = \frac{7500}{30} = 250\Omega$$

This value for R2 will tend to give a stage gain that is low, since the intrinsic emitter resistance, r_e, of the transistor has been neglected. A value of 220Ω is chosen for R2.

A value of 220Ω is also chosen for R3 to maintain circuit dc balance. The median current through Q2 is set equal to that in Q1 at 4 mA. The potential drop across R2 and R3 is, therefore, 4 x 0.22 ≈ 0.9 volt. The current through R4 would be, nominally, 8 mA for a potential drop of $(50 - V_{BE} - V_{R2}) = 50 - 0.6 - 0.9 = 48.5V$.

$$R4 = \frac{48.5}{0.008} \approx 6\Omega$$

Power dissipation = 48.5 x 0.008 = 0.39 watt

therefore select a 1/2 watt resistor

5.2.2.5 Closed Loop Gain

The input impedance, Z, of a stage such as Q1 is given approximately by

$$Z = (\beta + 1) R_e$$

where β is the usual term (typically 80 here)

R_e is the resistance in the emitter

Many other terms are neglected here, such as intrinsic emitter resistance, negative voltage feedback factor, and so on. One may expect the input impedance of Q1 to be

$$Z = 80 \times 220$$

$$= 17.6\ k\Omega$$

Applied to this differential input stage is negative feedback from the output stage. When a positive signal is applied to the input, Q1, the phasing through the amplifier is such that the output will also move positive. A small fraction of this output voltage is applied back to the input stage through the feedback network of R7 and R6. The base of Q2 will move positive, causing the R3 and R4 mode to move positive, which will reduce the input current drawn by Q1; i.e., the input impedance will be raised by the feedback factor.

$$\text{Feedback factor} = \frac{\text{open loop gain}}{\text{closed loop gain}}$$

Open loop gain is equal to the product of the stage gains of all four stages.

First stage (calculated)	30X
Voltage dropping stage (est. in.)	0.9
High voltage stage (calculated)	150X
Cathode follower output (est. in.)	0.98

Open loop gain = $30 \times 0.9 \times 150 \times 0.98$

= 3960X

Closed loop gain required 200X

For the amplifier shown in Fig. 44,

$$e_g = e_i - e_f$$

$$= e_i - \frac{R6}{R6 + R7} e_o$$

$$e_g = \frac{e_o}{A}$$

So

$$\frac{e_o}{A} = e_i - \frac{R6}{R6 + R7}$$

rearranging to give

$$\frac{e_o}{e_i} = A^1 = \frac{1}{\frac{1}{A} + \frac{R6}{R6 + R7}}$$

This formula will allow calculation of the value for either R6 or R7. It is desirable that R6 + R7, the internal load upon the output, be as light as possible. The maximum value that R6 can assume is related to the β of Q2 and the effective input impedance of the stage.

As previously noted the input impedance of the amplifier, 17.6 kΩ, will be raised by a factor of 3960/200, to give a value of about 350 kΩ. Assuming that the β of Q2 is 100X at 4 mA collector current, the base current drawn will be 40 μA; if an input resistor value of 10 kΩ were chosen, for R1 and R6 (they should be balanced for temperature compensations, one might expect the base potential of Q1 and Q2 to be at $-(10^4 \times 40 \times 10^{-6})$V with respect to ground, viz., -0.4 volt.

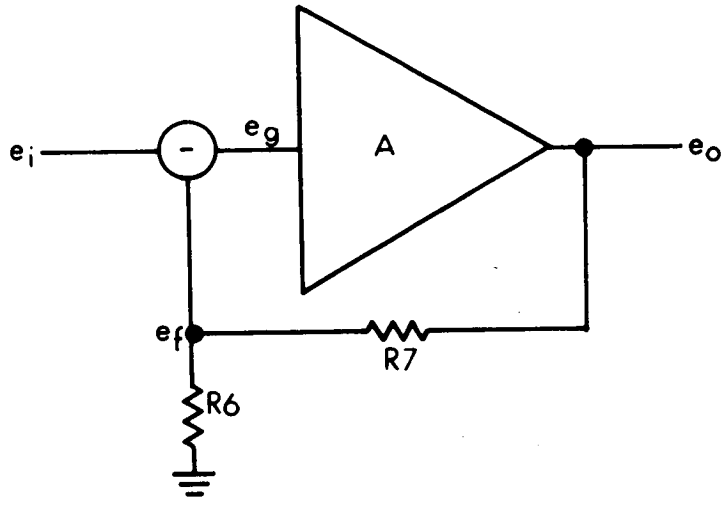

Figure 44. Feedback Amplifier

Now, from the closed loop gain equation we may calculate the value of R7 with respect to R6:

$$A^1 = \frac{1}{\frac{1}{A} + \frac{R6}{R6 + R7}}$$

$$R7 = \left(\frac{1}{\eta} - 1\right) R6$$

where $\eta = \frac{1}{A^1} - \frac{1}{A}$

Now $A^1 = 200$

$A = 3960$

so $\eta = .00475$

$\frac{1}{\eta} = 210$

thus

$R7 = 209 \times R6$

since

$R6 = 10\ k\Omega$ (neglecting the 350 $k\Omega$ load of Q2)

$R7 = 2.09\ M\Omega$

make

$R7 = 2.1\ M\Omega$

Now across R7 essentially 1500V potential may exist. The power dissipated in R7 under these conditions is E^2/R.

$$\text{Power} = 1500^2/2.1 \times 10^6$$

$$= 1.07 \text{ watts}$$

make

R7 a 2 watt resistor.

It might be advantageous that a modicum of high frequency peaking be added; this may be done through the effect of C1. As the frequency increases the shunting effect of C1 may be used to reduce the impedance at the base of Q2, reducing the negative feedback, and increasing the closed loop gain. This may be valuable but only up to a point since as the frequency increases further the amplifier gain may continue to rise with resultant problems of stability. One may settle for a maximum peaking effect of, say, 10 percent by placing in series with C1 a resistor of value 10 R6, viz., 100 kΩ. A suitable value for C1 is 0.1 μF which has an impedance of 1.6 kΩ at 1 kHz; this network is, of course, not essential to the operation. The circuit of the final amplifier is shown in Fig. 45.

The bleed resistor for the zener diode strip still requires calculation. A current of 5 mA appears more suitable than the 10 mA originally chosen, so the value of the resistor is given by

$$R8 = \frac{2000 - (50 + 6 + 150)}{5 \times 10^{-3}}$$

$$= \frac{1794}{5}\ k\Omega$$

$$= 360\ k\Omega$$

$$\text{Power dissipation} = 1794 \times 5 \times 10^{-3}$$

$$\approx 10 \text{ watt}$$

5.2.2.6 Power Supply Needs

±60 volt supply: maximum current drain ≈ 10 mA

±2 kV supply: The positive power supply will have a minimum current drain of 10 mA; i.e., 5 mA for each of the vacuum tubes.

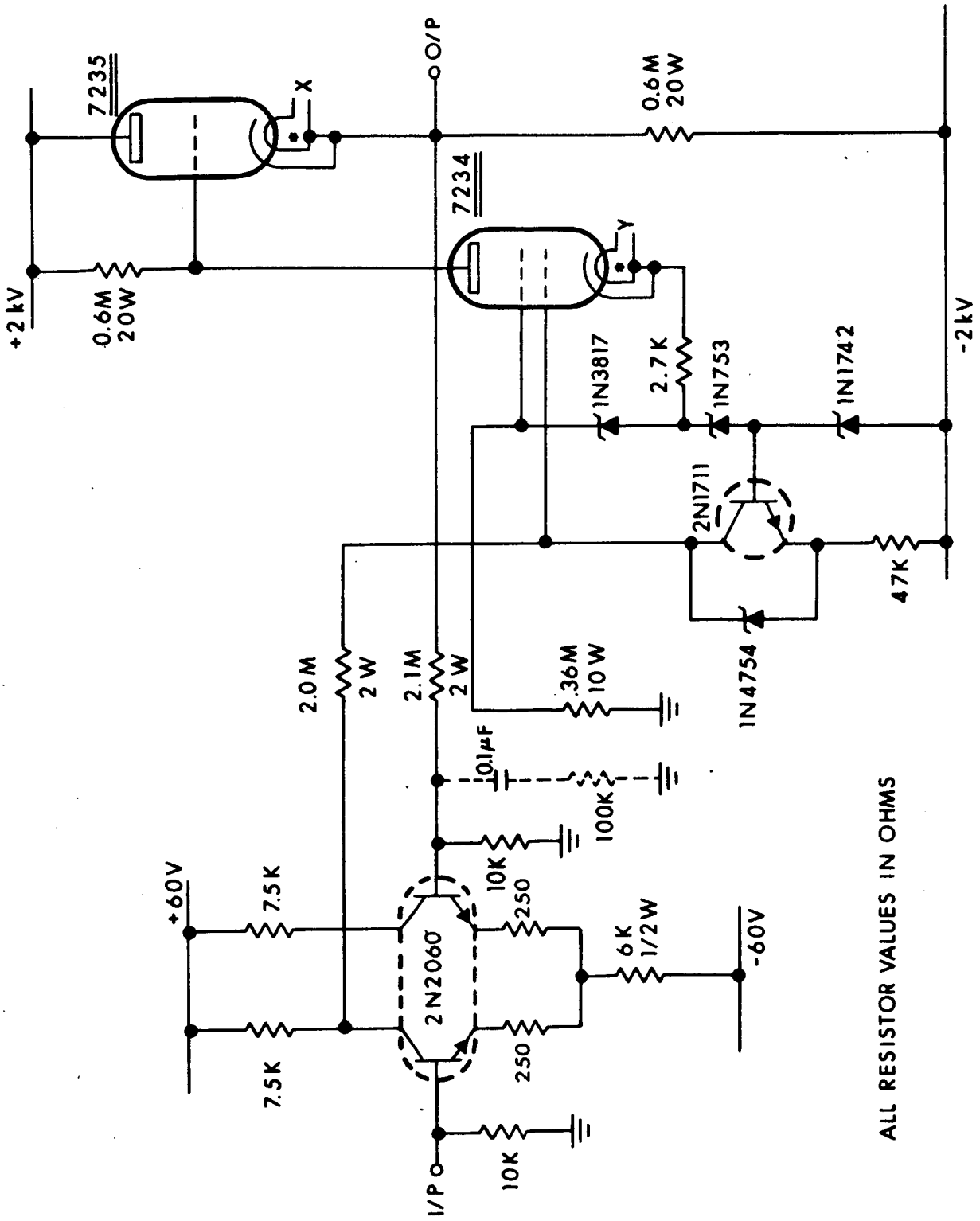

Figure 45. Final Amplifier Schematic

The negative supply will have an additional drain of 5 mA for the zener diode string, and 1 mA for the constant current dropping circuit.

+2 kV at 10 mA

-2 kV at 16 mA

5.3 LOW-FREQUENCY LENGTH CONTROL

The functional characteristics of the low-frequency length control were described in Subsection 4.3.4. It positions mirror M2 in response to error signals. A schematic is shown in Fig. 46.

The voltage, E_{17}, that appears at the slider of the 1500Ω feedback potentiometer can vary over the range of ±10V. In normal operation E_{17} will be within the range ±8V, corresponding to a total travel of 1000μ in. of mirror M2. A hard-over failure of the low-frequency servo would drive it out of this range until it reached the limit of its travel. The enormous torque (on the order of 1000 in.-oz) available at the shaft of the harmonic drive would destroy the internal mechanical stops in the feedback potentiometer. Such conditions might be more likely on a developmental prototype. Since the system moves comparatively slowly (on the order of 30 sec for full scale travel) such hard-over failures might not be detected visually. In order to guard against such damage normally-closed relay contacts open and remove power from the fixed phase of the servomotor if E_{17} drops below -9V or above +9V. A pair of operational amplifiers drive the relay coil. The outputs of both amplifiers are zero if $-9 < E_{17} < +9$. If E_{17} rises above +9V the output of the left hand amplifier switches to -6V and operates the relay. If E_{17} falls below -9V the output of the right hand amplifier switches to -6V and operates the relay.

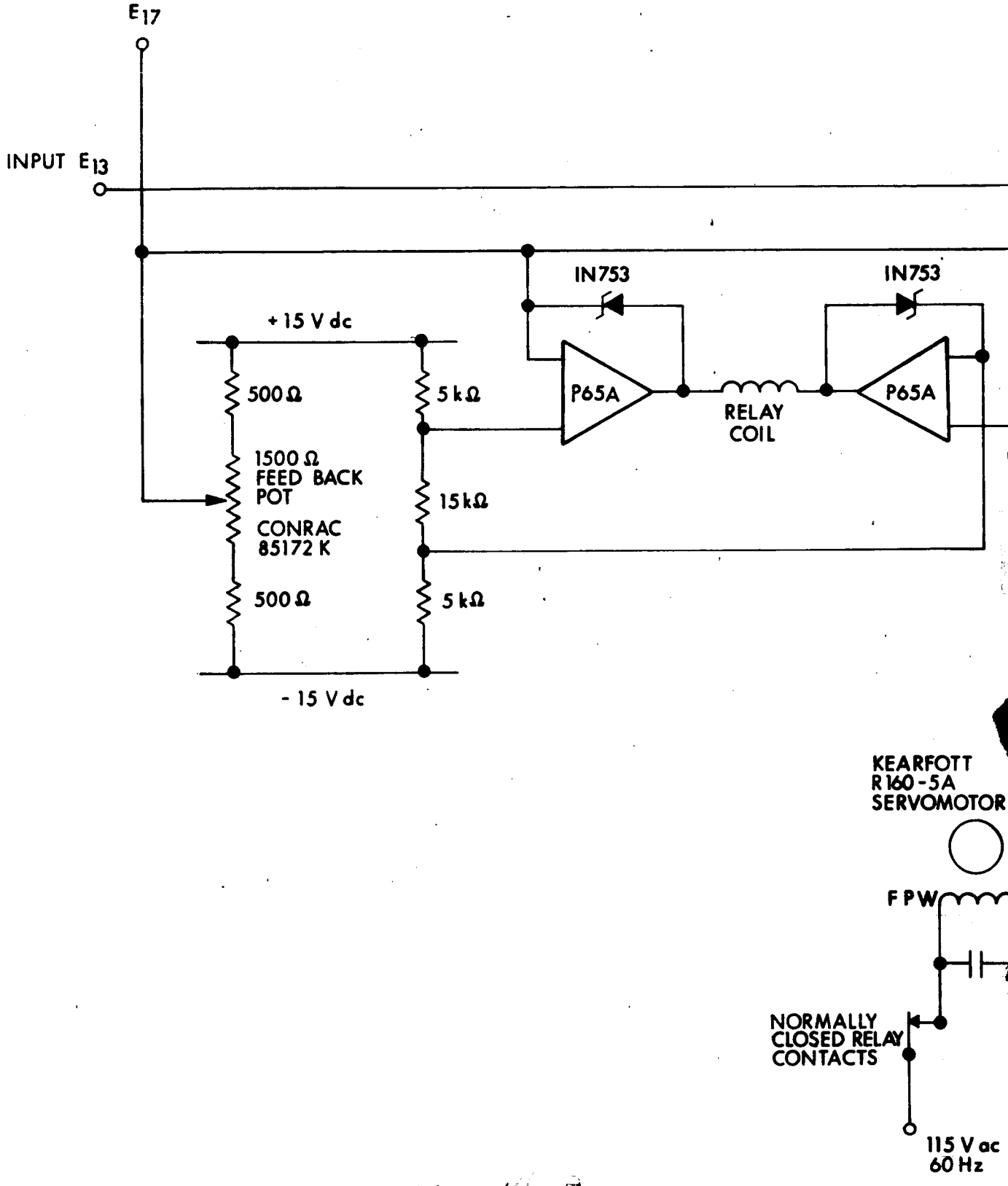
E17
INPUT E13
+15 V dc
500 Ω
1500 Ω
FEED BACK
POT
CONRAC
85172 K
500 Ω
- 15 V dc
5 kΩ
15 kΩ
5 kΩ
IN753
IN753
P65A
P65A
RELAY
COIL
KEARFOTT
R160-5A
SERVOMOTOR
F P W
NORMALLY
CLOSED RELAY
CONTACTS
115 V ac
60 Hz

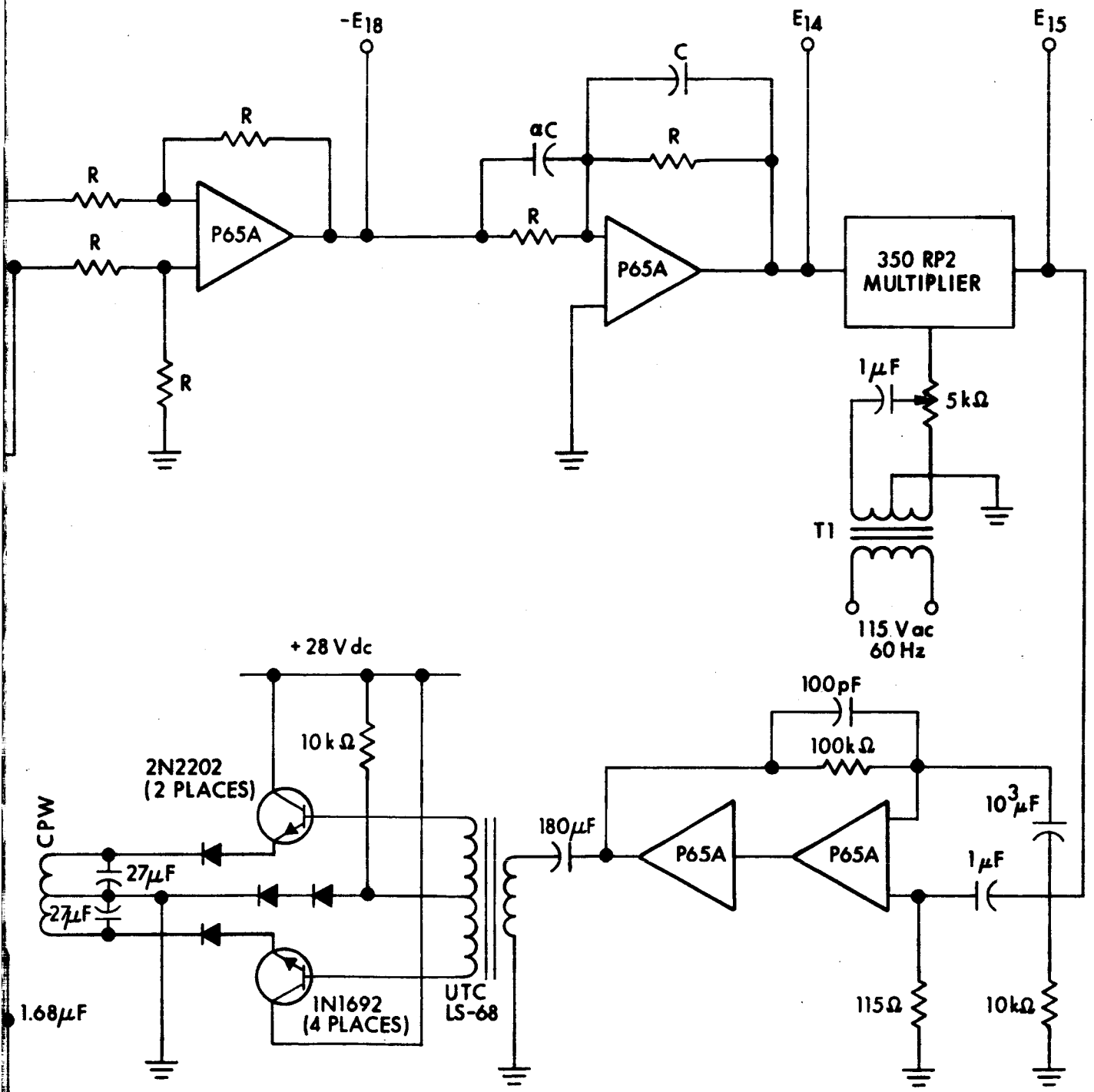

Figure 46.8 Schematic of Low-Frequency Length Control

The input voltage, E_{13}, is subtracted from the feedback signal, E_{17}, by a unity gain operational amplifier. The output, $-E_{18}$, of this amplifier to an active network with the transfer function

$$\frac{1 + \alpha RCs}{1 + RCs}$$

The characteristic described in Subsection 4.3.4 will be obtained if component values are selected so that

$$RC = 0.00586 \text{ seconds}$$

$$\alpha = 10$$

The output, E_{14}, of the active network is applied to one input of a Transmagnetics model 350RP2 multiplier. The second input of the multiplier is excited by a phase shift circuit consisting of a 1.0 μF condenser, a 5 kΩ potentiometer, and transformer, T1. The transformer has 14.14V RMS, center-tapped secondary. The condenser and potentiometer values are such that at mid-range the phase shift is approximately 90°. If the primary voltage is

$$115\sqrt{2} \sin 2\pi\ 60t$$

then at the input to the multiplier the voltage will be

$$10 \cos 2\pi\ 60t$$

The output, E_{15}, of the multiplier is equal to the product of the input voltages divided by 10. Thus, in this case

$$E_{15} = E_{14} \cos 2\pi\ 60t$$

which is seen to be a 60 Hz suppressed-carrier signal. The 90^{o} phase shift was made so that voltages on the fixed and control phases of the servo motor would have the required relationship.

The suppressed-carrier signal, E_{15}, is amplified by an ac amplifier composed of an operational amplifier and a Philbrick OSPB 50/50 current booster. Values selected provide a gain of 875. The booster provides sufficient power to drive the emitter-follower output stage. The output stage has a gain of 2, so that the voltage, E_{16}, accross the control phase of the servo motor is given by

$$E_{16} = 1750\, E_{15}$$

Both the control-phase winding (CPW) and the fixed-phase winding (FPW) are tuned to unity power factor by parallel capacitors.

5.4 OUTPUT CIRCUIT

The functional characteristics of the output circuit were described in Subsection 4.3.5. A schematic is shown in Fig. 47. The transfer function from E_3 to E_9 is given (Ref. 62) by

$$\frac{E_9(s)}{E_3(s)} = \frac{1 + \frac{2RC}{\alpha}\, s}{(1 + 2RCs)^2}\, K_{11}$$

This will have the desired characteristics if component values are chosen so that

$$RC = 2.5 \times 10^{-4} \text{ seconds}$$

$$\alpha = 10$$

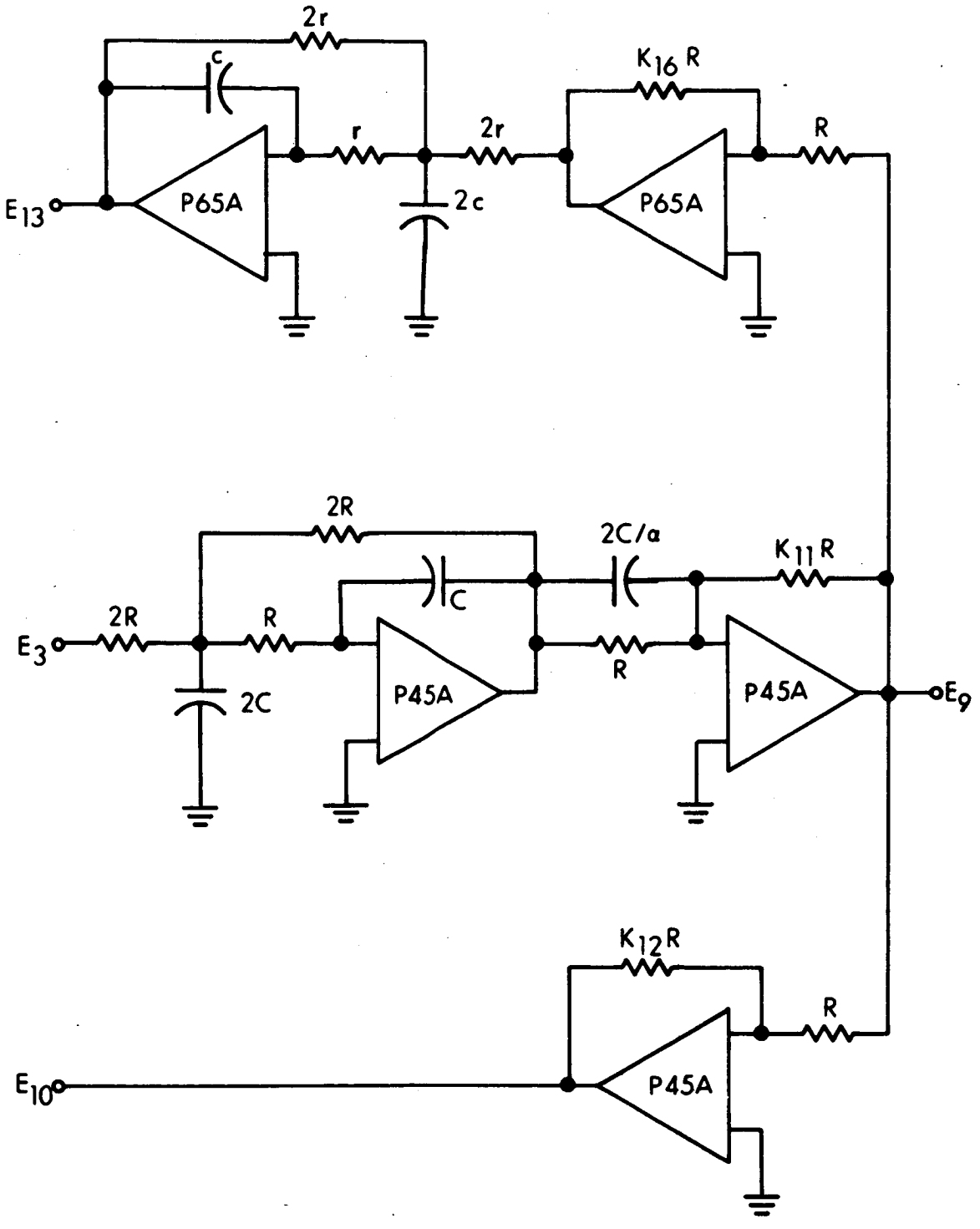

Figure 47. Schematic of Output Circuit

The transfer function from E_9 to E_{13} is given (Ref. 62) by

$$\frac{E_{13}(s)}{E_9(s)} = \frac{K_{16}}{(1 + 2rcs)^2}$$

The value of the time constant 2rc was discussed in Subsection 4.4.2. The transfer function between E_9 and E_{10} is simply K_{12}. A ganged switch will select values for the resistors $K_{11}R$, $K_{12}R$, and $K_{16}R$ in accordance with the chart in Subsection 4.3.5.

SECTION 6

OPTICAL DESIGN

The section describes the design of the resonator, its power output when discharge tubes are added, and the cavity used to modulate this output. It concludes with a description of the technique used to match the mode of the optical resonator to that of the modulated cavity. A schematic of the complete optical system is shown in Fig. 48.

6.1 OPTICAL RESONATOR

M3 is the remotely located mirror attached to the element the displacement of which is to be measured. M1 is the nearby fixed reference mirror. The radii, R_3 and R_1, of curvature of these two mirrors are both 2 meters. They are concave toward M2. They are coated so as to have maximum reflectivity. M4 is a plane ($R_4 = \infty$) mirror coated for maximum reflectivity. BS is a beam splitter coated so as to have 50 percent reflectivity for light incident at 45° in the s-polarization (perpendicular to the plane of incidence). The face of BS facing M1 is anti-reflection coated. M2 is concave toward M1 with a radius of curvature, R_2, of 44.3 meters. It is coated so as to have transmissivity on the order of 0.5 percent.

The distance from M1 to BS is $L_1 = 100$ cm. The distance from M3 to BS is $L_3 = L_1 + \Delta L = 110$ cm. The distance from the beam splitter to M2 is $L_2 = 5.7$ cm. The average resonator length, $L = d_1$, is

$$L = d_1 = \frac{L_1 + 2L_2 + L_3}{2} = 110.7 \text{ cm}$$

PRECEDING PAGE BLANK NOT FILMED.

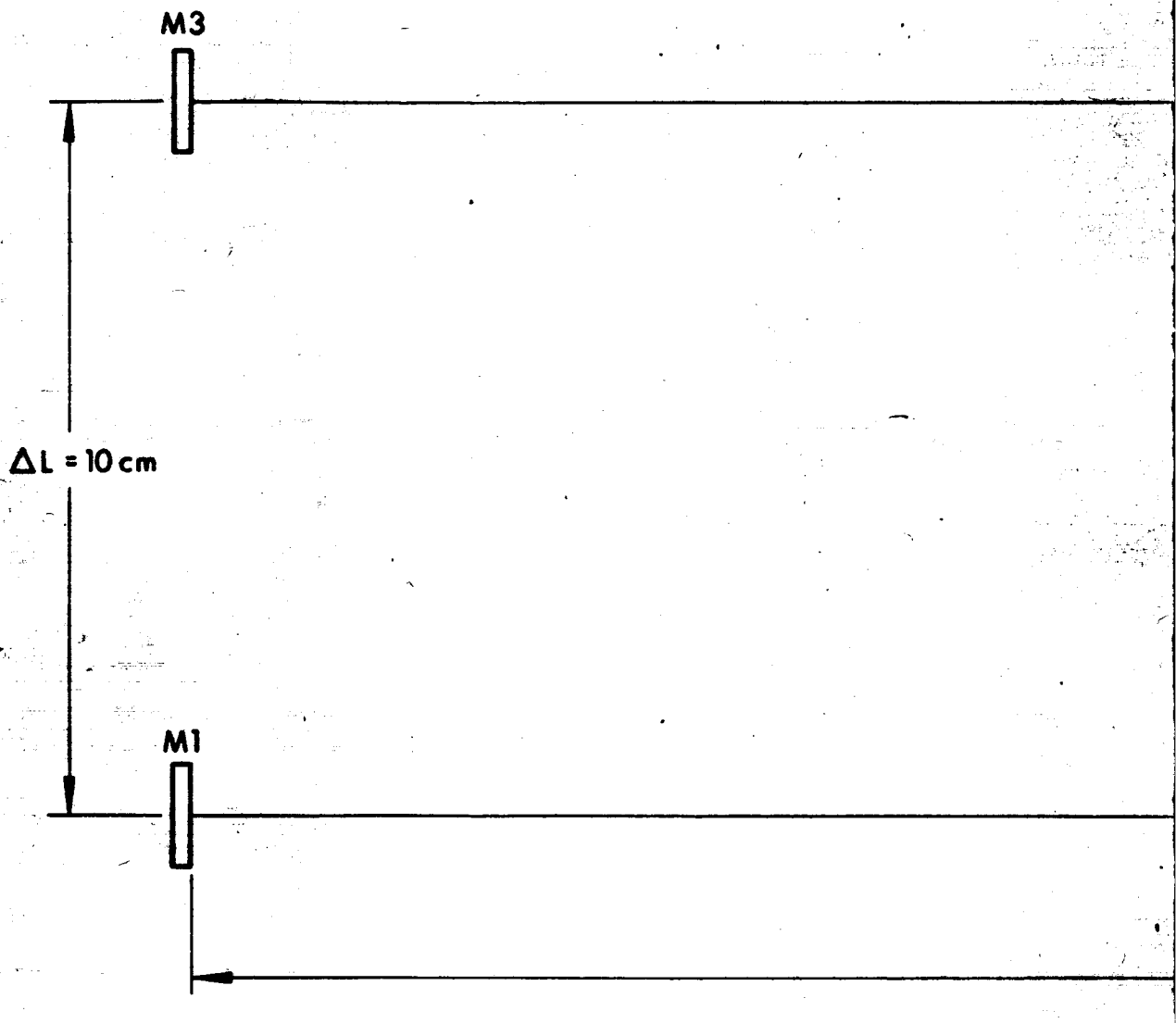

Fig. 48-A

141-A

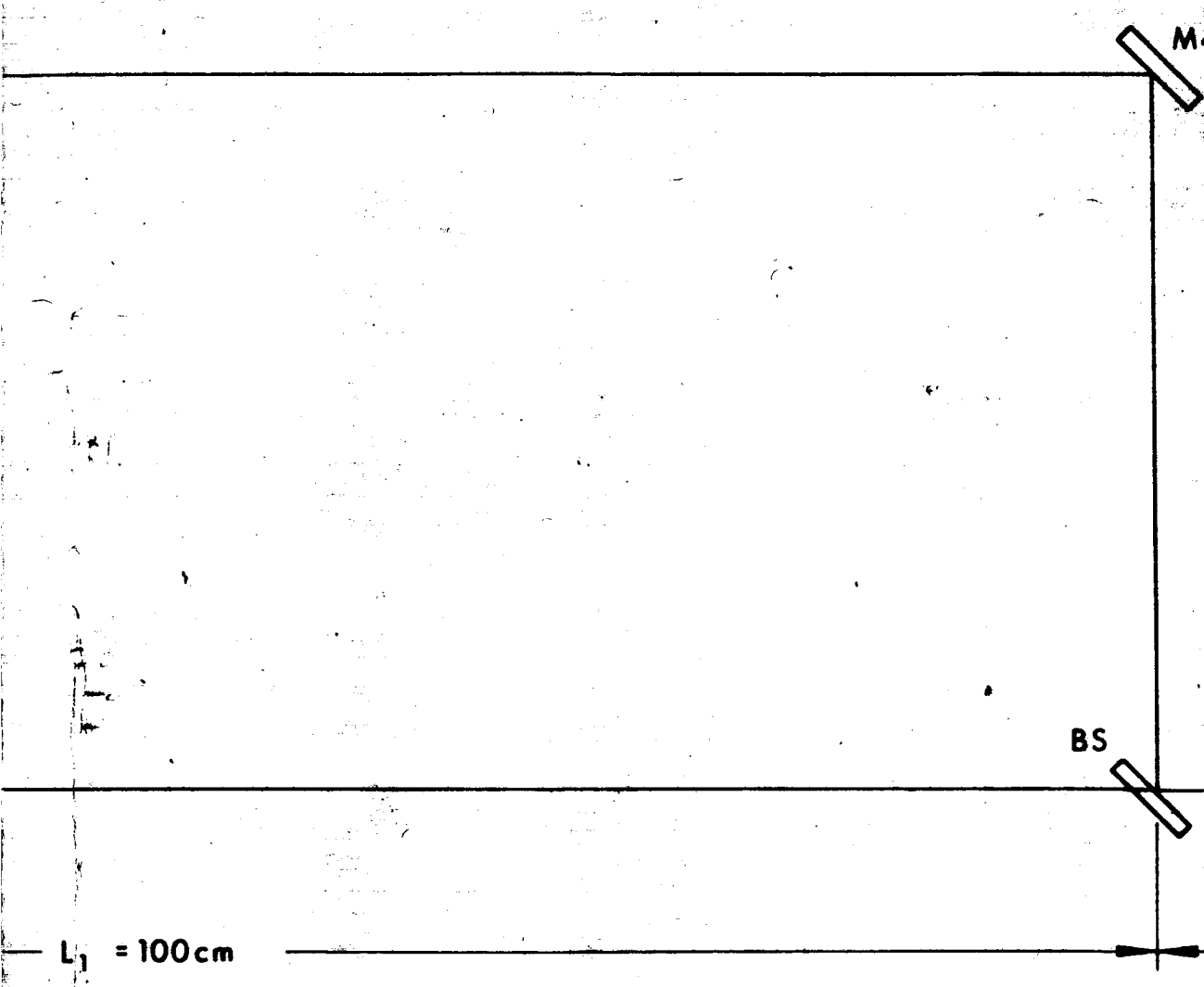

Fig. 48.B

141 - B

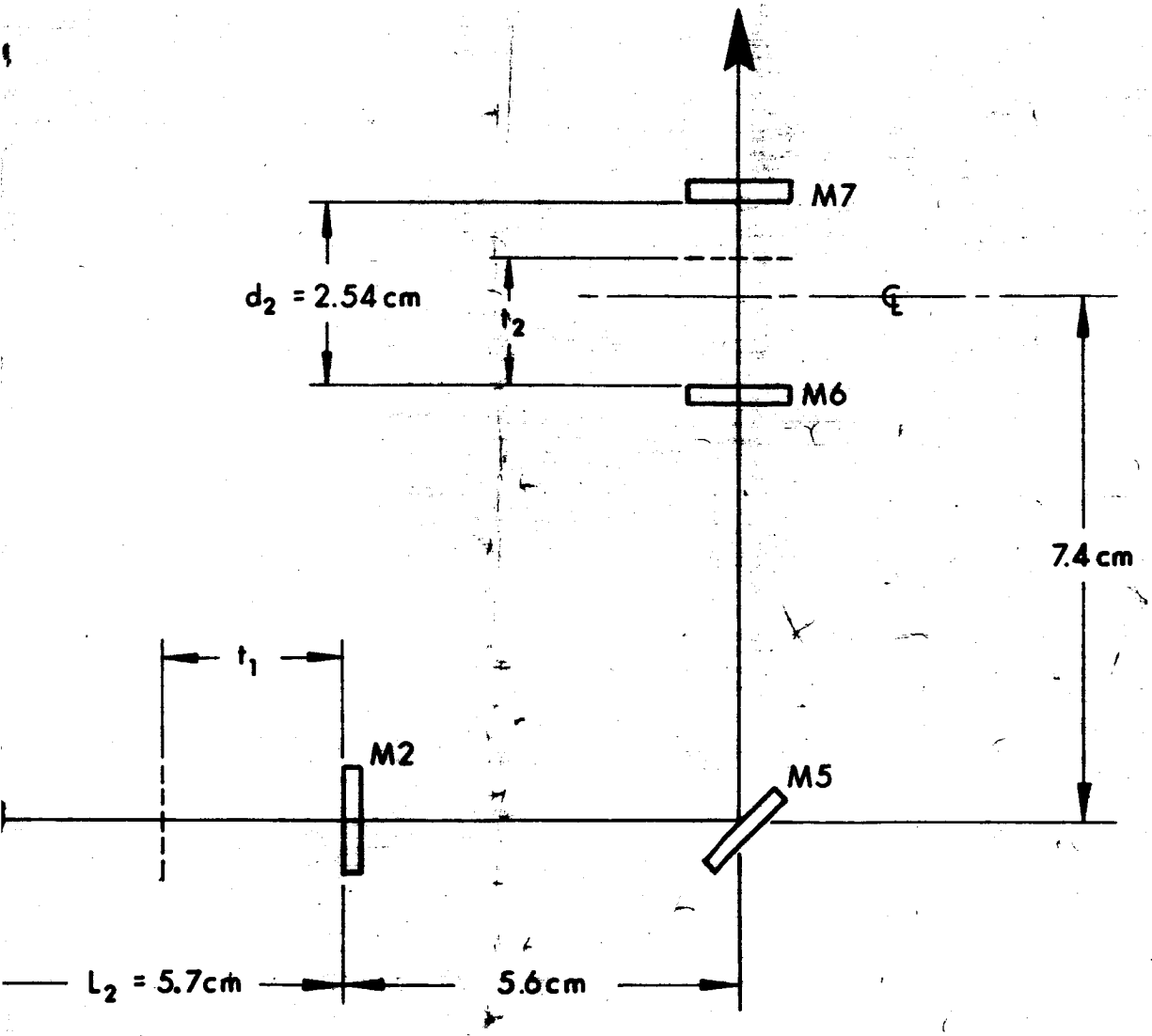

Figure 48. Schematic of Complete Optical System

A cavity of two mirrors M1 and M2 separated by d is semiconfocal if $R_1 = 2d$ and $R_2 = \infty$. The selection of $R_1 = R_3 = 2m$, $R_2 = 44.3$ m, and $d_1 = 1.107$ m makes this resonator essentially semiconfocal. It is located at $d/R_1 \simeq 0.55$, $d/R_2 \simeq 0.025$, on the Boyd-Kogelnik diagram (Fig. 24). This places it slightly above and to the right of the lower point marked ω in Fig. 24. This is in the stable region, and because of the proximity to ω, losses will be comparable to those of the confocal resonator.

6.2 POWER OUTPUT

The laser discharge tube consists of two 25 cm lengths, one in the M1-M2 arm, and one in the M3-M2 arm. The inside diameter, or bore, of both tubes is 2 mm. The incremental gain (Ref. 66) of the combined sections is

$$G_m = 3 \times 10^{-4} \frac{l}{d} = 0.075$$

or 7.5 percent per pass. The tube is filled with a mixture of 7 parts He to 1 part Ne. The optimum pressure (Ref. 66) is

$$p = \frac{4}{d} = 2 \text{ torr}$$

where d is in mm, and p in torr. The windows at either end of each tube are made from a borosilicate crown glass in order to introduce sufficient loss to suppress simultaneous oscillation at 3.39 μm (Ref. 67) in the infrared. These windows are set at Brewster's angle (Ref. 68) in order to reduce losses at 0.6328 μm to a minimum. The plane of the windows is oriented so that the emerging light is polarized with its electric field vector in the vertical plane. This is in consonance with the specification of the beam splitter in the previous section.

It can be assumed (Ref. 66) that aside from transmission out through M2, that the resonator losses are 0.2 percent per pass for each mirror surface and 0.05 percent per pass for each Brewster angle window. The losses are tabulated in Table III for both the M1-M2, and M3-M2 paths. For example, in the case of the M1-M2 path, a beam leaving M2 passes through the front surface, BS, and the rear surface, BS′, of the beam splitter, is reflected from M1, and returns through BS′ and BS. The contribution from the two Brewster angle windows is 0.1 percent for each path. The loss per pass is thus estimated to be 1.3 percent per path. If it is assumed that half of the energy is in each path, the average loss per path for the combined structure is also 1.3 percent.

TABLE III

Resonator Losses

Component	M1-M2	M3-M2
M2	0.2	0.2
BS	0.2	0.2
BS′	0.2	
M4		0.2
M1	0.2	
M3		0.2
M4		0.2
BS′	0.2	
BS	0.2	0.2
BL	0.1	0.1
	1.3%	1.3%

Having determined the gas pressure and gain of the discharge tube, and the loss due to the resonator, the power output can be calculated (Ref. 66, Ref. 69) as a function of the transmissivity of M2. The results of such calculations for three cases are as follows:

M2 Transmissivity, Percent	Power Output, Milliwatts
1.5	5.6
0.5	3.8
0.2	1.1

The optimum power output (Ref. 66) is 5.6 mW. For this design the highest power level is not required, and one of the more highly reflecting mirrors may be used. This will provide excess gain that can be utilized in looking at displacements through the window in a vacuum chamber.

These calculations assume complete suppression of the 3.39 μm oscillation and no loss out of BS (downward in Fig. 48). In order for the loss out BS to be minimized, the gains and losses of each path must be similar. Because of the difficulty in producing a beam splitter equal transmissivity and reflectivity, a series of several having reflectivities in a range extending a few percent on either side of 50 percent should be available during initial fabrication and checkout. As will be described in Section 7, the two discharge tubes are mechanically symmetrical and can be interchanged so as to optimize gain unbalance from this source. It is expected that by these techniques a power output of 2.0 mW will be obtained with a 0.5 percent mirror at M2.

6.3 MODULATED CAVITY

Light emerging from M2 is reflected through 90° by M5 and enters M6 of the modulated cavity. Light emerging from M7 falls on the photodetector. M6 has a radius of curvature, R_6, of 3.832 cm. It is concave toward M7, and coated so as to have a reflectivity of 98.5 percent. M7 is plane ($R_7 = \infty$) and coated so as to have a reflectivity of 98.5 percent. The mirrors are spaced at d_2 = 2.54 cm. The cavity is located at $d/R_1 \cong 0.65$, $d/R_2 = 0$, on the Boyd-Kogelnik diagram. This places it slightly to the

right of the lower point marked ω in Fig. 24. This is in the stable region, and close enough to ω that losses will be governed primarily by the reflectivity of the mirrors.

A layout of the cavity is shown in Fig. 49. Cavities of similar design have been found to have short term stability (Ref. 70) of better than two parts in 10^{10}. In the layout, items 1 and 2 are the mirrors M6 and M7. Item 3 is a hollow ceramic cylinder similar to that described in Section 5.2.1. It is supported on O-rings 4 and 5 that serve to decouple longitudinal changes in length of the aluminum cylinder, 6. The high thermal conductivity aluminum cylinder is heated by electric resistance heaters, 7 and 8. Its temperature is sensed by a resistance thermometer, 9. A temperature control system (Ref. 71) incorporating 7, 8, and 9 maintain the cavity at an average temperature that is controlled within $\pm$ 0.01°F. The cavity is isolated from atmospheric pressure fluctuations by hermetic seals, 10 and 11, and by end windows, 12 and 13. A satisfactory temperature gradient between the hermetically sealed, temperature-controlled aluminum cylinder, 6, and the local ambient is insured by enclosing it in a styrofoam liner, 14, within the outer housing, 15, end window, 16, and end plate, 17. The opening, 18, in the end plate, 17, will be closed by the photodetector. End windows (12, 13, and 16) are all antireflection coated on both surfaces. During local transportation, shock may cause longitudinal displacement of the cavity, 3. As long as the O-rings, 4 and 5, roll, and do not slip, the cavity will return to its original position after the cessation of the shock. The O-rings are restricted to their linear range by two fiber stop washers, 19 and 20.

The piezoelectric cylinder is 0.948 inch long, 0.572 inch outside diameter, and 0.328 inch inside diameter. It is supplied with two metallic electrodes, one covering the entire outer cylindrical surface, and one covering the entire inner cylindrical surface. This cylinder is made

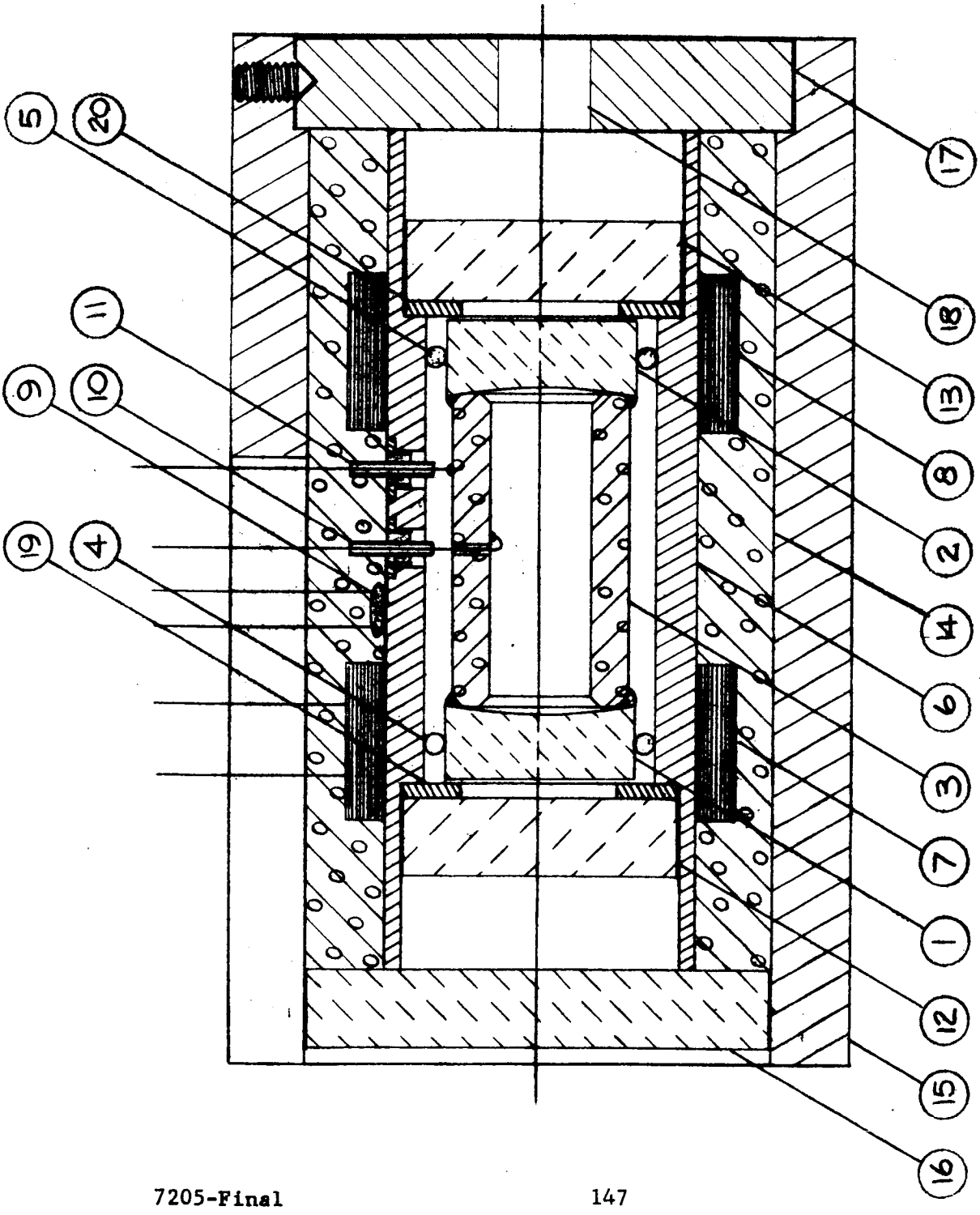

Figure 49. Optical Cavity Layout (overall dimensions 2.0 in. diam by 3.3 in. long)

from the same material described in Section 5.2.1. Based on similar considerations it is found that the application of 0.2V will cause a displacement of 2.67×10^{-10} meters, and change the optical resonant frequency by 5 MHz. Similarly the lowest mechanical resonance is found to on the order 37 kHz. This is far enough removed (because of its high Q) from the 52.5 kHz carrier, that frequency rate-of-change of phase angle will be small. Sensitivity will be decreased, but there is ample drive voltage available. Prior to setting the exact carrier frequency, and designing the various filters that depend upon it, the electrical/mechanical response of the cavity should be investigated experimentally in the region near 52.5 kHz.

6.4 MODE MATCHING

As mentioned in Section 4.3.2, the average effective cross-sectional area of the laser beam is on the order of 1/5 that of the discharge tube (Ref. 55). The beam diameter is not constant along the resonator length however. If both facing mirrors are concave, the beam will have a minimum diameter at some point between the two mirrors. If one mirror is plane, the beam diameter will be a minimum at that mirror. If the mirrors are of unequal radii of curvature, the minimum diameter will be nearest the mirror of the larger radius (more nearly plane). Any such point of minimum diameter is called a waist. The waists of the laser resonator and modulated cavity are designated on Fig. 48 by dashed lines.

In order to practically realize the theoretical resolution of the modulated cavity it is necessary to match the modes of the laser resonator to those of the cavity. This can be done based upon a knowledge of the beam diameters and waist locations of the two structures (Ref. 72). If a thin, convex, lens is inserted between the laser resonator (optical structure, 1) and the modulated cavity (optical structure, 2), their modes may be matched by the proper selection of three parameters. These

are the lens focal length, f; the distance, D_1, from waist 1 to the lens; and the distance, D_2, from waist 2 to the lens. They are related (Ref. 73) by

$$D_1 = f \pm \frac{b_1}{2} \sqrt{(f/f_o)^2 - 1}$$
$$D_2 = f \pm \frac{b_2}{2} \sqrt{(f/f_o)^2 - 1} \quad (64)$$

where b_1 and b_2 are the confocal parameters of the two structures, f_o is a characteristic length given by

$$f_o^2 = \left(\frac{b_1}{2}\right) \left(\frac{b_2}{2}\right) \quad (65)$$

and f in the focal length of the lens.

Mode matching may occur if $f \geq f_o$. The design of Fig. 48 is based on the particular case, $f = f_o$. For this case, Eq. 64 and Eq. 65 become

$$D_1 = D_2 = f = f_o = \frac{1}{2} \sqrt{b_1 b_2} \quad (66)$$

Mirror M5 is made concave of a radius of curvature suitable to fill the office of the thin lens.

The confocal parameter of the modulated cavity is given (Ref. 73) by

$$b_2 = \frac{R_6 \sqrt{d_2 (R_6 - d_2)}}{R_6 + d_2 (n^2 - 1)}$$

where R_6 and d_2 are as previously given, and n is the index of refraction of the glass blank from which M6 is made. The index of refraction enters because this mirror is plane on the M5 side and concave on the M7 side, thus acting like a diverging lens. M6 will be fabricated from a lanthanum flint optical glass with an index of refraction of 1.98.

Given that

$$R_6 = 3.832 \text{ cm}$$

$$d_2 = 2.54 \text{ cm}$$

$$n = 1.98$$

it is found that $b_2/2 = 0.61722$ cm.

The location of the waist is given (Ref. 73) by

$$t_2 = \frac{nd_2 R_6}{R_6 + d_2 (n^2 - 1)}$$

which, when evaluated under the above conditions, is found to be $t_2 = 1.713$ cm. The distance from this waist to the center of M5 must be f_o (because $D_2 = f_o$) and is

$$f_o = 7.4 - \frac{2.54}{2} + 1.713 = 7.843 \text{ cm}$$

The waist location of the laser resonator must be such that

$$f_o = 5.6 + t_1$$

$$t_1 = 7.843 - 5.6 = 2.243 \text{ cm}$$

The location of this waist is given (Ref. 73) by

$$t_1 = \frac{d_1 (R_1 - d_1)}{R_1 + R_2 - 2d_1}$$

If

$$d_1 = 1.107\text{m}$$

$$R_1 = 2.0\text{m}$$

$$t_1 = 0.02243\text{m}$$

it is found that $R_2 = 44.287$ m. This neglects effects due to the diverging lens characteristics of M2. However, because of its large radius such effects will be small.

Finally the confocal parameter of the laser resonator is given (Ref. 73 by

$$\frac{b_1}{2} = \sqrt{\frac{d_1(R_1-d_1)\ (R_2-d_2)\ (R_1+R_2-d_1)}{R_1+R_2-2d_1}}$$

If the above values are substituted into this expression, it is found that $b_1/2 = 0.9964$ m. Recalling the value of $b_2/2$, it is seen that

$$f_o = \frac{1}{2}\sqrt{b_1 b_2} = \sqrt{(.61722)(99.64)} = 7.842$$

which verifies that mode matching is in fact possible if the focal length of M5 is 7.842 cm. For waves of normal incidence, the focal length of a spherical mirror is one-half the radius (Ref. 74). Since M5 is set at 45° it will introduce appreciable astigmatism. If, during detail design, further analysis indicates this to be troublesome, it can be replaced by a single plane mirror and two symmeterically located thin lenses perpendicular to the optical paths.

SECTION 7

MECHANICAL DESIGN

Figure 50 is a photograph of a mock-up of the mechanical design. Figure 51 is a plan, or top, view layout, and Fig. 52 is a side view layout. M1 and M3 are shown for reference. In normal operation they would be remotely located.

The major optical components are mounted on a single plate, 1. This horizontal plate is supported between two vertical plates, 2 and 3. These plates carry vees, 4, that will allow the unit to rest on channel ways that are on 4 inch centers. One vee is relieved, 5, so as to permit three point support by the remaining three. During detail design, consideration should be given to moving the single vee aft of M4 in order to minimize distortion of plate 1.

M4 and its piezoelectric transducer are premanently secured to 1 on a vertical standard. A wire exists from the glass blank behind M4 and is dressed aft to the ±1500 Vdc amplifier, 6. The beam splitter is mounted on a two-axis adjustable mirror mount, 7. This is detailed on assembly drawing 881117, Appendix V. The inner and outer rings are mounted on flexure pivots. These are preloaded during assembly. The axes of the pivots pass through the front surface of the mirror so that angular adjustments do not move the mirror translationally.

M2 is mounted on an identical adjustable mirror mount, 8. This mount is arranged, by means of linear springs, 9 and 10, so that it can be moved fore and aft by the low frequency length control. This arrangement is shown in greater detail on assembly drawing 881118, Appendix V. The design of these springs (Ref. 75, Ref. 76) constrains the mirror to precise, parallel motion.

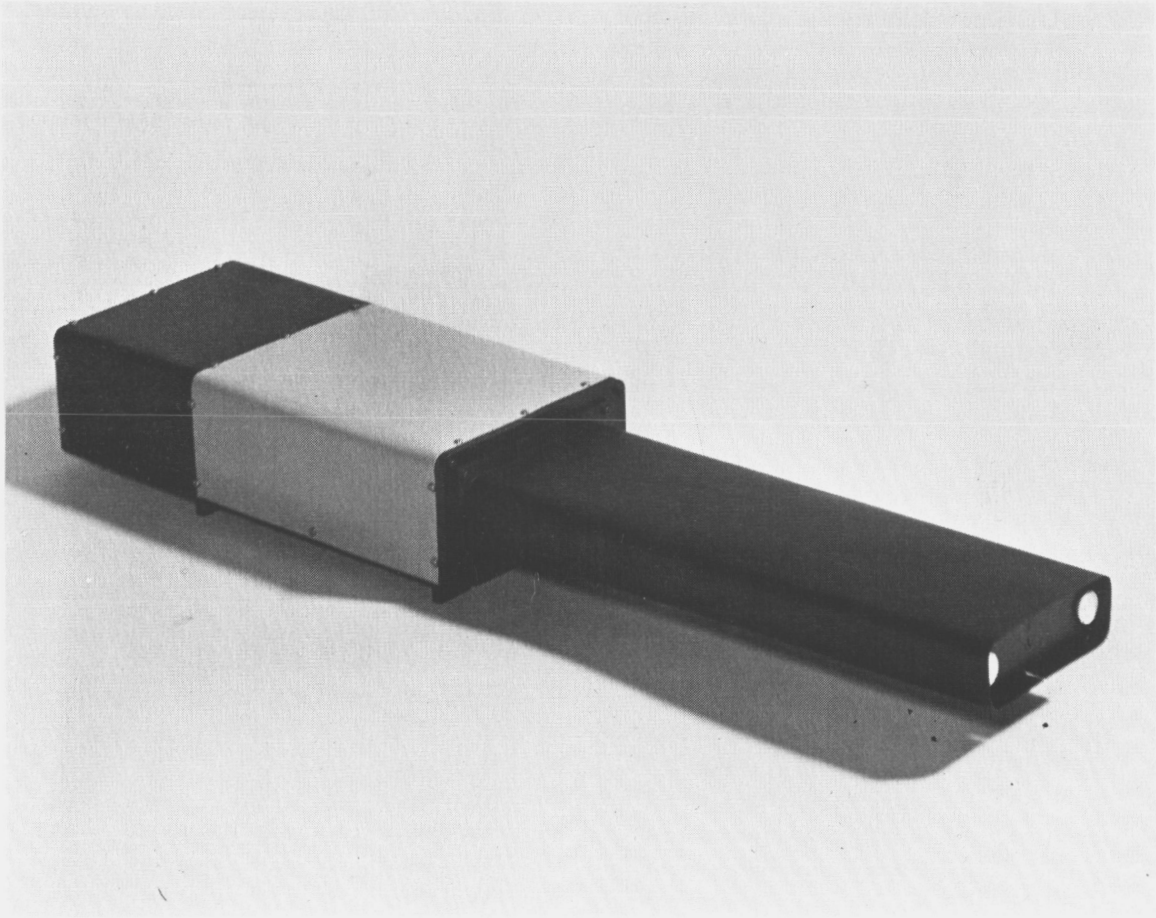

Figure 50. Photograph of Displacement Transducer Mockup

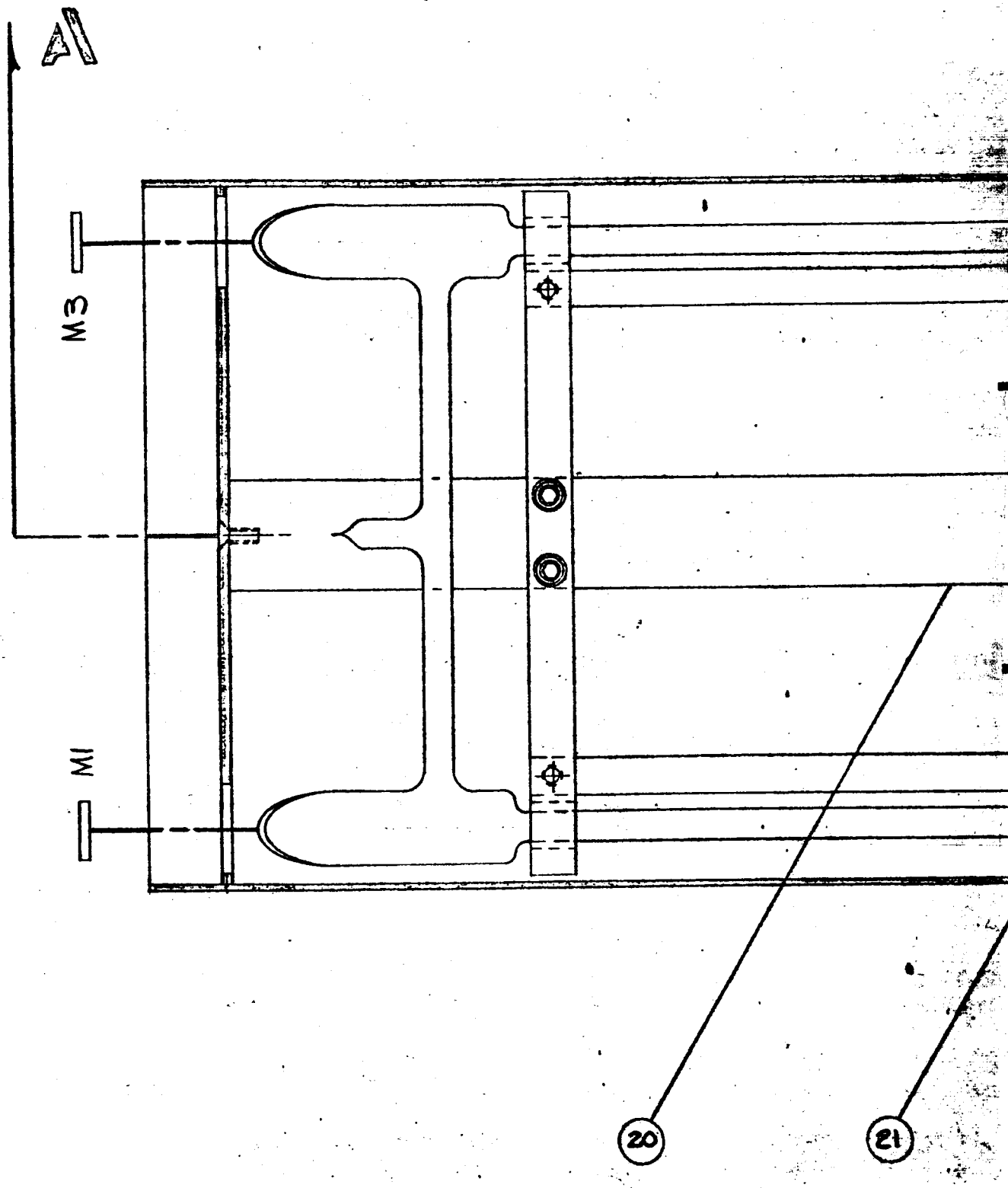

Fig. 51-A

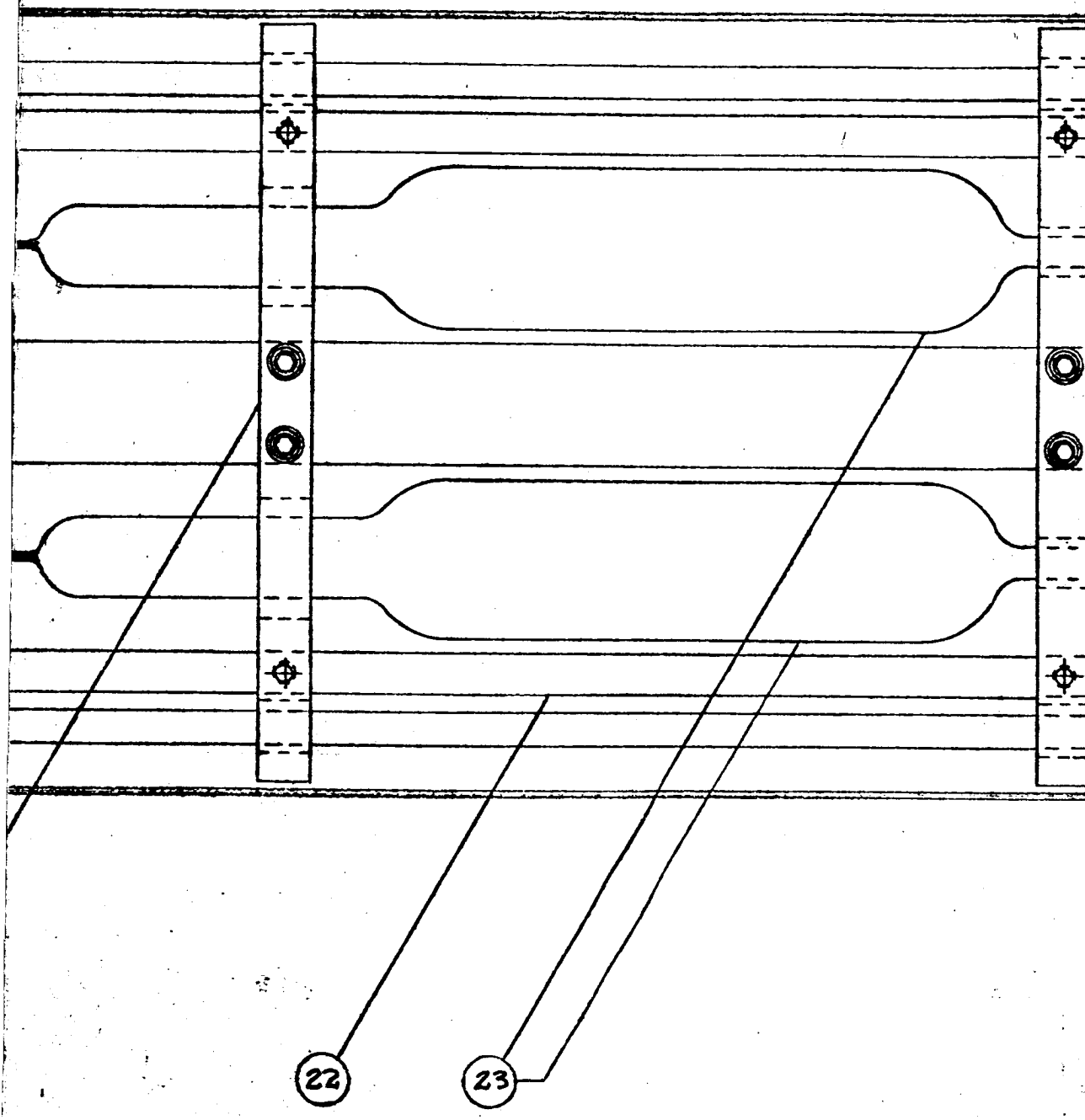

Fig. 51-B

155-B

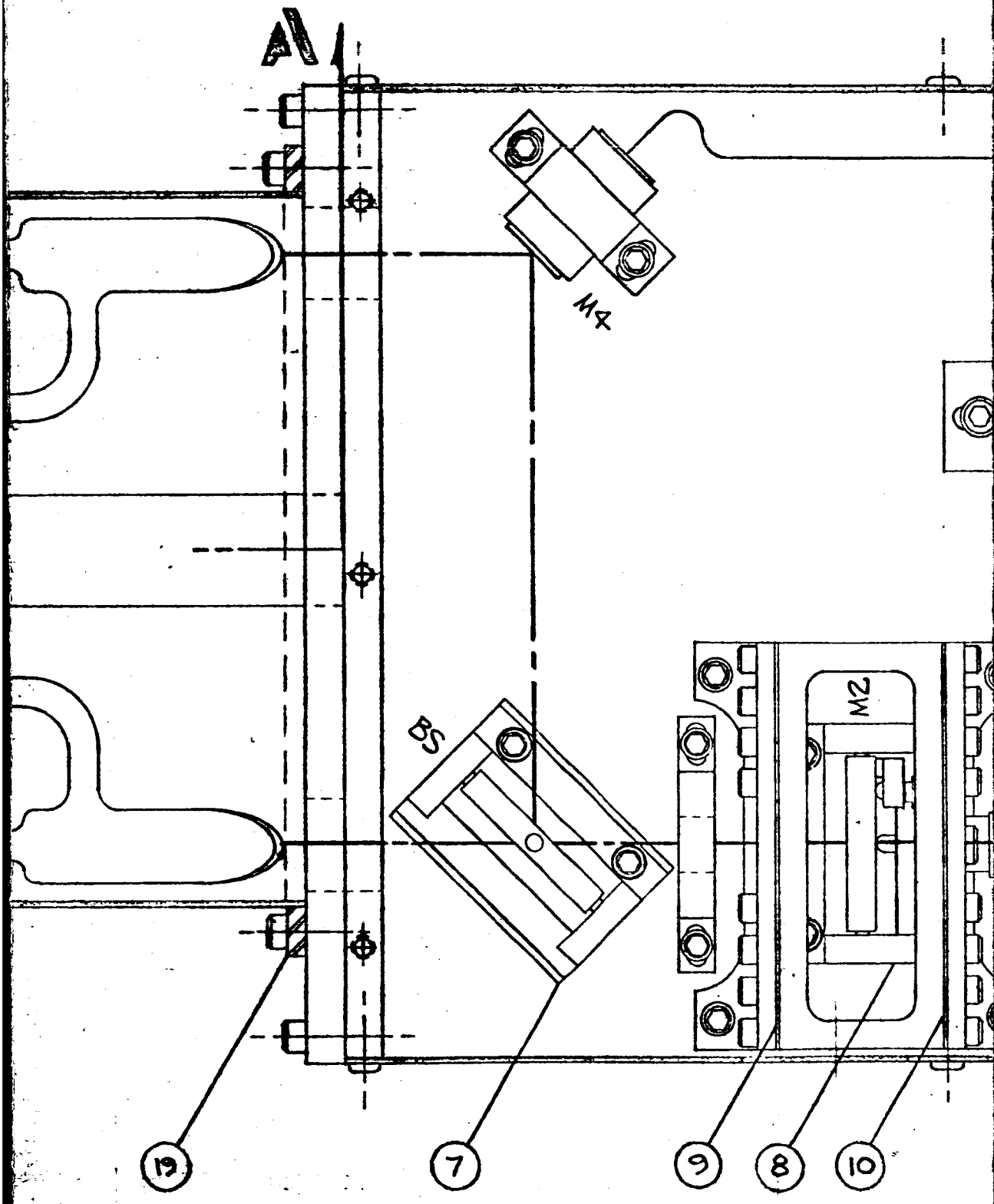

Fig 51-C

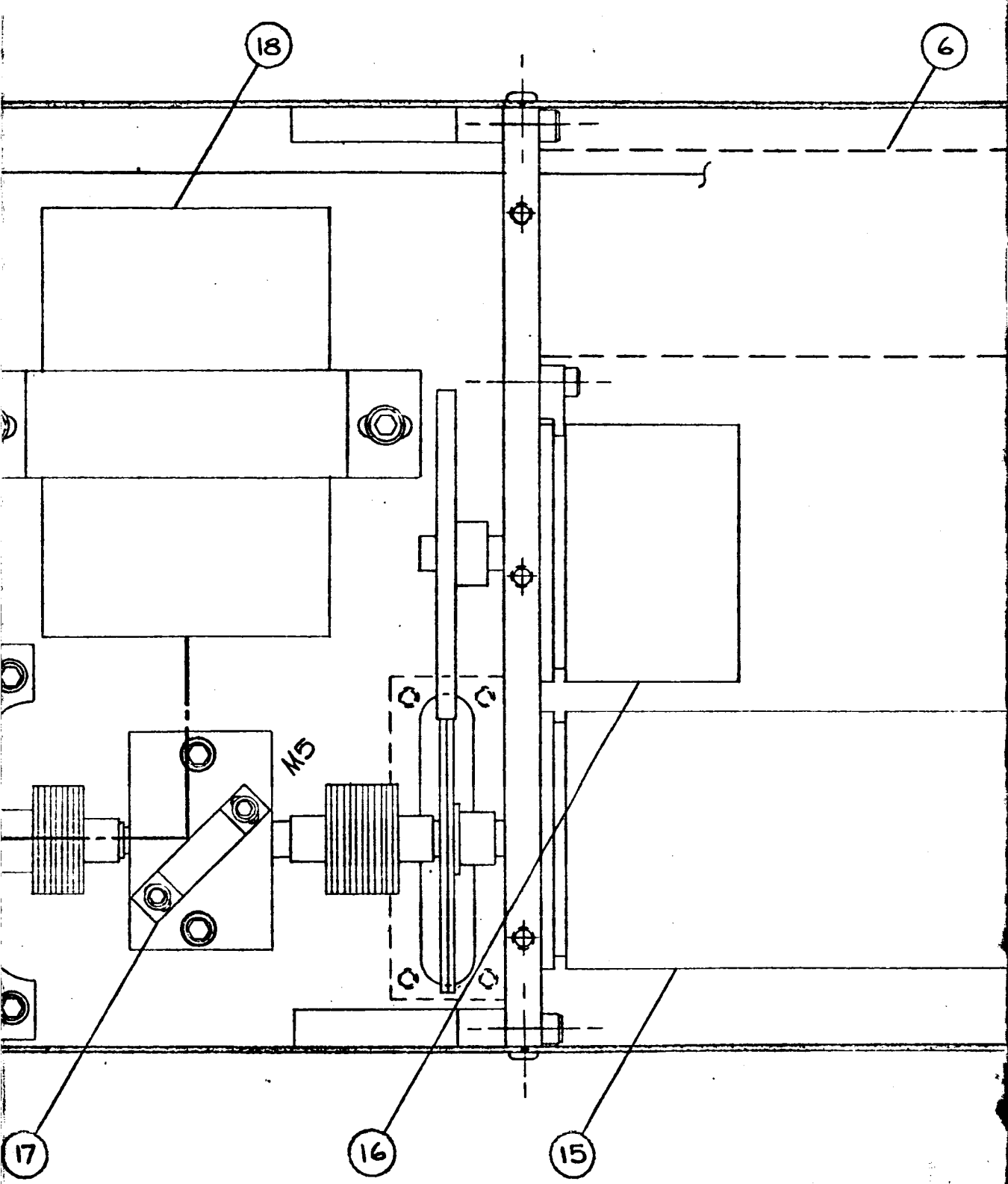

Fig. 51 - D
155 - D

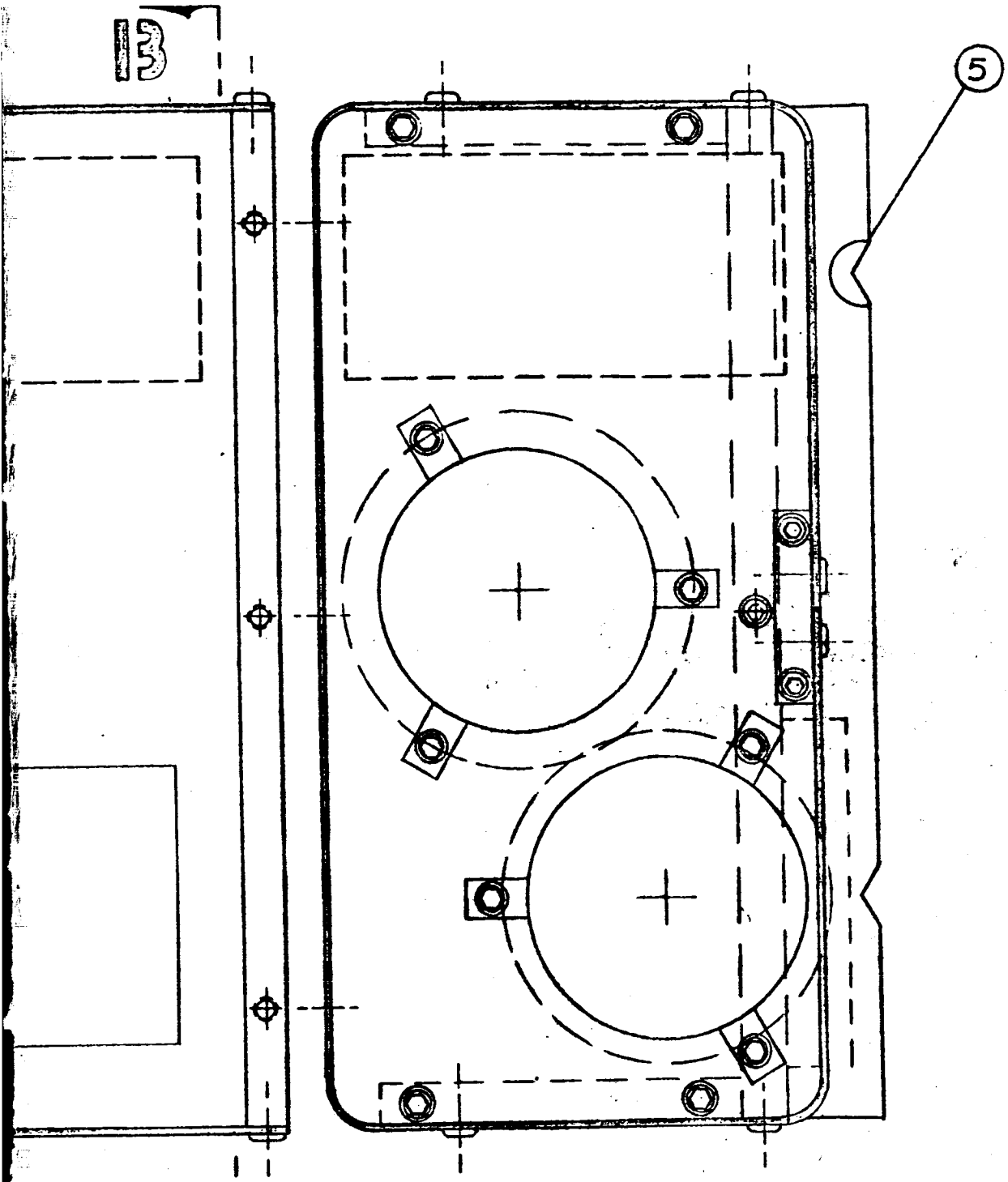

SECTION 13-13

Figure 51.5 Plan View Layout (overall dimensions, 6.7 in. by 28.1 in.)

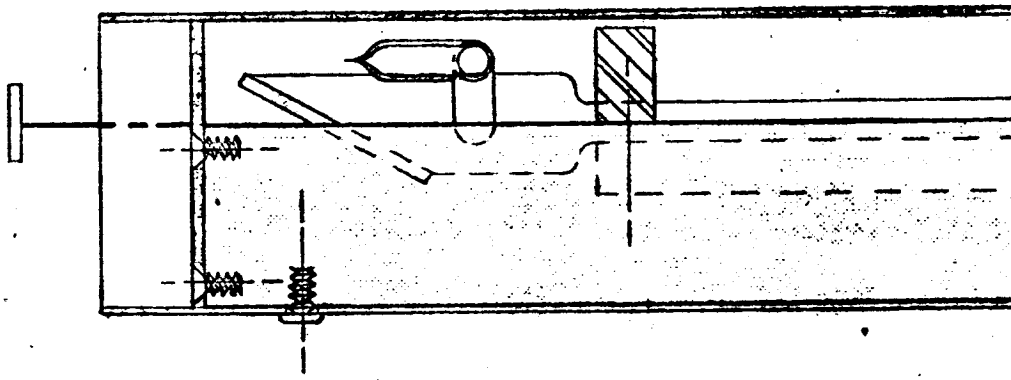

Fig. 52-A

157-A

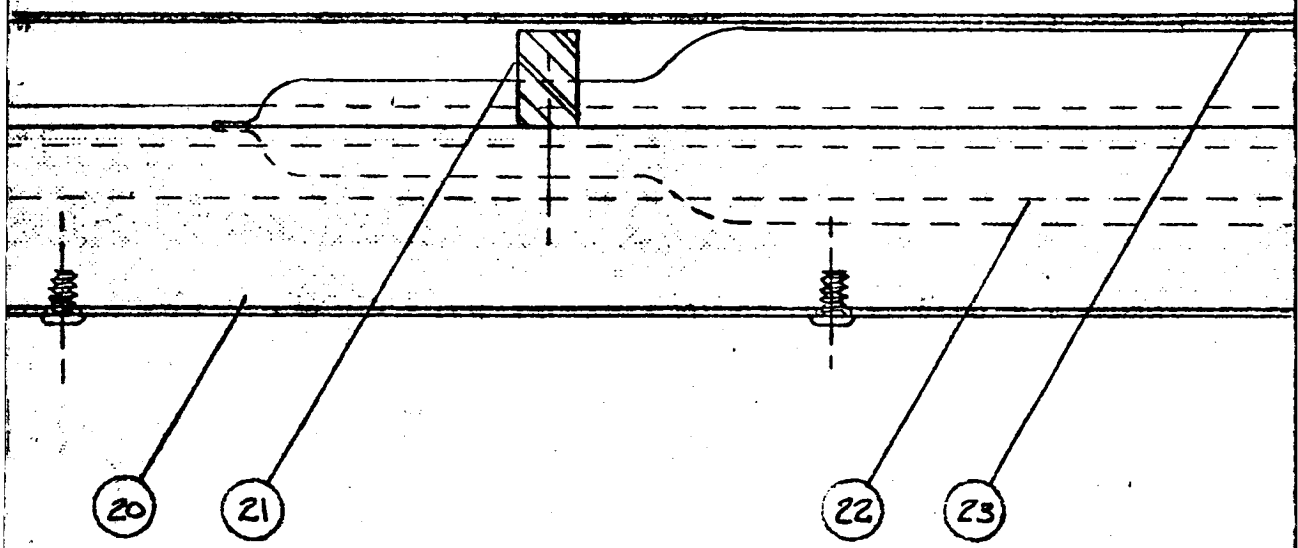

SECTION A-A

Fig. 52-B
157-B

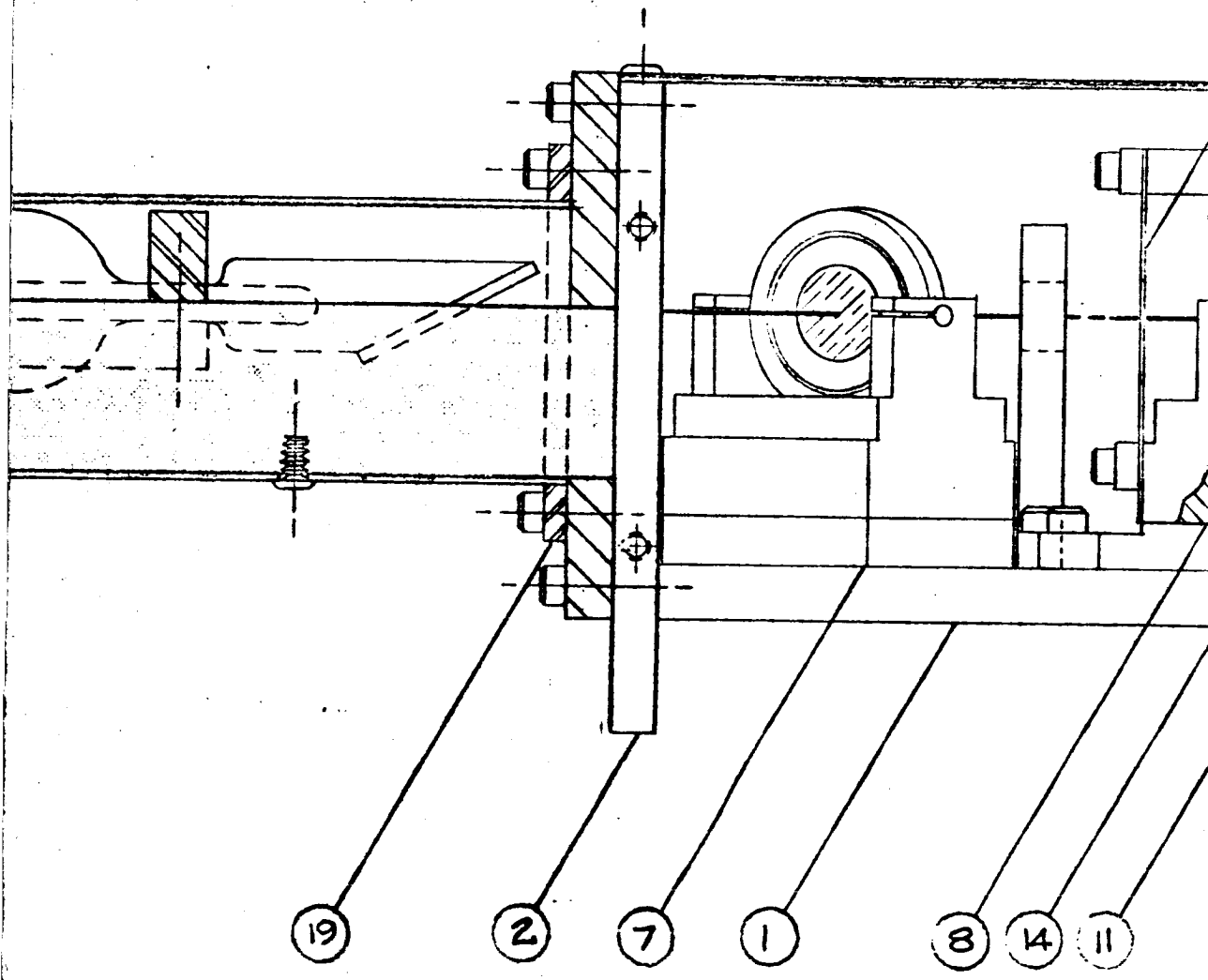

Fig. 52 - C

157 - C

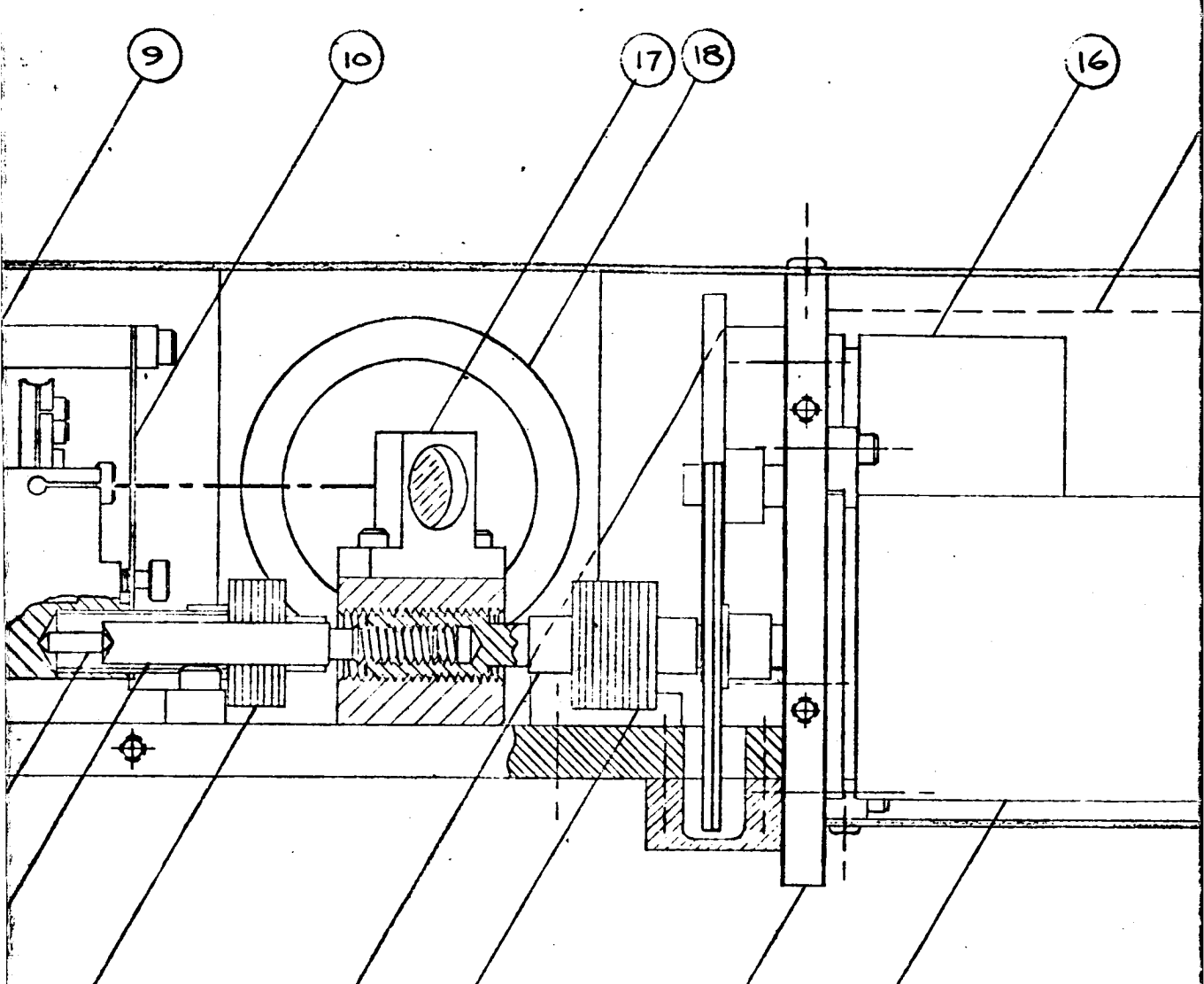

Fig 52 - D
157 - D

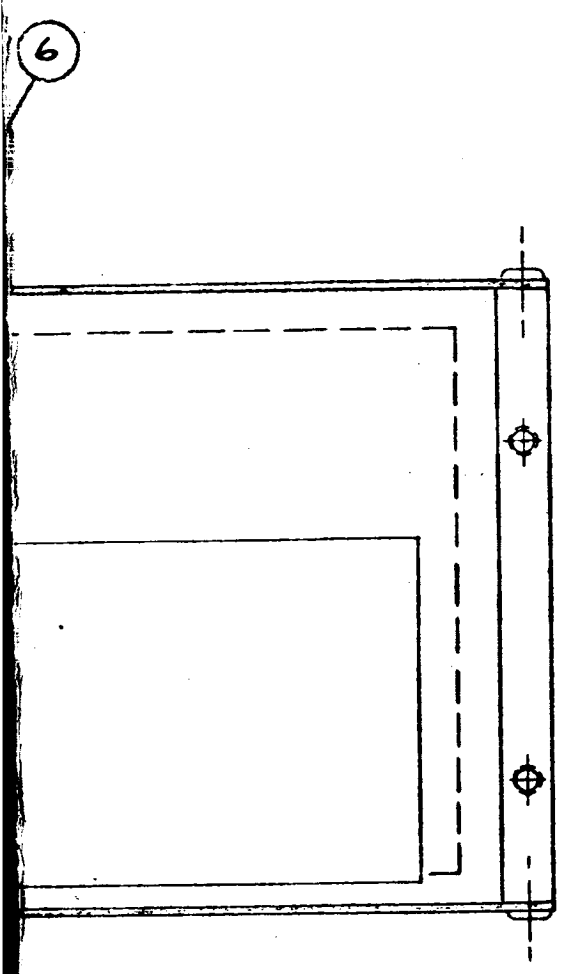

Figure 52. Side View Layout (overall dimensions, 3.7 in by 28.1 in.)

The M2 mirror assembly is moved by means of differential lead screws, 11 and 12. The former, 11, is prevented from rotating by a bellows coupling, 13, that is attached to the M2 mirror assembly. A link, 14, between this lead screw and the mirror base reduces moments due to lateral runout of 11. Since 12 can displace longitudinally about 0.06 inch during the 0.001 inch full scale travel of M2, a second bellows, 14, couples it to the output shaft of the harmonic drive, 15. A split, antibacklash, gear on this shaft meshes with a second gear that drives the feedback potentiometer, 16.

Mirror M5 is mounted, 17, on the fixed nut of the differential lead screw pair. It directs light to the modulated cavity, 18.

The forward vertical plate, 2, supports another plate, 19, to which a central box member, 20, is attached. This member carries a support, 21, to which the laser discharge tube, 22, is clipped. This support is symmetrical, so that by disconnecting the electrical leads to the discharge tube, it may be removed, rotated through 180° in the horizontal plane, and reinstalled. This effectively interchanges the two sides of the tube. The discharge tube is supplied with gas reservoirs, 23, so as to reduce pressure drop due to gettering over the operational life of the tube.

The discharge tube has a single, U-shaped, discharge path. The two long legs of the U lie along the M1-M2 and M3-M2 optical paths. The single discharge path insures that the two tubes will operate at the same average current density regardless of power supply regulation, and that the gas pressure will be the same in each tube. The two, 25 cm long, 2 mm bore, discharge tube sections will be cut from a single, selected, length of tubing. This will minimize variations that might otherwise result from the inverse dependence of gain on discharge tube radius.

There are three sources of heat in the transducer. The servomotor, 15, and the high voltage amplifier, 6, at one end, and the laser discharge tube, 22, at the other. It is anticipated that the (approximately) 25 watt power dissipation of the motor and amplifier will require a small, low-speed, blower in the area behind the potentiometer, 16. This must be selected with care in order to minimize vibration. It is not shown on the layout. The dissipation of the discharge tube is on the order of 10 watts. The large surface area of the, black, shroud that surrounds it may be sufficient to keep the temperature of plate 2 at the same temperature as 3. If not, louvers can be provided.

SECTION 8

SIGNAL CONDITIONING

Analog computer techniques, particularly those based on operational amplifiers, permit real-time operation on electrical signals. An ideal displacement transducer, in the sense of Section 2.1, has an output voltage, E, given by $E = K_x X$, where K_x is the transducer scale factor in volts per unit displacement. Analog operation on E permits such a transducer to be applied to the measurement of other mechanical quantities. This possibility was acknowledged in the system block diagram by the provision for signal conditioning (E-13) at the output of the transducer. This section considers the forms such signal conditioning may take when the basic transducer is applied to the measurement of velocity, acceleration, pressure, force, and impulse.

8.1 VELOCITY

Two cases are of interest. First, measurement of velocity with respect to the fixed coordinate system of the displacement transducer; and second, measurement with respect to some external, fixed, system when the transducer itself shares the velocity to be measured. In the former case the transducer input-output characteristic can be differentiated to obtain

$$\frac{dE}{dt} = K_x \frac{dx}{dt} = K_x v \qquad (67)$$

and it is clear that the required velocity measurement can be obtained by differentiation of the electrical output of the displacement transducer. A circuit that accomplishes this is shown in Fig. 53. Its transfer function is

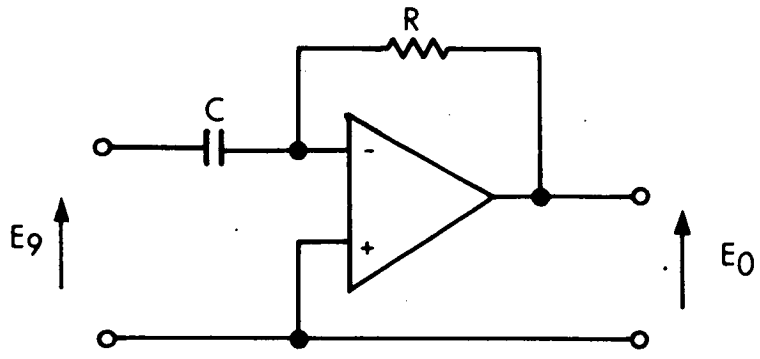

Figure 53. Ideal Operational Amplifier Differentiator

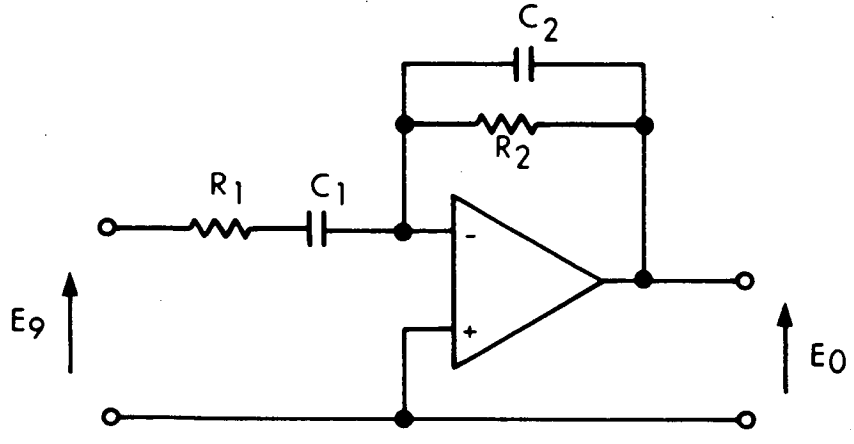

Figure 54. Stable, Low-Noise Differentiator

$$F_{27}(s) = \frac{E_o(s)}{E_9(s)} = RCs \tag{68}$$

Because the magnitude of this transfer function increases with frequency at a rate of 20 dB per decade, practical problems may arise as a result of noise and instability of the amplifier. A circuit that can be used to overcome these difficulties is shown in Fig. 54. Its transfer function is

$$F_{27}(s) = \frac{R_1C_1s}{(R_1C_1s+1)(R_2C_2s+1)} \tag{69}$$

The small condenser, C_2, is generally selected to insure stability. The input resistor, R_1, may be selected so that $1/R_1C_1$ is near the upper limit of signal frequencies at which differentiation is desired. Such a choice minimizes the amplification of noise above this range.

If the displacement transducer is in a moving coordinate system, the velocity of that system can be sensed by measuring the displacement of an inertial mass. If an inertial mass of m, kg, is restrained by a viscous damper of D, N-s/m, its displacement with respect to a uniformly moving coordinate system will be

$$X = \frac{m}{D} v \tag{70}$$

and the displacement transducer output will be directly proportional to velocity, no output signal conditioning being required. If the velocity varies, the transform of the displacement with respect to the moving coordinate system is

$$X(s) = \frac{\frac{m}{D}}{\frac{m}{D}s + 1} v(s) \qquad (71)$$

indicating that the displacement is only proportional to velocity at frequencies below the D/m corner frequency.

If an inertial mass of m kg is restrained by a spring of C m/N compliance, the transform of the displacement with respect to the moving coordinate system will be

$$X(s) = \frac{mCs}{mCs^2+1} v(s) \qquad (72)$$

The presence of an s as a factor in the numerator means that the output of the displacement transducer will have to be integrated in order to obtain a voltage proportional to velocity. This proportionality will only be good at frequencies sufficiently far below the $(mC)^{-1/2}$ resonant frequency. A circuit that will provide the required integration is shown in Fig. 55. Its transfer function is given by

$$F_{27}(s) = \frac{E_o(s)}{E_9(s)} = \frac{1}{RCs} \qquad (73)$$

Damping could be added to the spring restraint to control the response in the region near resonance.

8.2 ACCELERATION

As in the case of velocity, it will be of interest to consider the measurement of acceleration with the displacement transducer fixed, and again when it takes part in the motion. In the first case the transducer input-output characteristic can be doubly differentiated to obtain

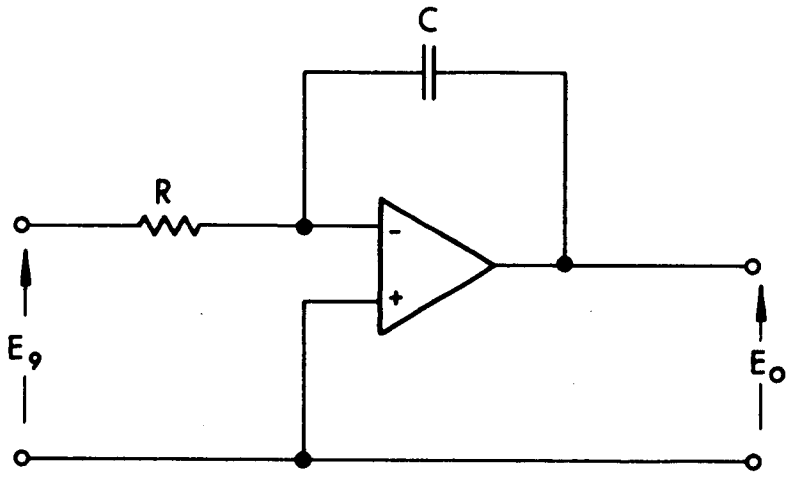

Figure 55. Stable Integrator

$$\frac{d^2E}{dt^2} = K_x \frac{d^2X}{dt^2} = K_x a \tag{74}$$

so that the displacement transducer output must also be differentiated twice in order to obtain a voltage proportional to acceleration. This may be accomplished by a two-fold replication of the circuit shown in Fig. 54.

If the displacement transducer is in a moving coordinate system, the acceleration of that system can be sensed by measuring the displacement of an inertial mass. If an inertial mass of m, kg, is restrained by a viscous damper of D, N-s/m, the transform of its displacement with respect to the moving coordinate system will be

$$X(s) = \frac{\frac{m}{D} \cdot \frac{1}{s}}{\frac{m}{D}s + 1} a(s) \tag{75}$$

The presence of the 1/s factor in the numerator indicates that the output of the displacement transducer will have to be differentiated in order to obtain an output voltage proportional to acceleration. This can be done by the circuit of Fig. 54. The accuracy of the measurement fails at frequencies on the order of D/m or above.

If an inertial mass of m kg is restrained by a spring of compliance C m/N, the transform of the displacement with respect to the moving coordinate system will be

$$X(s) = \frac{mC}{mCs^2 + 1} a(s) \tag{76}$$

At frequencies sufficiently far below the $(mC)^{-1/2}$ resonant frequency, the output of the displacement transducer will be directly proportional to acceleration and no signal conditioning will be required.

8.3 PRESSURE

The task of measuring velocity and acceleration with a displacement transducer is simplified by the fact that they are, respectively, the first and second derivatives of displacement. This happy result is not available in the case of pressure measurement. Mechanically, pressure may be converted to force by applying it across a known area. Ideally, this might be done with an infinitely stiff, massless, piston. The resulting force can then be converted to displacement by applying it to a spring, a damper, or a mass.

The spring restrained piston is of greatest interest since it can be closely approached by flat plates, and at low frequencies by bellows. If pressure, p, is applied to a piston of area, A, that is restrained by a spring of compliance C, the static displacement will be

$$X = ACp \tag{77}$$

The output of the displacement transducer would be directly proportional to pressure in this case, and no signal conditioning would be required.

A piston subject only to viscous restraint would have a velocity of

$$v = \frac{A}{D} p \tag{78}$$

and the displacement transducer would have to be differentiated in order to obtain a voltage proportional to pressure. A piston subject only to the restraint of mass (perhaps its own) would have an acceleration of

$$a = Amp \tag{79}$$

and the displacement transducer output would require double differentiation in order to obtain a voltage proportional to pressure.

8.4 FORCE

As suggested in the previous section, a displacement proportional to force can be produced by allowing the force to act on a linear element. For the cases of a compliance, C, a viscous damper, D, and a mass, m, the results are given by

$$X = CF \tag{80}$$

$$v = \frac{F}{D} \tag{81}$$

$$a = \frac{F}{m} \tag{82}$$

A displacement transducer will provide an output proportional force without signal conditioning in the first case. It will require one differentiation in the second case and two in the third case.

8.5 IMPULSE

Impulse, P, is sometimes defined as the integral of force with respect to time, that is, by

$$P = \int F \, dt \tag{83}$$

The force producing the impulse can be applied to one of linear elements just discussed. For the cases of a compliance, C, a viscous damper, D, and a mass, m, the results are

$$\int X dt = CP \tag{84}$$

$$X = \frac{P}{D} \tag{85}$$

$$v = \frac{P}{m} \tag{86}$$

In the first case the signal conditioner required is an integrator. In the second no conditioner is needed, and in the third case a differentiator is indicated.

In many cases of practical interest the force producing the impulse acts for only a brief interval. In the preceding sections it has been tacitly assumed that the quantity to be measured was static or slowly varying. Under such conditions it is generally possible to design the mechanical portion of the measurement so that, in the frequency range of interest, the system is primarily stiffness, viscous, or mass controlled. Short pulses have broad frequency spectra, and the dynamics of the measurement must be examined more generally.

If the force producing the impulse is applied to a mass that is restrained a parallel spring and viscous damper, the transform of the displacement will be

$$X(s) = \frac{C}{mCs^2 + CDs + 1} F(s) \tag{87}$$

If the force is assumed to be an infinitely narrow pulse of finite area, occurring at t = o, then

$$F(t) = P\delta(o)$$
$$F(s) = P \tag{88}$$

where $\delta(o)$ is the Dirac impulse function at t = o, and P is the magnitude of the impulse. Practical pulses of force can be so considered if their durations are much smaller than $\sqrt{mC}$ seconds. If the input defined by Eq. 88 is applied to the system defined by Eq. 87, the inverse transform yields

$$X(t) = \frac{P\omega_1}{\sqrt{1-\zeta^2}} e^{-\zeta\omega_1 t} \sin (\omega_1\sqrt{1-\zeta^2}t) \tag{89}$$

where

$$\omega_1 = \frac{1}{\sqrt{mC}}$$

$$\zeta = \frac{D}{2}\sqrt{\frac{C}{M}}$$

If the damping is low, the magnitude of the impulse can be determined by measuring the amplitude of the first overshoot. If the amplitudes of each of a repetitive string of pulses is to be measured, there will be a cumulative error if the displacement has not decayed substantially to zero.

If the output of the displacement transducer is applied to an integrator (Fig. 55) with the transfer function

$$F_{27}(s) = \frac{K_P}{s} \tag{90}$$

the response of the system will be

$$E_o(s) = \frac{K_x K_p}{s} x(s)$$

$$= \frac{K_x K_p C}{s(mCs^2 + CDs + 1)} F(s) \qquad (91)$$

If the input defined by Eq. 88 is applied to this system, the final value theorem can be used to show that the steady-state output is

$$E_o(t = \infty) = K_x K_p CP \qquad (92)$$

If, instead, the input is a string of impulses the cumulative error previously described will occur if attempts are made to separate the contribution of each pulse. This limitation can be effectively removed if the time of occurrence of the individual pulses is known in advance. Immediately prior to each pulse the output of the integrator is noted so as to determine the amplitude of the previous pulse. The integrator is then zeroed in preparation for the next pulse. A circuit that will accomplish this is shown in Fig. 56. With the switch open the integrator operates normally. Closing the switch allows the condenser to discharge. A small resistor, r, in series with the switch serves to limit the discharge current and protect the relay contacts. Opening the switch returns the integrator normal operation. Reed relays are available that will close, discharge the condenser, and open within the space of a few milliseconds. Relay operation could be controlled manually by the operator, or remotely by an appropriate signal from the system under test.

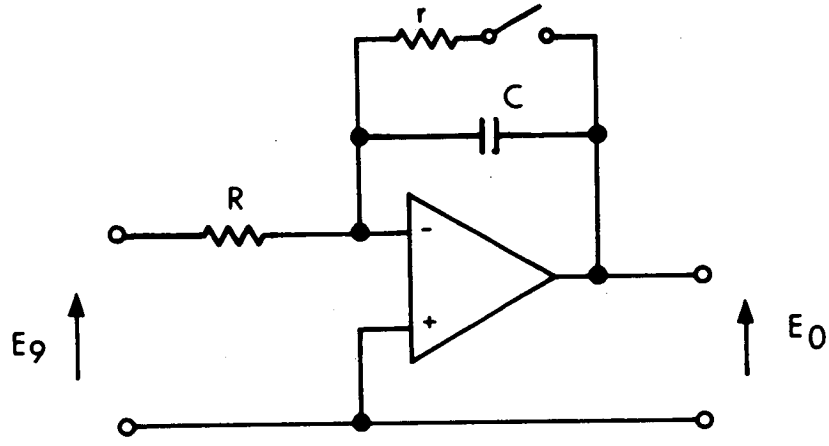

Figure 56. Integrator with Reset Switch

SECTION 9

CALIBRATION AND OPERATION

Initial alignment of the mirrors (Ref. 77) will make use of a calibration fixture that carries mirrors M1 and M3. The fixture will be arranged to rest, by means of a three-point support, on the same U-section channel (Section 7) that supports the transducer. Each mirror will be carried in a two-axis adjustable mount that is identical to those of the beam splitter and M2 in the transducer. M3 will, in addition, be able to be manually positioned by means of a differential lead screw like that of M2.

An access plate (not shown in the layouts) will permit the photodetector to be removed from the rear of the modulated cavity. This will allow light emerging from M2 to pass through the modulated cavity and out of side of the transducer housing. A black absorbing card is placed in front of M4 to prevent oscillation. A second card will be white on one side and black on the other. Fine black lines intersect at the center of the white face. At the intersection is a 0.04 inch diameter pin hole. On the black side of the card, the hole is covered with a deep red filter.

The white face of the card is placed against the back of the modulated cavity so that light from the discharge tube is centered in the pin hole. An image of the fine black lines will be seen reflected from the rear face of M2. By means of the adjustments on the M2 mirror mount, the intersection of the lines is centered in the beam of light from the tube. This assures that the plane of M2 is perpendicular to the axis of the M1-M2 discharge tube. M1 may now be adjusted for maximum brightness.

The black card is now moved from in front of M4 and placed in front (on the M1 side) of the beam splitter. The same alignment procedure is repeated except that the beam splitter is adjusted so as to center the intersection of the black lines in the light beam. This assures that, optically, the plane of M2 is perpendicular to the axis of the M3-M2 discharge tube. M2 is then adjusted for maximum brightness. If the black card is removed from in front of the beam splitter the laser should oscillate. Fine adjustments on each mirror may be made in order to maximize the power output as sensed by the photodetector.

The length, and hence the optical resonances, of the modulated cavity is determined by the set-point of its temperature controller. This should be allowed to stabilize prior to operation. A manual control by means of an offset voltage permits the cavity to be varied as a check to see that it is centered at the operating frequency of the laser. With the transducer feedback loops operating this control may be used to set the frequency of the laser to line center. Absolute calibration may be made by producing known displacements of M3 by means of its differential lead screw.

SECTION 10

CONCLUSIONS AND RECOMMENDATIONS

Based on the various analyses presented in this report it is concluded that the laser is well suited to the measurement of small displacements. In order to insure laser oscillation over a wide range of practical laboratory environments, a closed-loop frequency control was provided. This will reduce frequency response to about the level that might have been achieved with the interferometer. The response required by the Target Design Specification can, however, be obtained. In fact, the feasibility-design study has resulted in a specific approach that has a very high probability of meeting all of the target specifications. The transducer can be located outside of a vacuum chamber and used to measure displacements within, if the chamber is supplied with a low loss window. Such a window might either be set at the Brewster angle, or be antireflection coated. Output signal conditioning will allow the transducer to be applied to a wide range of measurement problems and variables. The full extent of the accuracy and flexibility of this design can only be assessed by the construction and test of a prototype. An estimate of the man hours required, and the cost of purchased parts, for such a prototype construction and test effort is given in Appendix VI.

APPENDIX I

EFFECTIVE REFLECTION COEFFICIENT OF A FABRY-PEROT CAVITY

Figure I-1a is a plane mirror with a partially reflecting coating on the face indicated by the dashed line. A collimated beam of coherent light with amplitude a_1 falls on the surface from the left. A similar beam of amplitude a_2 falls on the surface from the right.

It will be assumed that if $a_2 = 0$, then

$$b_1 = \rho\, a_1$$
$$b_2 = \tau\, a_1 \qquad \text{(I-1)}$$

and that if $a_1 = 0$, then

$$b_2 = \rho\, a_2$$
$$b_1 = \tau\, a_2 \qquad \text{(I-2)}$$

so that the mirror is symmetrical, and light from either direction is treated impartially. Combining Eq. I-1 and Eq. I-2 yields

$$b_1 = \rho\, a_1 + \tau\, a_2$$
$$b_2 = \tau\, a_1 + \rho\, a_2 \qquad \text{(I-3)}$$

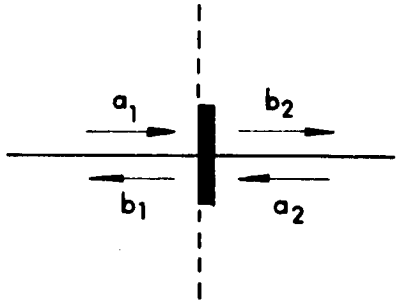

a. Partially Reflecting Mirror with Plane Waves Incident on Both Sides

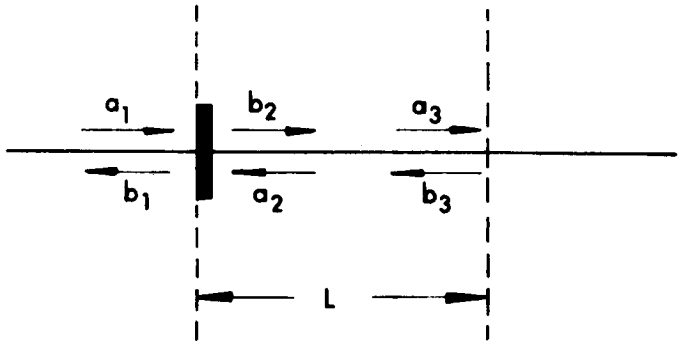

b. Wave Amplitude at Distance

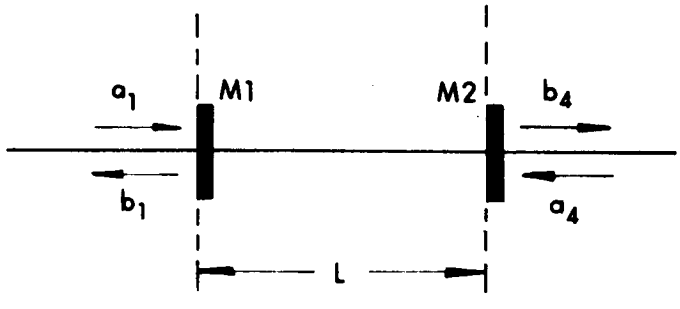

c. Second Mirror at Distance

Figure I-1. Plane Mirror with Partially Reflecting Coating on the Face

where, in general, all of the variables and coefficients can be complex. If the mirror is lossless, it can be shown (e.g., Ref. 78 and Ref. 79) that

$$|\tau|^2 = 1 - |\sigma|^2 \tag{I-4}$$

and that the phase of τ and ρ differ by $\pi/2$. These conditions will be met if

$$\begin{aligned} \rho &= re^{j(\alpha + \pi/4)} \\ \tau &= te^{j(\alpha - \pi/4)} \end{aligned} \tag{I-5}$$

where $r^2 + t^2 = 1$. Since it does not alter the form of the result (i.e., the mode spacing) it is customary to allow $\alpha = 0$.

Figure I-1b shows the same mirror with an imaginary plane located a distance, L, to the right of the partially reflecting surface. The wave of amplitude, b_2, leaving the mirror will have an amplitude, a_3, at the distance L. If the medium through which the wave travels is without attenuation, then the only effect will be a phase delay given by

$$a_3 = b_2 e^{-j\theta} \tag{I-6}$$

where

$$\theta = \frac{2\pi L}{\lambda} = \frac{2\pi f L}{c} \tag{I-7}$$

A similar relation

$$a_2 = b_3 e^{-j\theta} \tag{I-8}$$

applies to the wave leaving the plane and arriving at the mirror.

In Fig. I-1c the mirror is designated M1, and a second mirror designated M2 has been inserted at a distance, L, to the right. If M2 is identical to M1, the amplitude of the waves emerging from it will be

$$b_3 = \rho a_3 + \tau a_4$$

$$b_4 = \tau a_3 + \rho a_4 \tag{I-9}$$

If it is assumed that this wave (b_4) feeds into a black-body absorber, then $a_4 = 0$. Solving Eqs. I-3, I-5, I-6, I-8, and I-9 simultaneously yields

$$\frac{b_1}{a_1} = \frac{1 - e^{-j2(\theta - \frac{\pi}{4})}}{1 - r^2 e^{-j2(\theta - \pi/4)}} \, re^{-j\pi/4} \tag{I-10}$$

$$\frac{b_4}{a_1} = \frac{t^2 e^{-j(\theta + \pi/2)}}{1 - r^2 e^{-j2(\theta - \pi/4)}} \tag{I-11}$$

The incident wave, a_1, will be totally absorbed (i.e., $b_1 = 0$, $|b_4| = a_1$) if

$$\theta = (q + 1/4)\,\pi \tag{I-12}$$

where q is an integer. The incident wave will be substantially reflected if

$$\theta = (q + 1/2)\,\pi \tag{I-13}$$

Using Eq. I-7, the frequencies at which strong reflection takes place are given by

$$f = \frac{c}{2L}(q + 1/2) \qquad \text{(I-14)}$$

The magnitude of the amplitude of the reflected wave at these frequencies can be obtained from

$$\left|\frac{b_1}{a_1}\right|^2 = \frac{2r^2}{1 + r^4} \qquad \text{(I-15)}$$

It is seen that even moderate values of reflectivity, r^2, of the individual mirrors may result in quite high values of effective reflectivity, Eq. I-15, at selected frequencies. For example, if

$$r^2 = 90\%$$

then

$$\left|\frac{b_1}{a_1}\right|^2 = 99.4\%$$

where scattering and other internal losses in the physical structures of the mirrors are neglected.

APPENDIX II

THREE-MIRROR MICHELSON-TYPE RESONATOR

A schematic of the resonator is shown in Fig. II-1. The mirrors and arm lengths are designated to correspond to those of Fig. 27 and Fig. 28. The amplitudes of the waves impinging on the mirror are a_1, a_2, a_3, and a_4. The amplitudes of waves emerging from the mirror are designated by b_1, etc. For a symmetrical beam splitter a treatment similar to that of Appendix I yields:

$$\begin{aligned} b_1 &= \tau a_2 + \rho a_4 \\ b_2 &= \tau a_1 + \rho a_3 \\ b_3 &= \rho a_2 + \tau a_4 \\ b_4 &= \rho a_1 + \tau a_3 \end{aligned} \qquad \text{(II-1)}$$

If M1, M2, and M3 are perfect with a reflection coefficient of one, then:

$$\begin{aligned} a_1 &= b_1 e^{-j2\theta_1} \\ a_2 &= b_2 e^{-j2\theta_2} \\ a_3 &= b_3 e^{-j2\theta_3} \end{aligned} \qquad \text{(II-2)}$$

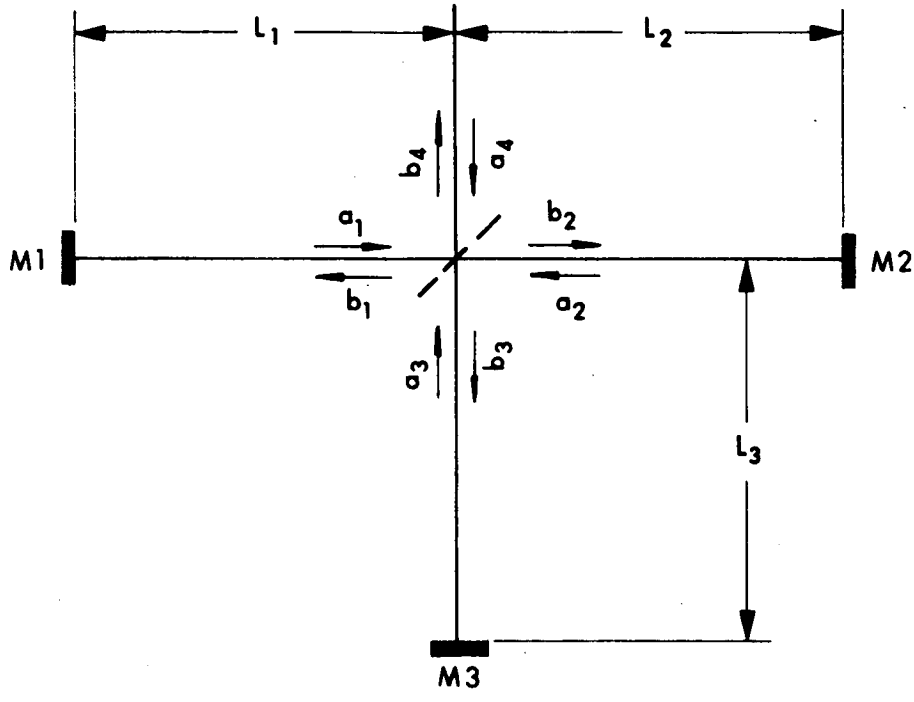

Figure II-1. Michelson-Type Three-Mirror Cavity

For an ideal 3 dB beam splitter (one that reduces the power at a plane wave incident at 45^{o} by one-half) it will be assumed that

$$\rho = \frac{e^{j\pi/4}}{\sqrt{2}}$$

$$\tau = \frac{e^{-j\pi/4}}{\sqrt{2}} \qquad \text{(II-3)}$$

where $\alpha = 0$ (see Eq. I-5).

If it is assumed that the output wave (b_4) feeds into a black-body absorber, then $a_4 = 0$. In order for the system of simultaneous equations that results from the substitution of Eq. II-2 into Eq. II-1 to have a solution in this case (i.e., $a_4 = 0$) it is necessary and sufficient that

$$1 = \rho^2 e^{-j2(\theta_2 + \theta_3)} + \tau^2 e^{-j2(\theta_1 + \theta_2)} \qquad \text{(II-4)}$$

If the values of ρ and τ given by Eq. II-3 are substituted into Eq. II-4, the resulting expression will be satisfied if

$$\theta_1 + \theta_2 = (m - 1/4)\,\pi$$

$$\theta_2 + \theta_3 = (n + 1/4)\,\pi \qquad \text{(II-5)}$$

If the values of θ_i ($i = 1, 2, 3$) are related to the path lengths, L_i, by Eq. I-7, then from Eq. II-5 it follows that

$$L_3 - L_1 = \frac{c}{2f}(n - m + 1/2) \qquad \text{(II-6)}$$

The frequencies that satisfy Eq. II-6 have separations given by

$$\Delta f = \frac{c}{2(L_3 - L_1)} \qquad \text{(II-7)}$$

The system of simultaneous equations referred to above also yields the result

$$\frac{b_4}{b_2} = \rho_T \left[e^{-j2(\theta_1 + \theta_2)} + e^{-j2(\theta_2 + \theta_3)} \right] \qquad \text{(II-8)}$$

If the values of $\theta_1 + \theta_2$ and $\theta_2 + \theta_3$ given by Eq. II-5 are substituted into Eq. II-8 it will be found that $b_4 = 0$. Since this is true regardless of the value of b_2 this is a resonance condition. That is, plane waves propagate back and forth along the arms of the resonator without "leaking out" of the beam splitter. Practically there will be diffraction losses and losses as result of transmission through less than perfect end mirrors. Further, there may be losses due to transmission out of the beam splitter (i.e., $b_4 \neq 0$) if the beam splitter is not symmetrical, or, in the case of the laser shown in Fig. 28, if the gains of the two discharge tubes are unequal. Losses due to these last two causes are discussed in greater detail by DiDomenico (Ref. 51).

APPENDIX III

FREQUENCY-DISPLACEMENT TRANSFER FUNCTION

This appendix considers the variation of frequency-selectivity of the three-mirror Michelson-type resonator in response to small displacements of any one of the three end mirrors. In Appendix II (Eq. II-5) it was shown that this structure has resonant frequencies given by

$$\begin{aligned} 2f(L_1 + L_2) &= (m - 1/4)c \\ 2f(L_2 + L_3) &= (n + 1/4)c \end{aligned} \qquad \text{(III-1)}$$

It is clear that these relations cannot be satisfied simultaneously for independent changes in L_1 and L_3. In order to investigate these possibilities, a steady state excitation may be applied to the resonator, and its response examined under the required conditions. Appendix II assumed that M1, M2, and M3 were perfectly reflecting. It is now assumed that they are partially reflecting and can be described by the coefficients ρ_1 and τ_1 for M1, ρ_2 and τ_2 for M2, and ρ_3 and τ_3 for M3. The resonator can now be excited by an external wave, e.g., a_1' in Fig. III-1 and the response observed by measuring an emerging wave, e.g., b_2' in Fig. III-1.

If the beam splitter of Fig. III-1 has characteristics like those of Appendix II, and if $a_4 = 0$, then the following result can be obtained

$$\frac{b_2'}{a_1'} = \frac{\tau_1\tau_2 e^{-j(\theta_1 + \theta_2)}}{1 - \rho^2\rho_2\rho_3 e^{-j2(\theta_2 + \theta_3)} - \tau^2\rho_1\rho_2 e^{-j2(\theta_1 + \theta_2)}} \qquad \text{(III-2)}$$

Had the resonator been excited by illuminating M3 with an external beam and again observing the response at M2, the result would be like Eq. III-2, except that the subscript 1 would be replaced by the subscript 3 when it occurs in the numerator. If the beam splitter and mirrors have coefficients given by

$$\rho = \frac{1}{\sqrt{2}} e^{+j\pi/4}$$

$$\tau = \frac{1}{\sqrt{2}} e^{-j\pi/4}$$

$$\rho_1 = \rho_3 = re^{+j\pi/4}$$

$$\tau_1 = \tau_3 = te^{-j\pi/4}$$

$$\rho_2 = re^{-j\pi/4}$$

$$\tau_2 = te^{+j\pi/4}$$

then Eq. III-2 becomes

$$\frac{b_2'}{a_1'} = \frac{t^2 e^{-j(\theta_1 + \theta_2)}}{1 - \frac{r^2}{2} e^{-j2(\theta_2 + \theta_3 - \pi/4)} - \frac{r^2}{2} e^{-j2(\theta_1 + \theta_2 + \pi/4)}} \qquad \text{(III-3)}$$

Under the conditions of resonance, that is, if

$$\theta_1 + \theta_2 = (m - 1/4)\pi$$

and

$$\theta_2 + \theta_3 = (n + 1/4)\pi$$

then Eq. III-3 reduces to

$$\frac{b_2'}{a_1'} = \frac{t^2 e^{-j(\theta_1 + \theta_2)}}{1 - r^2} = e^{-j(\theta_1 + \theta_2)}$$

indicating that the transmission is lossless and only a phase shift occurs.

The total power transmissivity, G, of the resonator when examined in the manner of Fig. III-1 is the square of the magnitude of Eq. III-3. This is found to be

$$G = \left| \frac{b_2'}{a_1'} \right|^2 = \frac{t^4}{\frac{r^4}{2}\left[1 - \cos 2(\theta_3 - \theta_1)\right] + r^2\left[\sin 2(\theta_1 + \theta_2) - \sin 2(\theta_2 + \theta_3)\right] + 1} \qquad \text{(III-4)}$$

Since G is a function of L_1, L_2, L_3, and f, it can be expanded in a Taylor's series in these variables. For partials through the second the series is

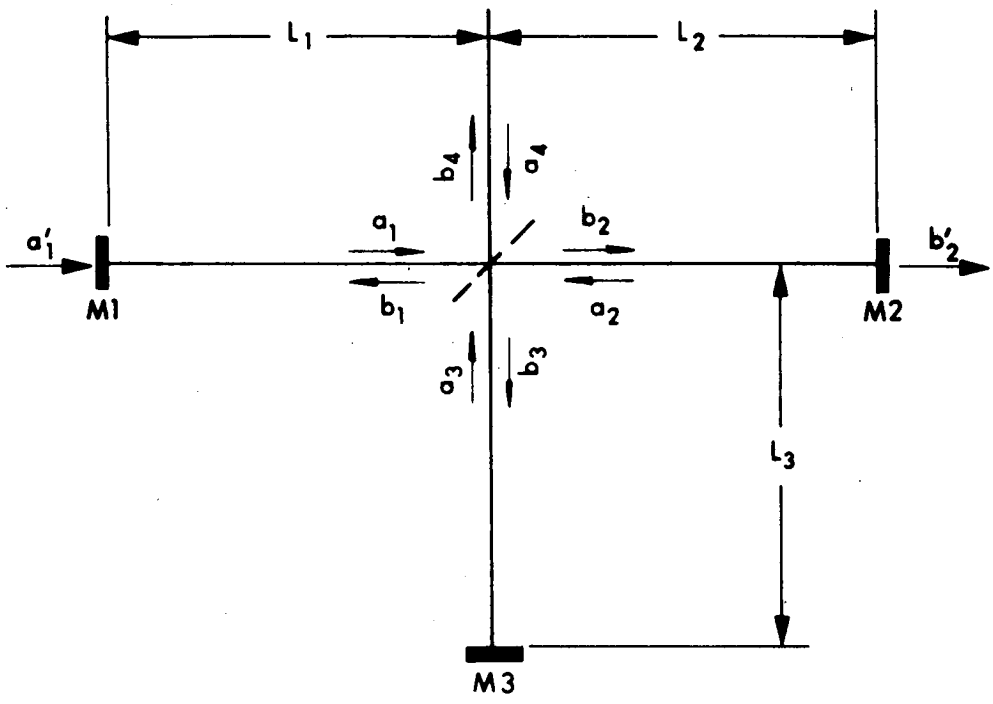

Figure III-1. Michelson-Type Three-Mirror Cavity with Partially Reflecting End Mirrors

$$G = G(\text{res.}) + \frac{\partial G}{\partial L_1}\Delta L_1 + \frac{\partial G}{\partial L_2}\Delta L_2 + \frac{\partial G}{\partial L_3}\Delta L_3 \qquad \text{(III-5)}$$

$$+ \frac{\partial G}{\partial f}\Delta f + \frac{1}{2}\frac{\partial^2 G}{\partial L_1^2}\Delta L_1^2 + \frac{1}{2}\frac{\partial^2 G}{\partial L_2^2}\Delta L_2^2$$

$$+ \frac{1}{2}\frac{\partial^2 G}{\partial L_3^2}\Delta L_3^2 + \frac{1}{2}\frac{\partial^2 G}{\partial f^2}\Delta f^2 + \frac{\partial^2 G}{\partial L_1 \partial L_2}\Delta L_1 \Delta L_2$$

$$+ \frac{\partial^2 G}{\partial L_1 \partial L_3}\Delta L_1 \Delta L_3 + \frac{\partial^2 G}{\partial L_2 \partial L_3}\Delta L_2 \Delta L_3$$

$$+ \frac{\partial^2 G}{\partial L_1 \partial f}\Delta L_1 \Delta f + \frac{\partial^2 G}{\partial L_2 \partial f}\Delta L_2 \Delta f + \frac{\partial^2 G}{\partial L_3 \partial f}\Delta L_3 \Delta f$$

$$+ \ldots$$

where it is assumed that the first partials exist and are continuous, so that the order of differentiation can be interchanged, and where all of the partial derivatives are evaluated at resonance. As expected all of the first partials become zero when evaluated at resonance. The remaining terms may be arranged to yield

$$G = 1 - \frac{2r^2}{t^4}\left(\frac{2\pi}{c}\right)^2 \Big\{\big[f\,\Delta L_1 + 2f\,\Delta L_2 + f\,\Delta L_3 \qquad \text{(III-6)}$$

$$+ (L_1 + 2L_2 + L_3)\,\Delta f\big]^2 + (1 - r^2)\,\big[f^2 \Delta L_1^2$$

$$+ 2(L_1 - L_3)\,f\,\Delta L \Delta f + f^2\,\Delta L_3^2 + 2(L_3 - L_1)\,f\,\Delta L_3 \Delta f\big]\Big\}$$

For highly reflective mirrors (e.g., $r \cong 1$), G is quite close to its maximum value when the first term in square brackets is zero, i.e., when

$$\Delta f = - \frac{\Delta L_1 + 2\Delta L_2 + \Delta L_3}{L_1 + 2L_2 + L_3} f \qquad \text{(III-7)}$$

This is the required transfer function between mirror displacement and change in resonant frequency. In the linear region where Eq. III-7 properly describes the resonator characteristics, it will sometimes be useful to consider the change in frequency produced by each mirror individually. Equation III-7 can be rewritten as follows

$$\Delta f_1 = - \frac{\Delta L_1}{2L} f$$

$$\Delta f_2 = - \frac{\Delta L_2}{L} f \qquad \text{(III-8)}$$

$$\Delta f_3 = - \frac{\Delta L_3}{2L} f$$

where

$$\Delta f = \Delta f_1 + \Delta f_2 + \Delta f_3 \qquad \text{(III-9)}$$

and L is defined as

$$L = \frac{L_1 + 2L_2 + L_3}{2} \qquad \text{(III-10)}$$

L may be recognized as the average cavity length on an intuitive basis, since, for an ideal beam splitter one expects that at resonance the power of the standing wave in L_2 will be twice that in either L_1 or L_3.

It should be noticed that if $\Delta L_1 = \Delta L_3 = 0$, the term in the second pair of square brackets in Eq. III-6 is zero. Under these conditions the

possibility of a low-loss resonance (i.e., G = 1) is assured regardless of the value of ΔL_2. If either ΔL_1 or ΔL_3 is not zero, the losses will be higher. In order to examine the restrictions that such losses impose, it will be useful to consider the Q of the resonator.

Equation III-4 can be written in the following form

$$G = \frac{1}{\left[\frac{1 - r^2 \sin(\theta_1 - \theta_3)}{1 - r^2}\right]^2 + 4 \frac{r^2}{t^4} \sin(\theta_1 - \theta_3) \cdot \cos^2 \left(\frac{\theta_1 + 2\theta_2 + \theta_3}{2}\right)} \qquad \text{(III-11)}$$

For small changes of frequency, Δf, about resonance in a resonator with highly reflecting mirrors, Eq. III-11 can be approximated by

$$G = \frac{1}{1 + \frac{4r^2}{t^4} \left(\frac{\theta_1 + 2\theta_2 + \theta_3}{2}\right)^2 \left(\frac{\Delta f}{f}\right)^2} \qquad \text{(III-12)}$$

When Δf is large enough that the power transmitted through the resonator has decreased to one-half the power at resonance, Eq. III-12 yields

$$\frac{\Delta f_{1/2}}{f} = \pm \frac{t^2 \lambda}{4r\pi L} \qquad \text{(III-13)}$$

where $\Delta f_{1/2}$ is the difference between the resonant frequency, and the frequency at which half-power transmission occurs. Under these conditions the Q of the resonator may be defined as the ratio of the frequency interval between the half-power points to the resonant frequency. From III-13

$$Q = \frac{f}{2\Delta f_{1/2}} = \frac{2\pi L}{t^2 \lambda}$$

where $r \cong 1$.

Returning to Eq. III-6, assume that $\Delta L_1 = \Delta L_2 = 0$, $\Delta L_3 \neq 0$, and that ΔL_3 and Δf_3 satisfy Eq. III-8. Under these conditions, the power transistivity is approximately

$$G = 1 - 2t^2 \left(\frac{2Q}{f} \Delta f_3\right) \left(1 - \frac{L_3 - L_1}{L}\right) \qquad \text{(III-15)}$$

If L_3 and L_1 are of comparable length, as in Fig. 29, and it is desired that losses not exceed about $2t^2$, then Δf_3 should not exceed about $f/2Q$. Similar remarks apply to independent changes in ΔL_1 and the resulting values of Δf_1. However, if L_1 and L_3 vary together such that $\Delta L_1 = \Delta L_3$, it is easy to show that the losses remain low just as in the previously considered case of an independent ΔL_2.

APPENDIX IV

MODULATED-CAVITY TRANSFER FUNCTION

In Appendix I the ratio of incident wave amplitude to emerging wave amplitude (Eq. I-11) was given for a passive Fabry-Perot cavity. The total power transmissivity, G, of the cavity is the square of the magnitude of this ratio, and is found to be

$$G = \frac{1}{1 + \frac{4r^2}{(1 - r^2)^2} \sin^2 (\theta - \frac{\pi}{4})} \qquad \text{(IV-1)}$$

At the condition of resonance, that is, if

$$\theta = (q + \tfrac{1}{4})\pi$$

Equation IV-1 reduces to G = 1, indicating that the transmission is lossless.

Since G is a function of L and f, it can be expanded in a Taylor's series in these two variables. If the first partial derivatives exist and are continuous, then the series through terms of the second order is

$$G = G\,(\text{res.}) + \frac{\partial G}{\partial L} \Delta L + \frac{\partial G}{\partial f} \Delta f \qquad \text{(IV-2)}$$

$$+ \frac{1}{2} \frac{\partial^2 G}{\partial L^2} \Delta L^2 + \frac{\partial^2 G}{\partial L \partial f} \Delta L \Delta f + \frac{1}{2} \frac{\partial^2 G}{\partial f^2} \Delta f^2 + \ldots$$

where all of the partials are evaluated at resonance. The first partials are zero as expected. The remaining terms are

$$G = 1 - \frac{8r^2}{t^4}\left(\frac{2\pi}{c}\right)^2\left[\frac{f^2}{2}\Delta L^2 + Lf\,\Delta L\Delta f + \frac{L^2}{2}\Delta f^2\right] \qquad \text{(IV-3)}$$

If the length of the cavity is modulated at a rate of f_c Hz, then ΔL can be represented at

$$\Delta L = \delta L \sin\omega_c t \qquad \text{(IV-4)}$$

where $\omega_c = 2\pi f$ and δL is the peak amplitude of the modulation. Since Δf may be a function of time, it will be convenient to represent it similarly

$$\Delta f = \delta f \sin\omega_s t \qquad \text{(IV-5)}$$

where δf is the peak amplitude of the incremental frequency variation and ω_s is the angular frequency of the signal. Substituting Eq. IV-4 and Eq. IV-5 into Eq. IV-3 and simplifying yields

$$G = 1 - \frac{8r^2}{t^4}\left(\frac{2\pi}{c}\right)^2\left\{\frac{f^2\delta L^2}{4}(1 - \cos 2\omega_c t)\right. \qquad \text{(IV-6)}$$

$$+ \frac{Lf\delta L\delta f}{2}\left[\cos(\omega_c - \omega_s)t - \cos(\omega_c + \omega_s)t\right]$$

$$\left. + \frac{L^2\delta f^2}{4}(1 - \cos 2\omega_s t)\right\}$$

The cos2 $\omega_c t$ term indicates that the output will contain a component at a frequency of twice the carrier, or modulating frequency. The cos2 $\omega_s t$ indicates a component at twice the signal frequency. The $\cos(\omega_c - \omega_s)t$ and $\cos(\omega_c + \omega_s)t$ terms indicate components at frequencies that are the difference and sum of the carrier and signal frequencies, and are characteristic of suppressed-carrier modulation. The absence of a discrete component at ω_c characterizes the process as balanced modulation. The presence of a component at 2 ω_s makes it similar to half-wave modulation.

The 2 ω_s component could be removed by the use of full-wave modulation. This might be accomplished by the addition of a second cavity the length of which was modulated in accordance with

$$\Delta L = -\delta L \sin\omega_c t$$

and then subtracting the outputs of the two cavities. This component can also be removed by filtering the output. If ω_m is the highest signal frequency that will occur, and if 3 $\omega_m < \omega_c$. then an ideal filter with a bandpass of $(\omega_c - \omega_m) < \omega < (\omega_c + \omega_m)$ will remove all components except the desired outputs at $\omega_c - \omega_s$ and $\omega_c + \omega_s$.

If the modulated cavity is illuminated by a laser with output power P_o, the power of the beam emerging from the cavity will be

$$P = GP_1 \qquad \text{(IV-7)}$$

The incremental change in power due to the desired signal component is

$$\Delta P = -\frac{8r^2}{t^4}\left(\frac{2\pi}{c}\right)^2 P_o L f \delta L \, \Delta f \sin\omega_c t \qquad \text{(IV-8)}$$

or

$$\Delta P = -\frac{8r^2}{t^4}\left(\frac{2\pi}{c}\right)^2 P_o L f \delta L \delta f \left[\frac{\cos(\omega_c - \omega_s)t - \cos(\omega_c + \omega_s)t}{2}\right] \quad \text{(IV-9)}$$

if

$$\Delta f = \delta f \sin\omega_s t.$$

APPENDIX V

ASSEMBLY DRAWINGS 881117 AND 881118

8 7 6 5

SECURITY CLASSIFICATION

D

NOTES:

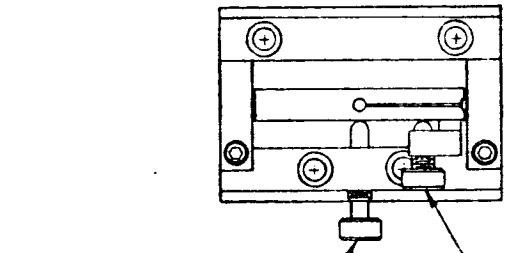

C

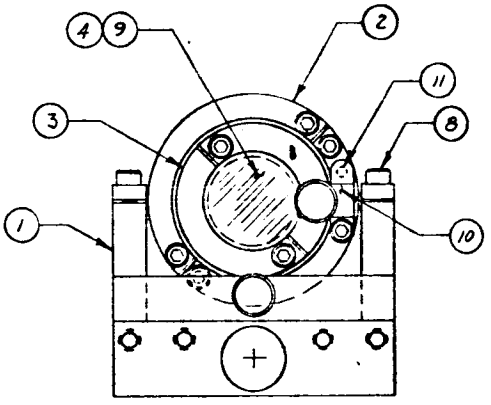

B

A

REVISIONS				
ZONE	LTR	DESCRIPTION	DATE	APPROVED

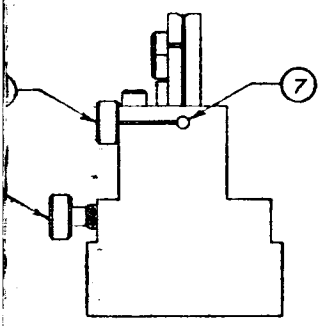

1.75H x 1.82W x 1.12D

QTY REQD	SYM	CODE IDENT	PART OR IDENTIFYING NO.	NOMENCLATURE OR DESCRIPTION	MATERIAL	SPECIFICATION	UNIT WT.	ZONE	ITEM NO.
1				PIN-ALIGNMENT	C1018 C.F.				11
1				SUPPORT	C1018 C.F.				10
AR				CEMENT-EPOXY	NO. 6203				9
9				SCREW-SKT HD CAP	416 SST	2-64 x 3/16			8
4			5004-400	FLEXURAL PIVOT	420 SST	BENDIX			7
1				SCREW-ADJ	416 SST	6-40 x 9/32			6
1				SCREW-ADJ	416 SST	6-40 x 9/16			5
1				MIRROR	QUARTZ				4
1				RING-INNER	C1018 C.F.				3
1				RING-OUTER	C1018 C.F.				2
1				FRAME	C1018 C.F.				1

LIST OF MATERIALS

881117

ON	THRU	PART DASH NO.	NEXT ASSY	USED ON
				7205

EFFECTIVE SERIAL NO. USAGE DATA

NEXT FINAL | QTY REQD PER ASSY | APPLICATION

DRAWING LEVEL

UNLESS OTHERWISE NOTED LINEAR DIMS. IN INCHES
TOLERANCES
DECIMAL FINISH ANGULAR
XX ± ±
XXX ± √ RMS
DO NOT SCALE

MATERIAL NOTED

TREATMENT/FINISH

SIMILAR TO | ACT. WT. | CALC. WT.

CONTRACT NO.

DRAWN PYCZ | DATE 1-9-67

CHECK

DESIGN

MFG.

DESIGN ACTIVITY APPD

CUSTOMER

ELECTRO-OPTICAL SYSTEMS, INC.
A Subsidiary of Xerox Corporation
300 N. Halstead St., Pasadena, California, 91107

TITLE
MIRROR ASSEMBLY-
ADJUSTABLE-TWO AXIS

DWG SIZE D | CODE IDENT NO. 12705 | DWG NO. 881117

SCALE 2x1 | RELEASE DATE | SHEET 1 OF 1

8 7 6 5

SECURITY CLASSIFICATION

D

NOTES:

1. BRAZE TUBE ITEM 8 TO MIRROR ASSY ITEM 1 TO DIM SHOWN, USING FLUX ITEM 9 AND BRAZING ALLOY ITEM 10.

C

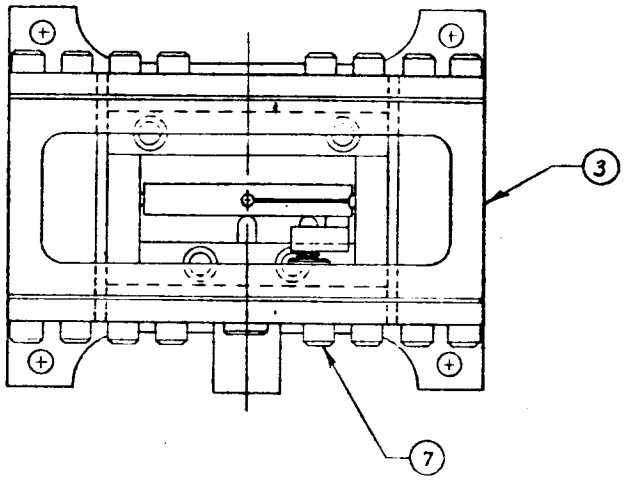

B

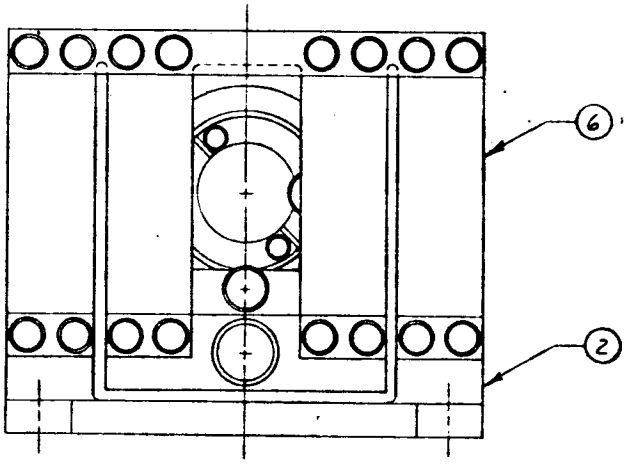

A

REVISIONS				
ZONE	LTR	DESCRIPTION	DATE	APPROVED

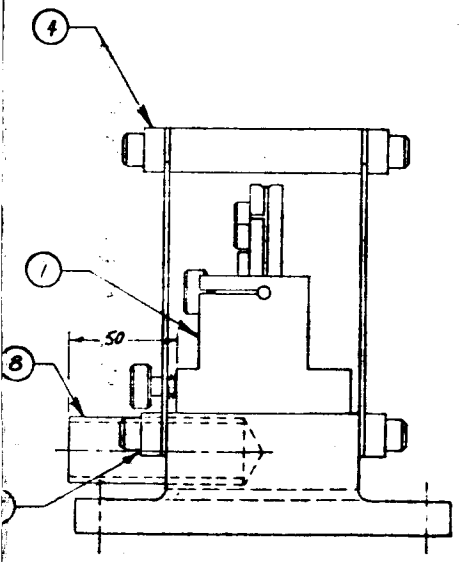

2.34H x 2.76W x 2.2D

QTY REQD	SYM	CODE IDENT	PART OR IDENTIFYING NO.	NOMENCLATURE OR DESCRIPTION	MATERIAL	SPECIFICATION	UNIT WT.	ZONE	ITEM NO.
AR				BRAZING ALLOY	EASY FLO-45				10
AR				FLUX	HANDY TYPE A-1				9
1				TUBE	3/8 OD x .022 WALL C.D.	AISI-MT-1015			8
32				SCREW-SKT HD CAP	400 SERIES SST	4-40 x 5/8			7
2				SPRING-FLEX	.010 THK SHIM STEEL	NO.1 ST.CR			6
8				SUPPORT-BTM					5
2				SUPPORT-TOP					4
1				PLATE					3
1				BASE					2
1			881117	MIRROR ASS'Y					1

881118

LIST OF MATERIALS

ON	THRU	USED ON
		7C05

EFFECTIVE SERIAL NO. — USAGE DATA

NEXT ASSY	NEXT FINAL	DASH NO.	QTY REQD PER ASSY	APPLICATION

DRAWING LEVEL

UNLESS OTHERWISE NOTED
LINEAR DIMS. IN INCHES.
TOLERANCES
DECIMAL: XX ± .01, XXX ± —
FINISH: — √ RMS
ANGULAR: ± —
DO NOT SCALE

MATERIAL: NOTED

TREATMENT FINISH: —

SIMILAR TO | ACT. WT. | CALC. WT.

CONTRACT NO.

DRAWN R.J. PYCZ — DATE 1-7-69

CHECK

DESIGN

MFG.

DESIGN ACTIVITY APPD

CUSTOMER

ELECTRO-OPTICAL SYSTEMS, INC.
A Subsidiary of Xerox Corporation
300 N. Halstead St., Pasadena, California, 91107

TITLE
MIRROR ASSEMBLY M2

DWG SIZE: D | CODE IDENT NO: 12705 | DWG NO: 881118

SCALE 2X/ | RELEASE DATE | SHEET 1 OF 1

APPENDIX VI

BREADBOARD ASSEMBLY COST ESTIMATE

This appendix is an estimate of the cost of a breadboard assembly. Electronic, optical, and mechanical component costs have been estimated on the basis of their dollar value even though some, e.g., machined parts, might be fabricated internally. The labor required for detail design, assembly, test, and reporting has been estimated on the basis of the man hours required in the appropriate labor grades.

The electronic components consist of all those described in Section 5, with the exception of the servomotor. It is assumed that all power supplies will be purchased. The optical components consist of all those described in Section 6 and include the laser discharge tube (and one spare) and the temperature regulated oven and control module for the modulated cavity. The mechanical components consist of those described in Section 7 and include the harmonic drive and servomotor. These estimates are

Electronic components	$ 5,500
Optical components	6,200
Mechanical components	2,700
Total, Components	$14,400

It must be emphasized that these costs are for a breadboard only. They could be substantially reduced if a number of instruments were subsequently fabricated.

Effort by engineers, designers, and technicians will be required to perform the following tasks:

a. Prepare sketches of detail parts
b. Manufacture detail parts
c. Breadboard electronic circuitry
d. Conduct developmental tests of circuitry
e. Finalize circuitry
f. Outline tests to be conducted during assembly
g. Assemble instrument and carry out concurrent tests
h. Interpret test results and outline alignment and checkout procedure
i. Make final electronic package and installation
j. Conduct alignment and checkout
k. Outline final performance tests
l. Conduct final performance tests
m. Draft final report

The total man hours, by labor grade, required to perform these tasks are estimated to be:

Senior Engineer, task leader	1000 hours
Senior Engineer, electronic	500 hours
Designer, mechanical	200 hours
Technician, electronic	500 hours
Technician, mechanical	500 hours

Here again it should be pointed out that an effort of this magnitude would only be required for the breadboard. Substantial reductions would obtain in the event a number of instruments were fabricated subsequently.

REFERENCES

1. "Feasibility Study of a Noncontacting, Remote Sensing Displacement Transducer," Contract No. NAS5-10345, 16 March 1967, National Aeronautics and Space Administration, Goddard Space Flight Center, Greenbelt, Maryland.

2. Ward, T. L., "Research Summary Report, Noncontacting, Remote Sensing Displacement Transducer," EOS Report 7205-RSR, 29 May 1967, Electro-Optical Systems, Pasadena, California.

3. Levy, S., and Droll, W. D., "Response of Accelerometers to Transient Accelerations," Journal of Research of the National Bureau of Standards, Vol. 45, No. 4, Oct. 1950, pp. 303-309.

4. Richard, R. R., and Bennett, S., "First Quarterly Progress Report, Resistojet Research and Development-- Phase II," NASA CR-54155, 25 Nov. 1964, National Aeronautics and Space Administration, Lewis Research Center, Cleveland, Ohio, pp. 23-31.

5. North, D. O., "An Analysis of the Factors Which Determine Signal-Noise Discrimination in Pulsed Carrier Systems (Radar)," unpublished RCA report cited by Freeman in Ref. 6 below.

6. Freeman, J. J., Principles of Noise, Wiley, New York, 1958, pp. 217-223.

7. Johnson, J. B., "Thermal Agitation of Electricity in Conductors," Physical Review, Vol. 32, No. 1, July 1928, pp. 97-109.

8. Nyquist, H., "Thermal Agitation of Electric Charge in Conductors," Physical Review, Vol. 32, No. 1, July 1928, pp. 110-113.

9. Paul, R. J. A., Fundamental Analogue Techniques, Macmillan, New York, 1966, pp. 84-90.

10. Olson, H. F., Acoustical Engineering, Van Nostrand, Princeton, 1957, pp. 335-339.

11. Kennedy, R. J., "A Refinement of the Mickelson-Morley Experiment," Proceedings of the National Academy of Sciences, Vol. 12, No. 11, 15 Nov. 1923, pp. 621-629.

12. Jaseja, T. S., Javan, A., and Townes, C. H., "Frequency Stability of He-Ne Masers and Measurements of Lengths," Physical Review Letters, Vol. 10, No. 5, 1 March 1963, pp. 165-167.

13. Van Veen, H. J., Savino, J., and Alsop, L. E., "An Optical Maser Strainmeter," Journal of Geophysical Research, Vol. 71, No. 22, 15 Nov. 1966, pp. 5478-5479.

14. Ahearn, W. E., and Crowe, J. W., "Linewidth Measurements of CW Gallium Arsenide Lasers at 77°K," IEEE Journal of Quantum Electronics, Vol. QE-2, April 1966, p. lxvi (digest of paper presented at 1966 International Quantum Electronics Conference, Phoenix, Arizona, 15 April 1966).

15. Nathan, M. I., "Semiconducting Lasers," Proceedings of the IEEE, Vol. 54, No. 10, Oct. 1966, pp. 1276-1290.

16. Kiss, Z. J. and Pressley, R. J., "Crystalline Solid Lasers," Proceeding of the IEEE, Vol. 54, No. 10, Oct. 1966, pp. 1236-1248.

17. Wittke, J. P., "Solid State Laser Explorations," AFAL-TR-64-344, Jan. 1964, Air Force Avionics Laboratory, Wright-Patterson Air Force Base, Ohio, pp. 88-90.

18. Snitzer, W., "Glass Lasers," Proceedings of the IEEE, Vol. 54, No. 10, Oct. 1967, pp. 1249-1261.

19. Javan, A., Ballik, E. A., and Bond, W. L., "Frequency Characteristics of a Continuous - Wave He-Ne Optical Maser," Journal of the Optical Society of America, Vol. 52, No. 1, Jan. 1962, pp. 96-98.

20. Einstein, A., "Zur Quantentheorie der Strahlung," Physikalische Zeitschrift, Vol. 18, No. 6, 15 March 1917, pp. 121-128.

21. Ditchburn, R. W., Light, 2nd ed., Interscience, 1963, pp. 681-683.

22. Tolman, R. C., "Duration of Molecules in Upper Quantum States," Physical Review, Vol. 23, No. 6, June 1924, pp. 693-709.

23. Javan, A., "Possibility of Production of Negative Temperature in Gas Discharges," Physical Review Letters, Vol. 3, No. 2, 15 July 1959, pp. 87-89.

24. Javan, A., Bennett, W. R., and Herriott, D. R., "Population Inversion and Continuous Optical Maser Oscillation in a Gas Discharge Containing a He-Ne Mixture," Physical Review Letters, Vol. 6, No. 3, 1 Feb. 1961, pp. 106-110.

25. White, A. D., and Rigden, J. D., "Continuous Gas Maser Operation in the Visible," Proceedings of the IRE, Vol. 50, No. 7, July 1962, p. 1697.

26. Garrett, C. G. B., Gas Lasers, McGraw-Hill, New York, 1967, p. 64.

27. Moore, C. E., Atomic Energy Levels, Circular 647, Vol. 1, National Bureau of Standards, Washington, 15 June 1949, pp. 4-7, pp. 76-88.

28. Bennett, W. R., Kindlman, P. J., and Mercer, G. N., "Measurement of Excited State Relaxation Times," Applied Optics Supplement 2: Chemical Lasers, 1965, pp. 34-57 (see Ne $2p_4$ level).

29. Garrett, op. cit., p. 133.

30. Garrett, op. cit., p. 68, pp. 43-44.

31. Gordon, E. I., and White, A. D., "Similarity Laws for the Effects of Pressure and Discharge Diameter on Gain of He-Ne Lasers," Applied Physics Letters, Vol. 3, No. 11, 1 Dec. 1963, pp. 199-201.

32. Rubin, S., "Concepts in Shock Data Analysis," Shock and Vibration Handbook, Vol. 2, McGraw-Hill, New York, 1961, 23.1-23.37.

33. Bloom, A. L., "Gas Lasers," Proceedings of the IEEE, Vol. 54, No. 10, Oct. 1966, pp. 1262-1276.

34. Walther, A., "Diffraction," Applied Optics and Optical Engineering, Vol. 1, Academic Press, New York, p. 264.

35. Fox, A. G., and Li, T., "Resonant Modes in a Maser Interferometer," Bell System Technical Journal, Vol. 40, No. 2, Sept. 1961, pp. 453-488.

36. Cochran, J. A., "The Existence of Eigenvalues for the Integral Equations of Laser Theory," Bell System Technical Journal, Vol. 44, No. 1, Jan. 1965, pp. 77-88.

37. Bennett, W. R., "Gaseous Optical Masers," Applied Optics Supplement: Optical Masers, 1962, pp. 24-61.

38. Morse, P. M., Vibration and Sound, 2nd ed., McGraw-Hill, New York, 1948.

39. Kogelnik, H., and Rigrod, W. W., "Visual Display of Isolated Optical-Resonator Modes," Proceedings of the IRE, Vol. 50, No. 2, Feb. 1962, p. 220.

40. Boyd, G. D., and Gordon, J. P., "Confocal Multimode Resonator for Millimeter Through Optical Wavelength Masers," Bell System Technical Journal, Vol. 40, No. 2, Mar. 1961, pp. 489-508.

41. Garrett, op. cit., p.16.

42. Kogelnik, H., "Modes in Optical Resonators," Lasers, Vol. 1, Marcel Dekker, New York, 1966, p. 312; see also, Ref. 68.

43. Boyd, G. D., and Kogelnik, H., "Generalized Confocal Resonator Theory," Bell System Technical Journal, Vol. 41, No. 4, July 1962, pp. 1347-1370.

44. Kogelnik, Lasers, op. cit., pp. 334-338; see also Ref. 72.

45. Garrett, op. cit., p. 17.

46. Kleinman, D. A., and Kisliuk, P. P., "Discrimination Against Unwanted Orders in the Fabry-Perot Resonator," Bell System Technical Journal, Vol. 41, No. 2, March 1962, pp. 453-462.

47. Kogelnik, H., and Patel, C. K. N., "Mode Suppression and Single Frequency Operation in Gaseous Optical Masers," Proceedings of the IRE. Vol. 50, No. 11, Nov. 1962, pp. 2365-2366.

48. Kumagai, N., Matsuhara, M., and Mori, H., "Design Considerations for Mode Selective Fabry-Perot Laser Resonator," IEEE Journal of Quantum Electronics, Vol. QE-1, No. 2, May 1965, pp. 85-94.

49. Smith, P. W., "Stabilized, Single-Frequency Output from a Long Laser Cavity," IEEE Journal of Quantum Electronics, Vol. QE-1, No. 8, Nov. 1965, pp. 343-348.

50. DiDomenico, M., "A Single-Frequency TEM_{00} Mode Gas Laser with High Power Output," Applied Physics Letters, Vol. 8, No. 1, 1 January 1966, pp. 20-22.

51. DiDomenico, M., "Characteristics of a Single-Frequency Michelson-Type He-Ne Gas Laser," IEEE Journal of Quantum Electronics, Vol. QE-2, No. 8, August 1966, pp. 311-322.

52. White, A. D., "Frequency Stabilization of Gas Lasers," IEEE Journal of Quantum Electronics, Vol. QE-1, No. 8, Nov. 1965, pp. 349-357.

53. Bloom, A. L., and Wright, D. L., "Pressure Shifts in a Stabilized Single Wavelength Helium-Neon Laser," Proceedings of the IEEE, Vol. 54, No. 10, Oct. 1966, pp. 1290-1294.

54. "Application Notes, SGD-100 and SGD-444 Diodes," EG&G Inc., Electronics Products Division, Boston, Mass., June 1967.

55. Li, T., "Diffraction Loss and Selection of Modes in Maser Resonators with Circular Mirrors," Bell System Technical Journal, Vol. 44, No. 5, May 1965, pp. 917-932.

56. Ivey, K. A., A-C Carrier Control Systems, Wiley, New York, pp. 144-146.

57. Weiss, G., and Levenstein, H., "A-C Servos," Control Engineers' Handbook, McGraw-Hill, New York, 1958, pp. 6-45 to 6-82.

58. "Piezoelectric Technology Data for Engineers," Clevite Corporation, Bedford, Ohio, 1965.

59. Berlincourt, D., and Krueger, H. H. A., "Properties of Clevite Ceramics," TP-226, Clevite Corporation, Bedford, Ohio.

60. Hansen, P. D., "New Approaches to the Design of Active Low Pass Filters," Part II, The Lightning Empiricist, Vol. 13, No. 3, July 1965, pp. 2-12.

61. Ivey, op. cit., pp. 216-219.

62. Hansen, P. D., "New Approaches to the Design of Active Filters," The Lightning Empiricist, Vol. 13, No. 1, Jan. 1965, pp. 3-16.

63. Olsen, H. F., Acoustical Engineering, Van Nostrand, Princeton, N. J., 1957, pp. 66-68.

64. White, A. D., "Method for Decoupling Laser Mirror Transducers from Mechanical Resonances of Laser Cavity," Review of Scientific Instruments, Vol. 37, No. 7, July 1966, pp. 976-977.

65. Smythe, W. R., Static and Dynamic Electricity, McGraw-Hill, New York, 1939, p. 28.

66. Smith, P. W., "On the Optimum Geometry of a 6328Å Laser Oscillator," IEEE Journal of Quantum Electronics, Vol. QE-2, No. 4, April 1966, pp. 77-79.

67. Bloom, A. L., Bell, W. E., and Rempel, R. C. "Laser Operation at 3.39μ in a Helium-Neon Mixture," Applied Optics, Vol. 2, No. 3, March 1963, pp. 317-318.

68. Rigrod, W. W., Kogelnik, H., Brangaccio, D. J., and Herriott, D. R., "Gaseous Optical Maser with External Concave Mirrors," Journal of Applied Physics, Vol. 33, No. 2, Feb. 1962, pp. 743-744.

69. Smith, P. W., "The Output Power of a 6328-Å He-Ne Gas Laser," IEEE Journal of Quantum Electronics, Vol. QE-2, No. 3, March 1966, pp. 62-68.

70. White, A. D., "Stable, Easily Fabricated, Tunable, Passive Optical Cavity," Review of Scientific Instruments, Vol. 37, No. 7, July 1966, pp. 968-969.

71. "Oven Assembly, Including Control Module," Part No. 2363, Cox and Company, Inc., 215 Park Avenue South, New York, N. Y. 10003.

72. Kogelnik, H. "Imaging of Optical Mode-Resonators with Internal Lenses," Bell System Technical Journal, Vol. 44, No. 3, March 1965, pp. 455-494.

73. Kogelnik, H., and Li, T., "Laser Beams and Resonators," Proceedings of the IEEE, Vol. 54, No. 10, Oct. 1966, pp. 1312-1329.

74. Kingslake, R., "Basic Geometrical Optics," Applied Optics and Optical Engineering, Vol. I, Academic Press, New York, 1965, pp. 224-225.

75. Jones, R. V., "Parallel and Rectilinear Spring Movements," Journal of Scientific Instruments, Vol. 28, No. 2, Feb. 1951, pp. 38-41.

76. Geary, P. J., Flexure Devices, British Scientific Instrument Research Association, 1954.

77. Vander Sluis, K. L., Werner, G. K., Griffin, P. M., Morgan, H. W., Rudolph, O. B., and Staats, P. A., "A Simplified Construction of a Helium-Neon Visible Laser," American Journal of Physics, Vol. 33, No. 3, March 1965, pp. 225-240.

78. Carlin, H. J., "The Scattering Matrix in Network Theory," IRE Transactions on Circuit Theory, Vol. CT-3, No . 2, June 1956, pp. 88-97.

79. Kerns, D. M., and Beatty, R. W., Basic Theory of Waveguide Junctions and Introductory Microwave Network Analysis, Pergamon, Oxford, 1967, pp. 41-48.